

# Reactions of Transition Metal Complexes with Fullerenes (C<sub>60</sub>, C<sub>70</sub>, etc.) and Related Materials

Alan L. Balch\* and Marilyn M. Olmstead

The Department of Chemistry, University of California, Davis, California 95616

Received August 18, 1997 (Revised Manuscript Received May 26, 1998)

## Contents

|   |      |
|---|------|
| I. Introduction   | 2123 |
| II. Brief Overview of Reactivity and Characterization of Isolated Fullerene Compounds   | 2125 |
| III. Survey of Isolated Fullerene Complexes across the Periodic Table   | 2126 |
| A. Lanthanum, Yttrium, and Scandium   | 2126 |
| B. Hafnium, Zirconium, and Titanium   | 2126 |
| C. Tantalum, Niobium, and Vanadium  | 2127 |
| D. Tungsten, Molybdenum, and Chromium   | 2127 |
| E. Rhenium, Technetium, and Manganese   | 2128 |
| F. Osmium, Ruthenium, and Iron  | 2128 |
| 1. Osmylation   | 2128 |
| 2. Reactions with Zerovalent Compounds  | 2131 |
| 3. Other Addition Reactions   | 2133 |
| 4. Redox Reactions  | 2134 |
| 5. Cocrystallizations   | 2134 |
| G. Iridium, Rhodium, and Cobalt   | 2135 |
| 1. Adduct Formation with Vaska-Type Complexes, Ir(CO)Cl(PR <sub>3</sub> ) <sub>2</sub>  | 2135 |
| 2. Addition of Ir <sub>2</sub> (μ-Cl) <sub>2</sub> (η <sup>4</sup> -C <sub>8</sub> H <sub>12</sub> ) <sub>2</sub> to C <sub>60</sub>        | 2144 |
| 3. Reaction of (η <sup>5</sup> -C <sub>9</sub> H <sub>7</sub> )Ir(CO)(η <sup>2</sup> -C <sub>8</sub> H <sub>12</sub> ) with C <sub>60</sub> | 2144 |
| 4. Reaction of C <sub>60</sub> with the Hydrogenation Catalyst, RhH(CO)(PPh <sub>3</sub> ) <sub>3</sub>                                     | 2145 |
| 5. Other Additions  | 2145 |
| 6. Redox Reactions  | 2146 |
| 7. Cocrystallizations   | 2147 |
| H. Platinum, Palladium, and Nickel  | 2147 |
| 1. Addition of M(PR <sub>3</sub> ) <sub>2</sub> Units to Fullerenes   | 2147 |
| 2. Formation of Pd(0) and Pt(0) Polymers  | 2151 |
| 3. Redox Reactions  | 2152 |
| 4. Cocrystallizations   | 2152 |
| I. Gold, Silver, and Copper   | 2152 |
| IV. Gas-Phase Studies of Fullerene Interactions with Transition Metal Ions  | 2153 |
| V. Theoretical Studies of the Electronic Structures of Metal Fullerene Complexes  | 2155 |
| VI. Fullerenes with Ligating Centers Attached   | 2156 |
| VII. Coordination Chemistry of Fullerene Fragments  | 2157 |
| VIII. Transition Metals and Carbon Nanotubes and Other Nanostructures   | 2158 |
| IX. Other Related Transition Metal–Carbon Compounds   | 2160 |
| X. Conclusions  | 2161 |
| XI. Acknowledgments   | 2162 |
| XII. References   | 2162 |

## I. Introduction

Within five years following the initial experimental identification of C<sub>60</sub> as a uniquely stable molecule,<sup>1</sup> synthetically useful amounts of C<sub>60</sub> and higher fullerenes (C<sub>70</sub>, C<sub>76</sub>, C<sub>78</sub>, C<sub>84</sub>)<sup>2</sup> became available to chemists for manipulation.<sup>3,4</sup> A portion of that synthetic manipulation has involved examination of the reactivity of the fullerenes toward transition metal compounds, which is the subject of this review.

The majority of studies of fullerene chemistry have involved C<sub>60</sub>, which is the most abundant species formed in the widely utilized carbon arc process of fullerene generation.<sup>4</sup> The structure of C<sub>60</sub> (Figure 1) consists of sixty identical carbon atoms, but there are two distinct types of C–C bonds. Those bonds at the 6:6 ring junctions are shorter (bond length 1.38 Å) than the bonds at the 6:5 ring junctions (bond length 1.45 Å).<sup>5</sup> The bonds at the 6:6 ring junction behave as olefinic units, and metal ions commonly coordinate to them in an η<sup>2</sup>-fashion. Since there are thirty identical 6:6 ring junctions, the reactivity of C<sub>60</sub> is complicated by the frequent occurrence of multiple additions to these 6:6 ring junctions, and by the regiochemistry of addition. Figure 2 outlines the eight possible regioisomers that can form when double addition is restricted to the bonds of 6:6 ring junctions. The nomenclature of Hirsh is useful in identifying these as three cis isomers with addenda on the same hemisphere, the unique equatorial isomer, and four trans isomers with the addenda on opposite hemispheres.<sup>6</sup>

Consideration of the electronic structure of C<sub>60</sub> has naturally focused on the surface π-orbitals. A molecular orbital energy diagram is shown in Figure 3. There are 30 filled π-type orbitals. The 5-fold degenerate h<sub>u</sub> orbitals are the HOMOs. The LUMOs are the triply degenerate t<sub>1u</sub> orbitals, and a second set of triply degenerate orbitals of t<sub>1g</sub> symmetry are the LUMO+1's. Since the LUMO is relatively low in energy, C<sub>60</sub> is readily reduced. As predicted by the nature of the LUMO, six-reversible one-electron reductions can be observed for C<sub>60</sub>.<sup>7–9</sup> The reduction potentials are uniformly spaced with a ca. 0.5 V difference between successive reduction waves in cyclic voltammetry. The reduction potentials show only modest variations when the solvent and/or supporting electrolyte are changed. In toluene/acetonitrile (4:1, v/v) with tetra(*n*-butyl)ammonium hexafluorophosphate as supporting electrolyte, the reduction potentials for C<sub>60</sub> are –0.98, –1.37, –1.87,



Alan L. Balch received his B.A. degree in chemistry from Cornell University in 1962. He was a Leeds and Northrop and NSF predoctoral student at Harvard University with R. H. Holm from 1962 to 1966 but spent the last of those years at the University of Wisconsin on traveling guidance from Harvard. He joined the faculty of the University of California, Los Angeles in 1966 and received the Ph.D from Harvard in 1967. In 1970 he moved to the University of California, Davis, where he is currently Professor of Chemistry after serving as Department Chair from 1994 to 1997. He has served on the editorial boards of *Inorganic Chemistry* and *Dalton Transactions* and on the NIH Metallobiochemistry Study Section (Chair, 1992–1994). His research interests include fullerene chemistry; supramolecular chemistry; synthesis, reactivity, and structure of metal–metal-bonded compounds; luminescence behavior of transition metal compounds; metalloporphyrin chemistry; heme degradation and bile pigment formation; and activation of molecular oxygen.



Marilyn M. Olmstead received her B.A. degree in chemistry from Reed College in 1965. She was a Woodrow Wilson Fellow from 1965 to 1967 at the University of Wisconsin, Madison, and earned her Ph.D. in inorganic chemistry under the direction of Richard F. Fenske in 1969. Since 1969 she has been a member of the Department of Chemistry at the University of California, Davis, as a Lecturer and Postdoctoral and Staff Research Associate. She served on the Board of Editors of *Inorganic Chemistry* from 1988 to 1991. At present, she manages the department's small molecule X-ray crystallographic facility. Her extensive collaborations have resulted in over 350 publications. Her research interests are as broad as her collaborations, but her favorite crystal structures are those of the fullerenes.

–2.35, –2.85, and –3.26 V versus a ferrocene/ferrocinium electrode. Numerous salts containing the fulleride ions have been prepared. Those salts of composition  $A_3C_{60}$ , where A is an alkali metal ion, have received considerable attention due to the observation of superconductivity at temperatures up to ~35 K.<sup>10</sup> Although reduction of  $C_{60}$  is relatively readily achieved, oxidation is more difficult. Cyclic voltammetry studies show that  $C_{60}$  undergoes a single one-electron oxidation at 1.26 mV versus a ferrocene/ferrocinium electrode in tetrachloroethyl-

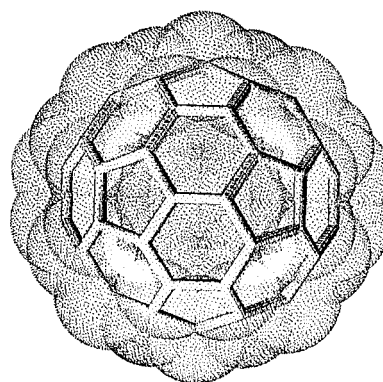
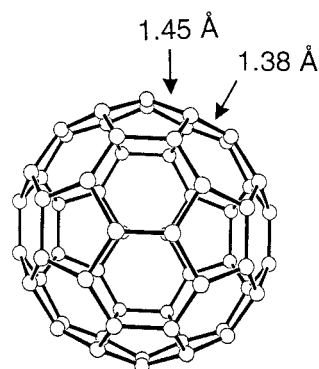


**Figure 1.** The idealized structure of the fullerene  $C_{60}$ .

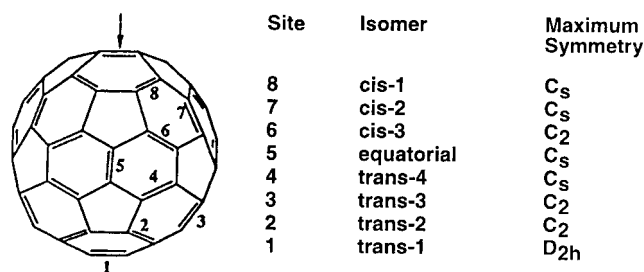


**Figure 2.** Regiochemistry of double-addition to  $C_{60}$ . The eight regioisomers that can form when addition is restricted to the carbon–carbon bonds at 6:6 ring junctions are named according to the scheme of Hirsh.<sup>6</sup>

ene solution with tetra(*n*-butyl)ammonium hexafluorophosphate as supporting electrolyte.<sup>11</sup>

Spectroscopically,  $C_{60}$  is characterized by a singlet in the  $^{13}C$  NMR spectrum at 143.2 ppm in benzene solution<sup>12</sup> and by four bands in the infrared spectrum at 1400, 1180, 580, and 510  $cm^{-1}$  with the band at 510  $cm^{-1}$  having the greatest intensity.<sup>13</sup> These infrared active modes are the four  $t_{1u}$  vibrations.  $C_{60}$  has 174 vibrational modes with 42 fundamentals of various symmetries. Of these only the four  $t_{1u}$  vibrations are infrared active.<sup>14</sup> The electronic absorption spectrum of  $C_{60}$  is dominated by three intense bands at 220, 270, and 340 nm which are due to allowed  $^1A_g \rightarrow ^3T_{1u}$  transitions. The purple color of  $C_{60}$  solutions results from a set of weaker transitions in the 400–600 nm region that are spin-forbidden, singlet–singlet transitions.<sup>15</sup>

In addition to  $C_{60}$ , the carbon arc process produces significant quantities of higher fullerenes of which  $C_{70}$  is the next most abundant species.<sup>16</sup>  $C_{70}$ , like  $C_{60}$ , has only one structure that conforms to the isolated pentagon rule.<sup>17</sup> That structure, which has  $D_{5h}$

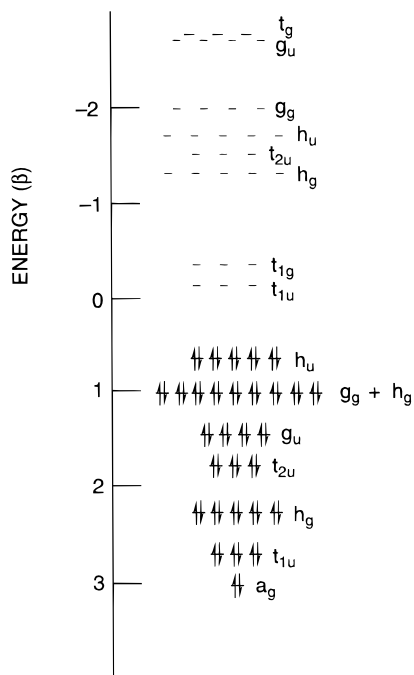


**Figure 3.** A molecular orbital energy diagram for  $C_{60}$  (adapted from ref 7).

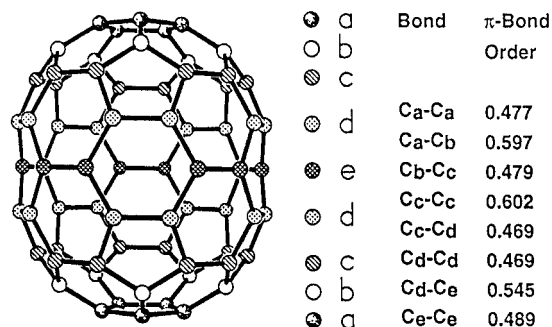


**Figure 4.** The idealized structure of  $C_{70}$ . The Hückel  $\pi$ -bond orders are from ref 18.

symmetry, is shown in Figure 4. The  $C_{70}$  molecule consists of two  $C_{60}$ -like hemispheres that are now bridged by a new set of 10 carbon atoms (labeled e in Figure 4). The  $C_{70}$  molecule has a layered structure that is unique among the isolated fullerenes. There are five types of carbon atoms (label a–e in Figure 4) that form nine layers. Connecting these carbon atoms are eight types of C–C bonds. Of these bonds, four occur between 6:6 ring junctions, and four involve 6:5 ring junctions. The C–C bond lengths at the 6:6 ring junctions are again shorter than the C–C bond lengths at the 6:5 ring junctions, and the shortest C–C bonds are found at the curved ends of the  $C_{70}$  molecule. The results of Hückel molecular orbital calculation are also shown in Figure 4.<sup>18</sup> The  $C_a$ – $C_b$  and  $C_c$ – $C_c$  bonds at the poles of the molecule have the highest  $\pi$  bond orders and are expected to be the most reactive by that criterion.

Multiple additions are also readily observed for  $C_{70}$ . So far, additions of transition metal complexes which are generally large relative to the fullerene surface occur at opposite poles of the molecule. Thus for double addition, there are three possible isomers if reactivity is confined to the  $C_a$ – $C_b$  bonds at opposite

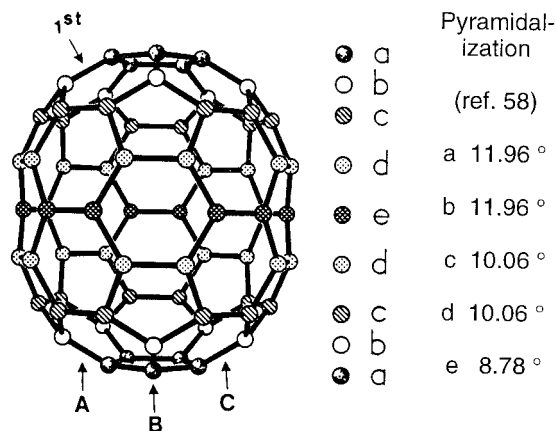


**Figure 5.** Sites for double addition to  $C_{70}$ .

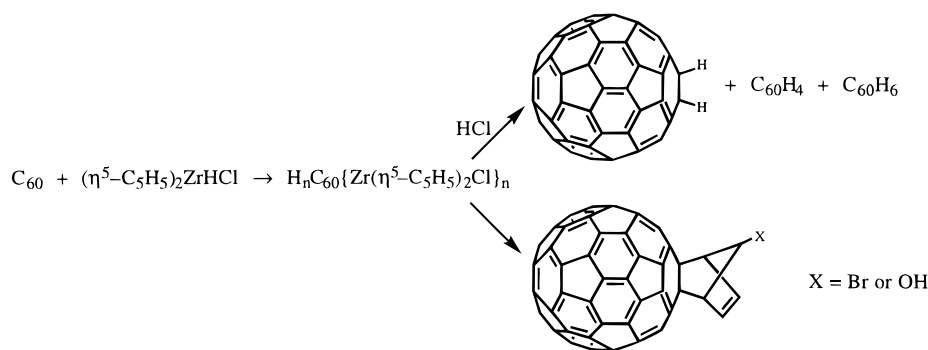
ends of the molecule. These three isomers are shown in Figure 5.

In addition to  $C_{60}$  and  $C_{70}$ , the carbon arc process also produces isolable quantities of  $C_{76}$ ,  $C_{78}$ , and  $C_{84}$  along with an array of even larger fullerenes in much lower abundances.<sup>14</sup> For  $C_{76}$  there is also only one structure that conforms to the isolated pentagon rule, but the molecule has  $D_2$  symmetry and exists in two enantiomeric forms.<sup>17</sup> The structural complexity of the higher fullerenes increases markedly with increasing number of carbon atoms. For  $C_{78}$ , there are five structures that conform to the isolated pentagon rule. These have the following symmetries:  $D_{3h}$  (two isomers),  $D_3$ , and  $C_{2v}$  (two isomers).<sup>17</sup> For  $C_{84}$ , 24 different isomeric structures are possible that obey the isolated pentagon rule.<sup>19</sup>

This review will cover the array of reactions that involve transition metal complexes and fullerenes. Of the fullerenes, most of the work involves  $C_{60}$ , but a substantial number of studies on  $C_{70}$  have been conducted as well. Because of limitations in availability of the parent fullerenes, in only a few cases have metal complexes been reported to react with higher fullerenes:  $C_{76}$ ,  $C_{78}$ , and  $C_{84}$ . Only the exposed, outer surface of the fullerenes is readily accessible to chemical reactions, and thus this review is restricted to the exohedral chemistry of the fullerenes. The formation and reactivity of endohedral species in which an atom, generally a non-transition metal atom, is encapsulated within a fullerene, are not covered here, but several reviews are available.<sup>20</sup> Several complementary reviews cover related chemistry. The present review is an update of an earlier article on transition metal fullerene complexes.<sup>21</sup> Aspects of the organometallic reactivity of fullerenes have been covered in two reviews,<sup>22,23</sup> while another article deals with both endo- and exohedral metal fullerene interactions.<sup>24</sup>

## II. Brief Overview of Reactivity and Characterization of Isolated Fullerene Compounds

The reactions of transition metal complexes with fullerenes result in the formation of an interesting array of new compounds. Four major types of reactions that yield complexes which may be isolated can be ascertained: (1) addition of the metal to the

**Scheme 1. Hydrozirconation of C<sub>60</sub>**

olefinic C–C bonds at 6:6 ring junctions to form  $\eta^2$ -coordination complexes, (2) reduction of the fullerene to form fulleride salts, (3) addition of ligating groups to the fullerene so that the metal center is attached to the fullerene through some type of bridging arrangement, and (4) the formation of solids in which the fullerene and a metal complex are cocrystallized.<sup>21</sup> The last reaction type may involve some degree of charge transfer between the individual components. The survey in Section III reports on the specific compounds that have been prepared so far via the routes outlined above for each of the transition elements across the periodic table.

Characterization of the products of the reactions of fullerenes with transition metal complexes has involved an array of structural probes. Single-crystal X-ray diffraction is particularly valuable in providing metric details about the structure and measuring structural distortion that results from chemical modification of the fullerene. X-ray diffraction studies are also important in identifying not only the primary site of chemical interaction but in specifying regiochemistry and identifying secondary features within structures that may contribute to the overall stability. Of course in cases where the interaction between the components is weak and generally referred to as cocrystallization or intercalation,<sup>25</sup> X-ray crystallography is particularly important in defining the nature of the products. Due to the high symmetry of the fullerenes and many chemically modified fullerenes, disorder is a common problem that plagues the analysis of single-crystal diffraction data. Appending a bulky metal complex to the surface of the fullerene lowers the symmetry and can produce ordered materials that are structurally more informative.

In considering spectroscopic probes for the characterization of fullerene compounds in solution, it has frequently been more informative to use probes that involve parts of the molecule that came from the parent transition metal complex itself rather than the fullerene portion. Thus infrared spectroscopy can readily monitor metal ligand characteristics such as metal hydride or metal carbonyl vibrations rather than the fullerene vibrations. However the most intense fullerene band at  $\sim 510\text{ cm}^{-1}$  is one that has had considerable use in characterization of fullerene compounds. NMR spectroscopic observations that focus for example on the <sup>31</sup>P NMR spectra of metal-bound phosphines have also proven to be useful

structural probes. In contrast, <sup>13</sup>C NMR studies of the fullerene portions, while potentially informative, are frequently hampered by problems that arise from poor solubility, lability of the compounds involved, and spectral complexity that results from both lowering of the fullerene symmetry, and, in many reactions, the formation of a variety of products. The electronic spectra of fullerenes do show changes upon chemical reactions. Profound alterations in the UV/vis absorption spectra are seen upon reduction of the fullerenes.<sup>26</sup> The fulleride salts display unique features, particularly at low energies. On the other hand, coordination of a metal complex to the fullerene exterior produces small changes in the absorption spectra, and those that are observed do not appear to contain useful information for structural determination.

### III. Survey of Isolated Fullerene Complexes across the Periodic Table

#### A. Lanthanum, Yttrium, and Scandium

To date no exohedral compounds that involve these elements have been reported, but extensive work on endohedral fullerenes with Sc and La has been described.<sup>20</sup>

#### B. Hafnium, Zirconium, and Titanium

Within this group, the only work reported involves hydrozirconation of C<sub>60</sub>.<sup>27,28</sup> Thus, treatment of C<sub>60</sub> with  $(\eta^5\text{-C}_5\text{H}_5)_2\text{ZrHCl}$  in benzene yields a deep red solution which is believed to contain (on the basis of <sup>1</sup>H NMR measurements) a mixture of adducts:  $\{\eta^5\text{-C}_5\text{H}_5\}_2\text{ZrCl}\}_n\text{C}_{60}\text{H}_n$  with  $n = 1, 2,$  and  $3$  as shown in Scheme 1. Hydrolysis of this mixture produces C<sub>60</sub>H<sub>2</sub> in 60% yield along with C<sub>60</sub>H<sub>4</sub> and C<sub>60</sub>H<sub>6</sub> which can be separated by HPLC; these hydrides of C<sub>60</sub> have also been made by other routes.<sup>30</sup> Additionally, treatment of the C<sub>60</sub> hydrozirconation adducts with *N*-bromosuccinimide or *m*-chloroperoxybenzoic acid results in the formation of Diels–Alder-type adducts with bromocyclopentadiene or hydroxycyclopentadiene.<sup>28</sup> The authors concluded that the hydrozirconation product is cleaved by the added electrophile to form free C<sub>60</sub> and a substituted cyclopentadiene (presumably from the  $(\eta^5\text{-C}_5\text{H}_5)_2\text{Zr}$  unit). Subsequent Diels–Alder addition of the substituted cyclopentadiene to C<sub>60</sub> occurs to form the product.

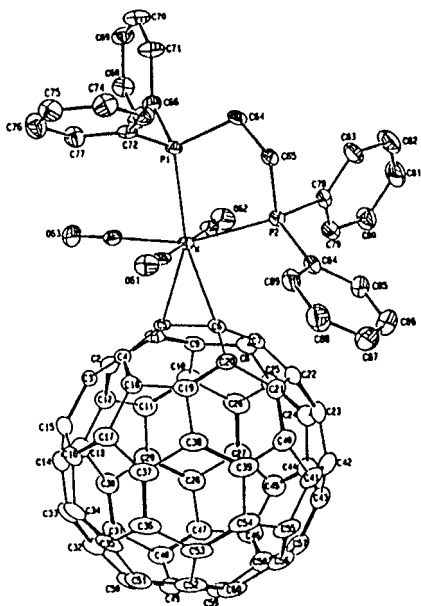


**Figure 6.** The structure of *mer*-( $\eta^2$ -C<sub>60</sub>)W(CO)<sub>3</sub>(Ph<sub>2</sub>PCH<sub>2</sub>CH<sub>2</sub>PPh<sub>2</sub>) as determined by X-ray crystallography (Reprinted with permission from ref 32. Copyright 1994 Electrochemical Society.)

### C. Tantalum, Niobium, and Vanadium

Treatment of C<sub>60</sub> with ( $\eta^5$ -C<sub>5</sub>H<sub>5</sub>)<sub>2</sub>TaH<sub>3</sub> in benzene yields brown microcrystals of ( $\eta^5$ -C<sub>5</sub>H<sub>5</sub>)<sub>2</sub>Ta( $\eta^2$ -C<sub>60</sub>), which has been characterized by infrared spectroscopy ( $\nu$ (Ta–H), 1791 cm<sup>-1</sup>, characteristic fullerene bands at 518 and 529 cm<sup>-1</sup>).<sup>30</sup> Additionally, the interaction between ( $\eta^5$ -C<sub>5</sub>H<sub>5</sub>)<sub>2</sub>V and C<sub>60</sub> has been monitored in solution by EPR spectroscopy.<sup>31</sup> An adduct, ( $\eta^5$ -C<sub>5</sub>H<sub>5</sub>)<sub>2</sub>V( $\eta^2$ -C<sub>60</sub>) is formed reversibly and detected by its EPR spectrum with *g* (isotropic) of 2.0001 and A(<sup>51</sup>V) (isotropic) of -4.58 mT. The adduct has been isolated from concentrated solutions.

### D. Tungsten, Molybdenum, and Chromium

A number of stable  $\eta^2$ -C<sub>60</sub> complexes of tungsten and molybdenum have been prepared, and some of these are particularly stable with respect to loss of the fullerene. Photolysis of W(CO)<sub>4</sub>(Ph<sub>2</sub>PCH<sub>2</sub>CH<sub>2</sub>PPh<sub>2</sub>) and C<sub>60</sub> in 1,2-dichlorobenzene produces both green ( $\eta^2$ -C<sub>60</sub>)W(CO)<sub>3</sub>(Ph<sub>2</sub>PCH<sub>2</sub>CH<sub>2</sub>PPh<sub>2</sub>) in 80% yield and deep green (C<sub>60</sub>){W(CO)<sub>3</sub>(Ph<sub>2</sub>PCH<sub>2</sub>CH<sub>2</sub>PPh<sub>2</sub>)<sub>2</sub> in 10% yield.<sup>32</sup> The two products are separable by chromatography on activated alumina. Both complexes display exceptional stability. The half-life of ( $\eta^2$ -C<sub>60</sub>)W(CO)<sub>3</sub>(Ph<sub>2</sub>PCH<sub>2</sub>CH<sub>2</sub>PPh<sub>2</sub>) in solution at 110 °C under 60 psig of carbon monoxide is 7 h. An X-ray crystallographic study of the monoadduct confirms the  $\eta^2$ -bonding mode of the fullerene. The structure of the complex with its three meridional carbon monoxide ligands is shown in Figure 6. Electrochemical studies of ( $\eta^2$ -C<sub>60</sub>)W(CO)<sub>3</sub>(Ph<sub>2</sub>PCH<sub>2</sub>CH<sub>2</sub>PPh<sub>2</sub>) as shown in Figure 7 reveal that the complex undergoes three reversible one-electron reductions at potentials that are shifted by about 0.2 V to more negative potentials relative to C<sub>60</sub> itself. Similar shifts to negative potentials are characteristic of a range of compounds with both organic and inorganic (*vide infra*) groups added to the fullerene nucleus.<sup>33</sup>

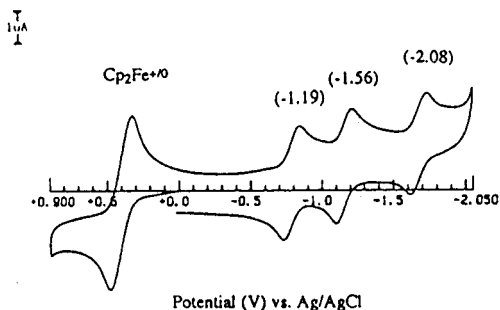


**Figure 7.** The cyclic voltammogram of *mer*-( $\eta^2$ -C<sub>60</sub>)W(CO)<sub>3</sub>(Ph<sub>2</sub>PCH<sub>2</sub>CH<sub>2</sub>PPh<sub>2</sub>) in toluene/acetonitrile, with 0.1 M[(*n*-Bu)<sub>4</sub>N]PF<sub>6</sub> as supporting electrolyte vs an Ag/AgCl reference electrode. Ferrocene has been added as a standard (Reprinted with permission from ref 32. Copyright 1994 Electrochemical Society).

Such behavior is typical of coordinated fullerenes in which the reductions are localized on the fullerene portion.

Similarly, photolysis of a 2:1 mixture of Mo(CO)<sub>4</sub>(Ph<sub>2</sub>PCH<sub>2</sub>CH<sub>2</sub>PPh<sub>2</sub>) and C<sub>60</sub> in chlorobenzene produces bright green *mer*-( $\eta^2$ -C<sub>60</sub>)Mo(CO)<sub>3</sub>(Ph<sub>2</sub>PCH<sub>2</sub>CH<sub>2</sub>PPh<sub>2</sub>) in 30% yield along with a 40% yield of a mixture of isomers of C<sub>60</sub>{Mo(CO)<sub>3</sub>(Ph<sub>2</sub>PCH<sub>2</sub>CH<sub>2</sub>PPh<sub>2</sub>)<sub>2</sub> and 5% of C<sub>60</sub>{Mo(CO)<sub>3</sub>(Ph<sub>2</sub>PCH<sub>2</sub>CH<sub>2</sub>PPh<sub>2</sub>)<sub>3</sub>.<sup>34</sup> These are also remarkably stable with respect to displacement of the coordinated fullerene. No decomposition occurred in a solution of ( $\eta^2$ -C<sub>60</sub>)Mo(CO)<sub>3</sub>(Ph<sub>2</sub>PCH<sub>2</sub>CH<sub>2</sub>PPh<sub>2</sub>) that had been heated under reflux for 6 h. Analysis of the <sup>31</sup>P NMR spectra of the double addition product, C<sub>60</sub>{Mo(CO)<sub>3</sub>(Ph<sub>2</sub>PCH<sub>2</sub>CH<sub>2</sub>PPh<sub>2</sub>)<sub>2</sub>, reveals that five isomers are formed in a 3:29:44:9:15 ratio with the equatorial isomer (see Figure 2) unambiguously found to be the one with relative abundance of 15 and the other four isomers believed to be the four *trans*-type regioisomers.

Thermolysis of *fac*-Mo(CO)<sub>3</sub>(MeCN)(Ph<sub>2</sub>PCH<sub>2</sub>CH<sub>2</sub>PPh<sub>2</sub>) in the presence of C<sub>60</sub> in chlorobenzene at 80 °C produces the *fac* isomer of ( $\eta^2$ -C<sub>60</sub>)Mo(CO)<sub>3</sub>(Ph<sub>2</sub>PCH<sub>2</sub>CH<sub>2</sub>PPh<sub>2</sub>) which has been characterized by <sup>31</sup>P (singlet, 51.5 ppm), <sup>1</sup>H, and <sup>13</sup>C NMR spectroscopy, infrared spectroscopy and mass spectrometry.<sup>35</sup> The *fac* isomer appears to be more reactive than *mer*-( $\eta^2$ -C<sub>60</sub>)Mo(CO)<sub>3</sub>(Ph<sub>2</sub>PCH<sub>2</sub>CH<sub>2</sub>PPh<sub>2</sub>); since the *fac* isomer reacts with CO at 100 °C in chlorobenzene to produce 61% of Mo(CO)<sub>4</sub>(Ph<sub>2</sub>PCH<sub>2</sub>CH<sub>2</sub>PPh<sub>2</sub>) in 4 h.

In a related reaction, C<sub>60</sub> and *fac*-W(CO)<sub>3</sub>(MeCN)-(1,2-Ph<sub>2</sub>PC<sub>6</sub>H<sub>4</sub>PPh<sub>2</sub>) react to form a mixture of *fac*- and *mer*-( $\eta^2$ -C<sub>60</sub>)W(CO)<sub>3</sub>(1,2-Ph<sub>2</sub>PC<sub>6</sub>H<sub>4</sub>PPh<sub>2</sub>).<sup>36</sup>

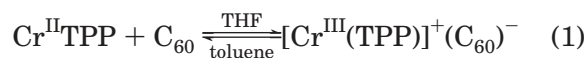
Treatment of C<sub>60</sub> with ( $\eta^5$ -RC<sub>5</sub>H<sub>4</sub>)<sub>2</sub>MoH<sub>2</sub> in toluene produces green ( $\eta^2$ -C<sub>60</sub>)Mo( $\eta^5$ -RC<sub>5</sub>H<sub>4</sub>)<sub>2</sub> (R = H, *n*-Bu) which has been characterized spectroscopically.<sup>30</sup>

The reaction between C<sub>60</sub> and Mo(CO)<sub>4</sub>(diacetyldihydrazone) or Mo(CO)<sub>2</sub>(diacetyldihydrazone)(PPh<sub>3</sub>)<sub>2</sub> yields black precipitates that are formulated as (C<sub>60</sub>)-{Mo(CO)<sub>3</sub>(diacetyldihydrazone)}<sub>2</sub> and (C<sub>60</sub>)Mo(CO)<sub>2</sub>(PPh<sub>3</sub>)<sub>2</sub>(diacetyldihydrazone) on the basis of elemental analysis, <sup>1</sup>H NMR, and infrared spectroscopy.<sup>37</sup>

Air-stable molybdenum and tungsten complexes, {( $\eta^2$ -C<sub>60</sub>)M(CO)<sub>2</sub>(1,10-phenanthroline)(dibutyl maleate)}, have been obtained from the reaction of M(CO)<sub>4</sub>(1,10-phenanthroline) and C<sub>60</sub> in the presence of dibutylmaleate.<sup>38</sup> X-ray crystallographic studies of

the Mo and W complexes reveal a six-coordinate geometry about each metal with the cis-CO groups and the 1,10-phenanthroline ligand lying in a plane and with the C<sub>60</sub> moiety bound in η<sup>2</sup>-fashion.

In contrast to the preceding reactions which all produce η<sup>2</sup>-type complexes, Cr<sup>II</sup>(tetraphenylporphyrin), Cr<sup>III</sup>TPP, reacts with C<sub>60</sub> in tetrahydrofuran solution through electron-transfer according to eq 1.<sup>39,40</sup>

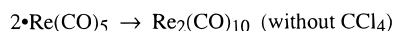
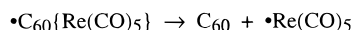
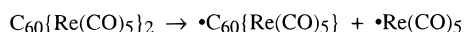


A purple-black, solid material with the composition Cr(TPP)(C<sub>60</sub>)(THF)<sub>3</sub> has been isolated. In toluene solution, this compound reverts back to Cr<sup>II</sup>TPP and free C<sub>60</sub> as shown by the shift in the intense Soret UV/vis absorption from 451 nm (for Cr<sup>III</sup>(TPP)) to 421 nm (for Cr<sup>II</sup>(TPP)). Magnetic susceptibility measurements show Curie–Weiss behavior that results in a room-temperature magnetic moment of 4.2(1) μ<sub>B</sub> which corresponds to the spin only value of 4.27 μ<sub>B</sub> for noninteracting S = 3/2 (Cr<sup>III</sup>) and S = 1/2 (C<sub>60</sub><sup>-</sup>) centers.

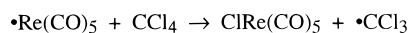
## E. Rhenium, Technetium, and Manganese

The radical Re(CO)<sub>5</sub>, as obtained from Re<sub>2</sub>(CO)<sub>10</sub> through photolysis or from (η<sup>3</sup>-Ph<sub>3</sub>C)Re(CO)<sub>4</sub> through thermolysis in the presence of CO, adds to C<sub>60</sub> to produce C<sub>60</sub>{Re(CO)<sub>5</sub>}<sub>2</sub>.<sup>41</sup> The photolytic reaction has been carefully monitored by infrared spectroscopy which shows that a new set of carbonyl absorptions appear at 2134, 2130(sh), 2036, and 1993 cm<sup>-1</sup> (vs 2070, 2011, and 1969 cm<sup>-1</sup> for Re<sub>2</sub>(CO)<sub>10</sub>). Photo-generated C<sub>60</sub>{Re(CO)<sub>5</sub>}<sub>2</sub> is unstable in solution and has not been isolated. Solutions of C<sub>60</sub>{Re(CO)<sub>5</sub>}<sub>2</sub> may be obtained in ~90% conversion from Re<sub>2</sub>(CO)<sub>10</sub> by photolysis, but these solutions decompose in a day to re-form Re<sub>2</sub>(CO)<sub>10</sub> and free C<sub>60</sub>. In the presence of carbon tetrachloride, the intermediate C<sub>60</sub>{Re(CO)<sub>5</sub>}<sub>2</sub> decomposes to form C<sub>60</sub> and ClRe(CO)<sub>5</sub>, but no Re<sub>2</sub>(CO)<sub>10</sub> is formed. Thus it has been suggested that the adduct decomposes via Scheme 2. The

### Scheme 2. Radical Dissociation from C<sub>60</sub>{Re(CO)<sub>5</sub>}<sub>2</sub>



or



structure proposed for the adduct, which is shown in Figure 8, involves σ-addition. The two Re-centered radicals bond to opposite ends of a hexagonal face of the fullerene in 1,4 positions.

The anion, C<sub>60</sub>H<sup>-</sup>, which is prepared by treatment of C<sub>60</sub> with Li[BET<sub>3</sub>H], adds to the coordinated ethylene in [(η<sup>2</sup>-C<sub>2</sub>H<sub>4</sub>)Re(CO)<sub>5</sub>]<sup>+</sup> according to the reaction in eq 2.<sup>42</sup> The product, which has been characterized spectroscopically, has the fullerene linked to the metal through a hydrocarbon bridge. In a similar

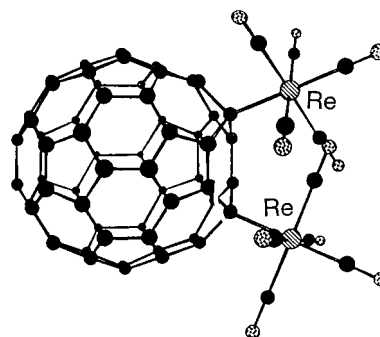
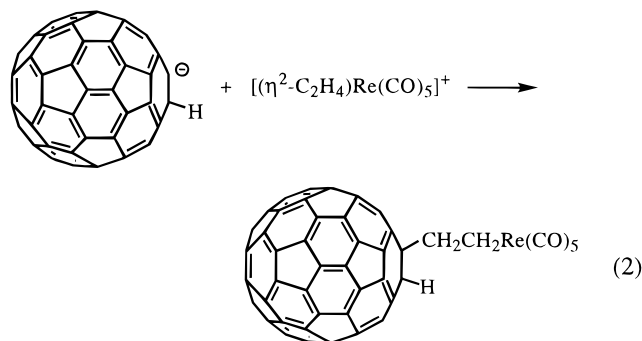


**Figure 8.** The proposed structure for C<sub>60</sub>{Re(CO)<sub>5</sub>}<sub>2</sub> (Reprinted from ref 41. Copyright 1993 American Chemical Society.)

reaction, [(η<sup>6</sup>-C<sub>6</sub>H<sub>6</sub>)Mn(CO)<sub>3</sub>](PF<sub>6</sub>) undergoes addition of C<sub>60</sub>H<sup>-</sup> to form C<sub>60</sub>H(η<sup>5</sup>-C<sub>6</sub>H<sub>6</sub>)Mn(CO)<sub>3</sub>.



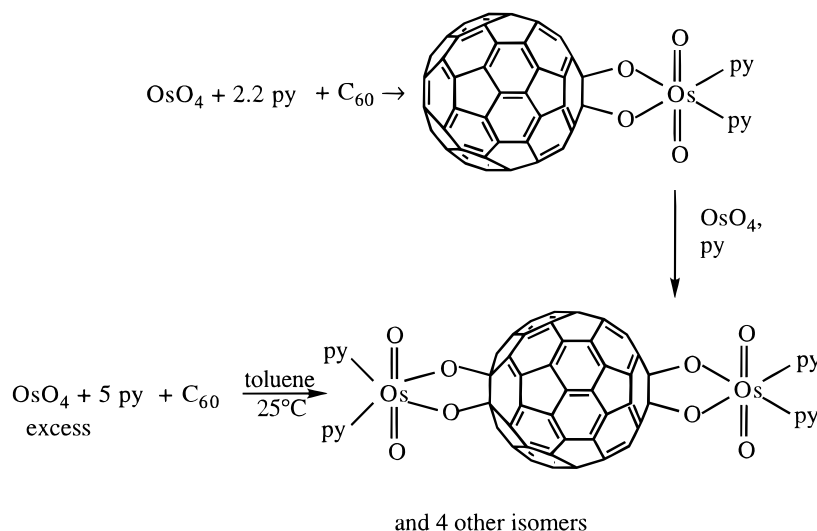
In a different vein, reactions of toluene solutions of (η<sup>5</sup>-C<sub>5</sub>Me<sub>5</sub>)<sub>2</sub>Mn with toluene solution of either C<sub>60</sub> or C<sub>70</sub> produce brown solids: [(η<sup>5</sup>-C<sub>5</sub>Me<sub>5</sub>)<sub>2</sub>Mn]·2C<sub>60</sub> and [(η<sup>5</sup>-C<sub>5</sub>Me<sub>5</sub>)<sub>2</sub>Mn]·2C<sub>70</sub>.<sup>43</sup> The effective magnetic moments of the compounds (3.13 μ<sub>B</sub> for the C<sub>60</sub> material, 3.34 μ<sub>B</sub> for the C<sub>70</sub> material) are consistent with the presence of [(η<sup>5</sup>-C<sub>5</sub>Me<sub>5</sub>)<sub>2</sub>Mn]<sup>+</sup> with S = 1 and a fullerene component with S = 1/2. The anionic component may consist of dimeric (C<sub>60</sub>)<sub>2</sub><sup>-</sup> or of C<sub>60</sub><sup>-</sup> with C<sub>60</sub> cocrystallized. The EPR spectrum shows a single line with g = 2.0023 and a peak to peak width of 1.6 G. These parameters are consistent with the presence of (C<sub>60</sub>)<sup>-</sup>.

The reaction between K[(η<sup>5</sup>-Me<sub>5</sub>C<sub>5</sub>)<sub>2</sub>Mn] and C<sub>60</sub> proceeds via electron transfer and produces deep red crystals of K<sub>3</sub>C<sub>60</sub>·7(THF) as well as (Me<sub>5</sub>C<sub>5</sub>)<sub>2</sub>Mn, which is readily removed because of its higher solubility.<sup>44</sup> K[(η<sup>5</sup>-Me<sub>5</sub>C<sub>5</sub>)<sub>2</sub>Mn] is a strong reductant (E<sub>1/2</sub> = -2.17 V vs SCE) that is readily capable of reducing C<sub>60</sub> to the trianion (E<sub>1/2</sub> for C<sub>60</sub><sup>2-</sup> to C<sub>60</sub><sup>3-</sup> = -1.3 V vs SCE). The red crystals of K<sub>3</sub>C<sub>60</sub>·7(THF) as formed in this reaction are not superconducting as are the M<sub>3</sub>C<sub>60</sub> materials that are formed by vapor transport from C<sub>60</sub> and the alkali metals.<sup>10</sup> However, removal of the THF by vacuum-drying at room temperature followed by annealing at 300 °C for 12 h did yield superconducting K<sub>3</sub>C<sub>60</sub>.

## F. Osmium, Ruthenium, and Iron

### 1. Osmylation

The powerful oxidant, osmium tetroxide, is widely used to convert olefins into diols.<sup>45</sup> Osmate esters are isolable intermediates in this process. In the

Scheme 3. Osmylation of C<sub>60</sub>

presence of pyridine, osmium tetroxide also forms stable adducts with polycyclic aromatic hydrocarbons.<sup>46</sup> Treatment of C<sub>60</sub> with osmium tetroxide in the presence of pyridine (py) yields either the single addition product, C<sub>60</sub>O<sub>2</sub>OsO<sub>2</sub>(py)<sub>2</sub>, and/or a mixture of five double addition products, C<sub>60</sub>{O<sub>2</sub>OsO<sub>2</sub>(py)<sub>2</sub>}<sub>2</sub> as shown in Scheme 3.<sup>47–51</sup> The yields of the single and double addition products can be altered by controlling the stoichiometry of the reaction. The single addition product can be separated from the double addition products, since the single addition product has a higher solubility in toluene. Exchange of 4-*tert*-butylpyridine for the pyridine ligands gives an even more soluble derivative that can be crystallized. A drawing of the structure of this adduct, C<sub>60</sub>O<sub>2</sub>OsO<sub>2</sub>(4-*tert*-butylpyridine)<sub>2</sub>·2.5 toluene, as determined from a single-crystal X-ray diffraction study, is shown in Figure 9.<sup>48</sup> Two oxygen atoms of the osmyl group have been added to the fullerene at a C–C bond of a 6:6 ring fusion. Addition of this osmyl group produces a structural perturbation of the fullerene which is restricted to the vicinity of the addition site. The unreacted atoms of the fullerene lie in a shell with a radius of 3.46–3.56 Å about the center with an average center-to-carbon distance of 3.512 Å. However, the two carbon atoms that are

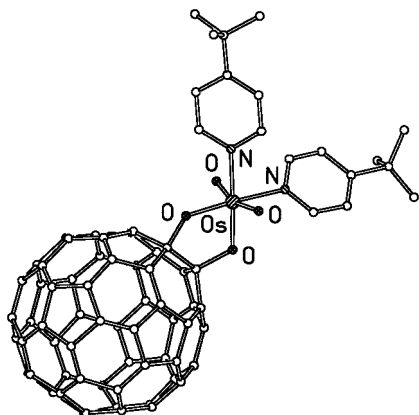


**Figure 9.** The structure of C<sub>60</sub>O<sub>2</sub>OsO<sub>2</sub>(4-*tert*-butylpyridine)<sub>2</sub> as determined by X-ray crystallography (from data in ref 48).

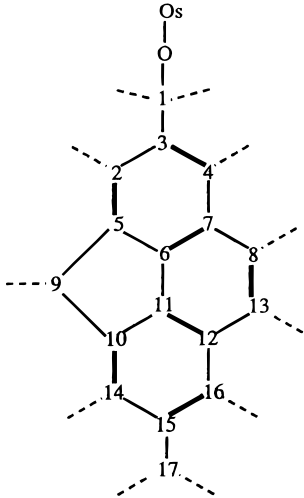
connected to the osmyl function are 3.80(2) and 3.81(2) Å away from the center. The structure shown in Figure 9 has special significance; since it was the first crystallographic demonstration that the C<sub>60</sub> moiety possessed the soccer ball structure.

The <sup>13</sup>C NMR spectrum of C<sub>60</sub>O<sub>2</sub>OsO<sub>2</sub>(*t*-Bupy)<sub>2</sub> that was enriched in <sup>13</sup>C in the fullerene portion has been thoroughly analyzed. Bond connectivities within the fullerene moiety have been determined from a 2D NMR INADEQUATE experiment.<sup>51</sup> The chemical shifts and coupling constants for the 17 different types of carbon atoms in the fullerene portion of the molecule are given in Table 1. The two tetracoordinate carbons produce a resonance that is well upfield of the resonances of the tricoordinate carbon atoms, which lie in the 137–153 ppm range. While the chemical shifts within the 137–153 ppm range do not show a well-defined pattern that correlates with structure, the C–C coupling constants do show such a correlation. The C–C coupling constants in the range 54–57 Hz correspond to C–C bonds at 5:6 ring junctions, while coupling constants in the 65–71 Hz range correspond to bonds at 6:6 ring junctions. A unique 48 Hz coupling constant is found for the C–C bond at those 6:5 ring junctions which involve the oxygenated carbon atoms.

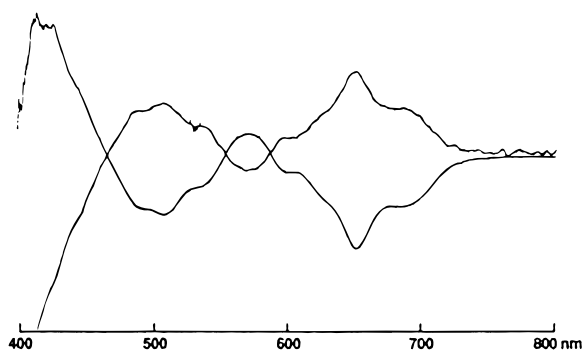
The results of a theoretical analysis of the nature of the molecular orbitals in C<sub>60</sub>O<sub>2</sub>OsO<sub>2</sub>(py)<sub>2</sub> are discussed in Section V.<sup>52</sup>

Double addition of osmium tetroxide to C<sub>60</sub> produces five of the eight expected regioisomers shown in Figure 2. These isomers of C<sub>60</sub>{O<sub>2</sub>OsO<sub>2</sub>(py)<sub>2</sub>}<sub>2</sub> have been separated by HPLC.<sup>53</sup> Four of the double addition products have been studied by <sup>13</sup>C NMR and <sup>1</sup>H NMR spectroscopy. The data indicate that two of the isolated isomers have C<sub>s</sub> symmetry and that the other two have C<sub>2</sub> symmetry. 2D NMR studies on samples that were <sup>13</sup>C-enriched in the fullerene portion led to the identification of one of the C<sub>s</sub> isomers as the equatorial isomer and one of the C<sub>2</sub> isomers as the *trans*-3 isomer (see Figure 2). With the assumption that steric effects preclude the formation of the three *cis* isomers, it was concluded that the other C<sub>2</sub> isomer was the *trans*-2 isomer and that

**Table 1.**  $^{13}\text{C}$  NMR Parameters for  $\text{C}_{60}\text{O}_2\text{OsO}_2(\text{tert-butylpyridine})_2$  (from ref 51)

|   | carbon type | chemical shift (ppm) | $^1J(\text{C,C})$ , Hz (to carbon type) |
|---|-------------|----------------------|---|
|  | 1           | 105.38               | 48(3)                                   |
|   | 2           | 145.76               | 57(3), 68(5)                            |
|   | 3           | 153.03               | 48(1), 57(2), 71(4)                     |
|   | 4           | 137.02               | 71(3), 56(7)                            |
|   | 5           | 139.42               | 68(2), 56(6), 56(9)                     |
|   | 6           | 145.77               | 56(5), 67(7), 54(11)                    |
|   | 7           | 142.75               | 56(4), 67(6), 55(8)                     |
|   | 8           | 146.10               | 55(7), 67(13)                           |
|   | 9           | 141.81               | 56(5), <sup>a</sup> (10)                |
|   | 10          | 142.32               | (9) <sup>a</sup> 56(11)                 |
|   | 11          | 144.85               | 54(6), 56(10), 68(12)                   |
|   | 12          | 146.32               | 68(11), 56(13), 56(16)                  |
|   | 13          | 142.55               | 67(8), 56(12)                           |
|   | 14          | 142.48               | 56(15)                                  |
|   | 15          | 145.99               | 56(14), 65(16), 56(17)                  |
|   | 16          | 145.04               | 56(12), 65(15)                          |
|   | 17          | 148.41               | 56(15)                                  |

<sup>a</sup> Not first order.

**Figure 10.** The CD spectra of the (+) and (-) forms of  $\text{C}_{60}\{\text{O}_2\text{OsO}_2(\text{py})_2\}_2$ . (Reprinted from ref 54. Copyright 1993 American Chemical Society.)

the remaining  $C_s$  isomer was the trans-4 isomer. The most rapidly eluting isomer was not sufficiently soluble for NMR analysis, and consequently this isomer was believed to be the nonpolar, trans-1 isomer.

The trans-2 and trans-3 double addition products,  $\text{C}_{60}\{\text{O}_2\text{OsO}_2(\text{py})_2\}_2$ , are chiral molecules with  $C_2$  symmetry, and it has been possible to resolve the two enantiomers for each.<sup>54</sup> By using the Sharpless cinchona alkaloid ligands during the addition process,<sup>55,56</sup> asymmetric bis-osmylation of  $\text{C}_{60}$  occurs. Figure 10 shows the CD spectra of the (+) and (-) forms of the trans-3 isomer of  $\text{C}_{60}\{\text{O}_2\text{OsO}_2(\text{py})_2\}_2$ . These isomers were obtained after the asymmetric bis-osmylation by replacement of the chiral Sharpless ligands with pyridine.<sup>54</sup> The array of CD features in the 500–800 nm region has been ascribed to a chiral, band-shaped  $\pi$  system. In contrast, a related chiral osmium complex prepared from a simple olefin shows only a broad tail in the corresponding region of its CD spectrum. The enantioselectivity in the bis-osmylation process has been attributed to attractive electronic interactions between the ligands coordinated to the osmium reagent and the fullerenes rather than repulsive, steric effects. There is ample crystallographic evidence for attractive interactions between aromatic groups and fullerene surfaces as

will be seen in a number of structures in later parts of this review.

Osmylation of  $\text{C}_{70}$  in pyridine produces two single addition products,  $\text{C}_{70}\{\text{O}_2\text{OsO}_2(\text{py})_2\}$ , which have been separated by chromatography.<sup>57</sup> Analysis of the  $^{13}\text{C}$  NMR spectra of the two products has shown that they have the osmyl groups added to the  $C_a-C_b$  and to the  $C_c-C_c$  bonds of the fullerene, respectively (see Figure 4). The ratio of the amount of the  $C_a-C_b$  addition product to the amount of the  $C_c-C_c$  addition product is 2.1:1. The pattern of addition seen for the osmylation is kinetically controlled and appears to be governed by two factors: the degree of local curvature within the fullerene, and the reactivity as expressed in the  $\pi$ -bond order. The  $C_a-C_b$  and  $C_c-C_c$  bonds have the highest  $\pi$ -bond order, and consequently should be the most reactive sites within the fullerene. However, on this criterion alone, the  $C_c-C_c$  bond should be the most reactive, yet the isomer formed by addition to the  $C_a-C_b$  bond is more prevalent. The greater reactivity of the  $C_a-C_b$  bond has been attributed to the greater degree of curvature at that site and the degree of pyramidalization of the carbon atoms.<sup>58</sup> A similar trend in reactivity has been observed for the reaction of Vaska-type iridium complexes with  $\text{C}_{70}$  where addition occurs preferentially at the  $C_a-C_b$  bond (vide infra).

Distinctly different mixtures of double-addition products are obtained when additional amounts of osmium tetroxide are added to the individual isomers of  $\text{C}_{70}\{\text{O}_2\text{OsO}_2(\text{py})_2\}$ . Six double-addition products have been obtained from the reaction of the  $C_a-C_b$  isomer of  $\text{C}_{70}\{\text{O}_2\text{OsO}_2(\text{py})_2\}$  with  $\text{OsO}_4$ , but with the  $C_c-C_c$  isomer of  $\text{C}_{70}\{\text{O}_2\text{OsO}_2(\text{py})_2\}$ , seven double-addition products were obtained. Four of the products in the two sets had similar chromatographic behavior and were believed to be the same set of isomeric double addition products. The formation of these distinct sets of double-addition products is further evidence that the osmylation reaction occurs under kinetic control.



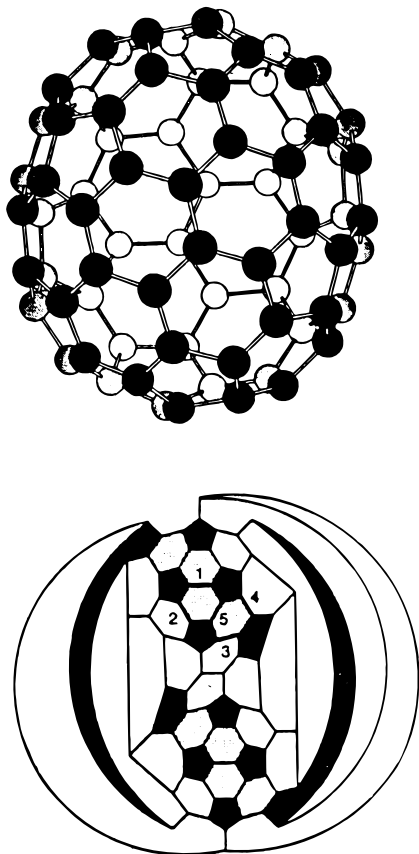


**Figure 11.** The idealized structure of  $C_{76}$  (from refs 59 and 60).

The higher fullerene,  $C_{76}$ , is a chiral molecule with  $D_2$  symmetry.<sup>17</sup> Figure 11 shows idealized drawings of  $C_{76}$  with 30 different carbon-carbon bonds with

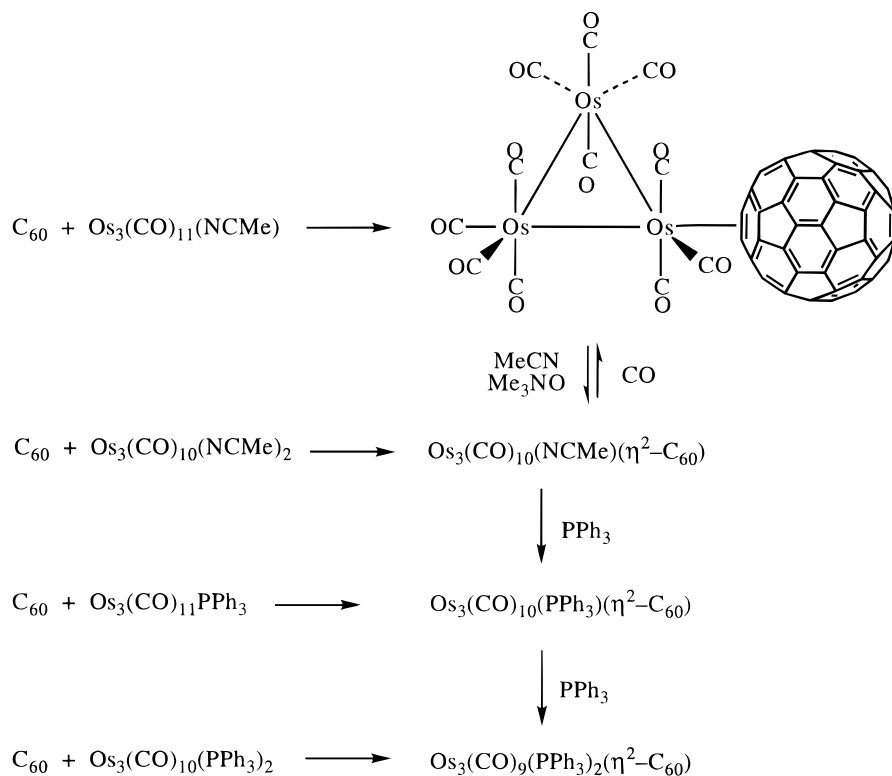
fifteen of these at 6:6 ring fusions.<sup>59,60</sup> Kinetic resolution of  $C_{76}$  has been achieved through the use of the chiral Sharpless cinchona alkaloid ligands during the osmylation process.<sup>59</sup> If osmylation occurs at the sites of highest curvature or pyramidalization (as it does in  $C_{70}$ ) then the two bonds designated 1 and 5 in Figure 11 are the likely sites for reaction. The resolution process involved addition of 1 equiv of osmium tetroxide to racemic  $C_{76}$  in the presence of an excess of the chiral ligand. Unreacted  $C_{76}$  was chromatographically separated from the complexed fullerene, and the complexed fullerene was reduced with tin(II) chloride in pyridine to liberate  $C_{76}$ . The resolved, purified enantiomers of uncomplexed  $C_{76}$  show a rich array of features in the 300–800 nm region of their CD spectra.<sup>59</sup>

This method of kinetic resolution method has also been applied to samples of  $C_{78}$  and  $C_{84}$ . Again CD spectra of the kinetically resolved samples of  $C_{78}$  and  $C_{84}$  have been obtained.<sup>61</sup> The optically active samples of  $C_{78}$  and  $C_{84}$  were found to be configurationally stable under thermolysis at 600–700 °C and photolysis at 193 nm. As a result, the barrier for the Stone–Wales rearrangement in these fullerenes is quite high.

## 2. Reactions with Zerovalent Compounds

Low-valent compounds of Os, Ru, and Fe, particularly the carbonyls, also react with  $C_{60}$ . Heating toluene solution of  $C_{60}$  and  $Os_3(CO)_{11}(NCMe)$  or related compounds results in the transformations shown in Scheme 4.<sup>62,63</sup> The products have been characterized by matching the infrared and  $^{13}C$  NMR spectroscopic features for the carbonyl groups with those of similarly substituted analogues of  $Os_3(CO)_{12}$ .

### Scheme 4. Reactions of Triangular $Os_3$ Compounds with $C_{60}$



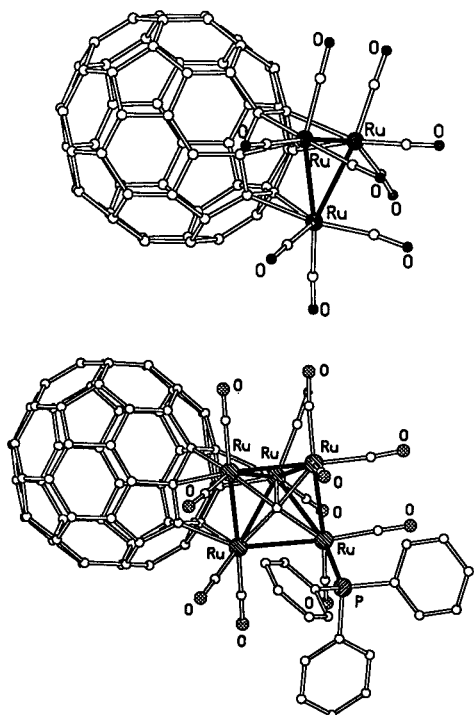


**Figure 12.** Top, the structure of  $\text{Ru}_3(\text{CO})_9(\mu_3\text{-}\eta^2, \eta^2, \eta^2\text{-C}_{60})$  as determined by X-ray crystallography (from data in ref 65 and 69). Bottom, the structure of  $\text{Ru}_5\text{C}(\text{CO})_{11}(\text{PPh}_3)(\mu_3\text{-}\eta^2, \eta^2, \eta^2\text{-C}_{60})$  as determined by X-ray crystallography (from data in ref 69).

Limited amounts of double-addition products (i.e.,  $\text{C}_{60}\{\text{Os}_3(\text{CO})_{11}\}_2$ ) are also produced in these reactions. The structure of  $(\eta^2\text{-C}_{60})\text{Os}_3(\text{CO})_{11}$  has been determined by a single-crystal X-ray diffraction study.<sup>63</sup> Electrochemical studies of  $(\eta^2\text{-C}_{60})\text{Os}_3(\text{CO})_{11}$  have been interpreted to give evidence of  $\text{C}_{60}$ -mediated electron transfer to the osmium cluster for the addition of a second electron to the complex, while the first electron is simply added to the fullerene ligand.<sup>64</sup>

In contrast,  $\text{Ru}_3(\text{CO})_{12}$  reacts with  $\text{C}_{60}$  to form two very different products: soluble,  $\text{Ru}_3(\text{CO})_9(\mu_3\text{-}\eta^2, \eta^2, \eta^2\text{-C}_{60})$ <sup>65</sup> and insoluble “ $\text{Ru}_3\text{C}_{60}$ ”.<sup>66,67</sup> Red, crystalline  $\text{Ru}_3(\text{CO})_9(\mu_3\text{-}\eta^2, \eta^2, \eta^2\text{-C}_{60})$  is formed in 4% yield by heating  $\text{C}_{60}$  and  $\text{Ru}_3(\text{CO})_{12}$  in refluxing hexane solution for 2 days followed by thin-layer chromatography on silica with carbon disulfide as eluant.<sup>65</sup> The structure of the product reveals the novel hexahapto mode of coordination of the fullerene to three ruthenium atoms as shown in Figure 12. The ruthenium atoms are positioned over 6:6 ring junctions. The pattern of coordination, with slight alteration in C–C bond distances (average short distance, 1.427(19) Å; average long distance, 1.466(15) Å) around the Ru-bound hexagon, resembles the situation observed for the benzene complex,  $\text{Ru}_3(\text{CO})_9(\mu_3\text{-}\eta^2, \eta^2, \eta^2\text{-C}_6\text{H}_6)$ .<sup>68</sup> The osmium analogue,  $\text{Os}_3(\text{CO})_9(\mu_3\text{-}\eta^2, \eta^2, \eta^2\text{-C}_{60})$ , has also been prepared.<sup>63</sup>

Insoluble black “ $\text{Ru}_3\text{C}_{60}$ ” is obtained by heating a mixture of  $\text{Ru}_3(\text{CO})_{12}$  and  $\text{C}_{60}$  in toluene for 7 days.<sup>66,67</sup> TEM images of the black residue show that it consists of an amorphous matrix in which small particles of ruthenium metal (diameter, 2–5 nm) are imbedded. Some coordinated carbon monoxide and some toluene are also found in the sample. The material has

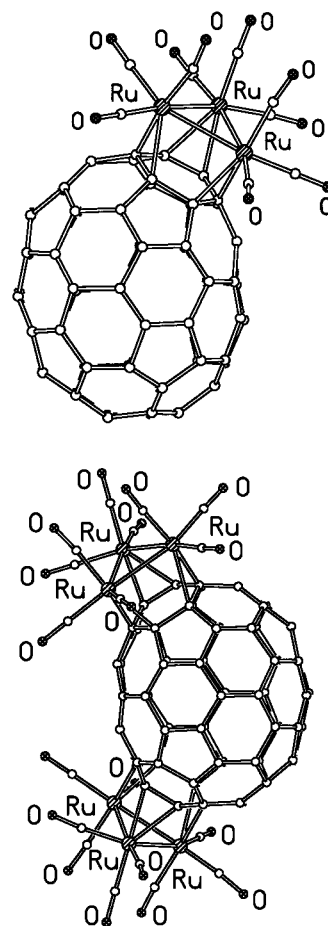


**Figure 13.** The structures of (top)  $\text{Ru}_3(\text{CO})_9(\mu_3\text{-}\eta^2, \eta^2, \eta^2\text{-C}_{70})$  and (bottom)  $\{\text{Ru}_3(\text{CO})_9\}_2\text{C}_{70}$  from X-ray crystallographic studies (from data in ref 70).

catalytic activity in the liquid-phase hydrogenation of cyclohexenes at 300 K and in the Fischer–Tropsch hydrogenation of CO at 500 K. The relationship of this polymer with that of other polymeric materials such as  $\text{C}_{60}\text{Pd}_n$  and  $\text{C}_{60}\text{Eu}_n$  ( $n = 4\text{--}6$ ) deserves examination (vide infra).

The ruthenium carbide clusters,  $\text{Ru}_5\text{C}(\text{CO})_{15}$  and  $\text{Ru}_6\text{C}(\text{CO})_{17}$ , react with  $\text{C}_{60}$  followed by treatment with a tertiary phosphine to form  $\text{Ru}_5\text{C}(\text{CO})_{11}(\text{PPh}_3)(\mu_3\text{-}\eta^2, \eta^2, \eta^2\text{-C}_{60})$  and  $\text{Ru}_6\text{C}(\text{CO})_{12}(\text{Ph}_2\text{PCH}_2\text{PPh}_2)(\mu_3\text{-}\eta^2, \eta^2, \eta^2\text{-C}_{60})$  in which a triangular face of the ruthenium cluster is capped by the fullerene.<sup>69</sup> The structure of  $\text{Ru}_5\text{C}(\text{CO})_{11}(\text{PPh}_3)(\mu_3\text{-}\eta^2, \eta^2, \eta^2\text{-C}_{60})$  is compared to that of  $\text{Ru}_3(\text{CO})_9(\mu_3\text{-}\eta^2, \eta^2, \eta^2\text{-C}_{60})$  in Figure 12.

$\text{Ru}_3(\text{CO})_{12}$  also reacts with  $\text{C}_{70}$  to form two products,  $\text{Ru}_3(\text{CO})_9(\mu_3\text{-}\eta^2, \eta^2, \eta^2\text{-C}_{70})$  and  $\{\text{Ru}_3(\text{CO})_9\}_2\text{C}_{70}$ .<sup>70</sup> The structures of these are shown in Figure 13. In both products, the triangular ruthenium complexes have added to hexagons that involve the highly pyramidalized carbon atoms at the poles of the fullerene moiety. Note that the addition of two triangular complexes occurs at opposite ends of the  $\text{C}_{70}$  moiety and positions these groups in an analogous fashion to that seen in the addition of two Ir(CO)Cl(PPh<sub>3</sub>)<sub>2</sub> groups so that the added groups are neither as close to one another nor as far apart as they could be (vide infra).

$\text{C}_{60}$  reacts with  $\text{Fe}_2(\text{CO})_9$  and  $\text{Ru}(\text{CO})_5$  to form  $(\eta^2\text{-C}_{60})\text{Fe}(\text{CO})_4$  and  $(\eta^2\text{-C}_{60})\text{Ru}(\text{CO})_4$ , respectively.<sup>31,71</sup>

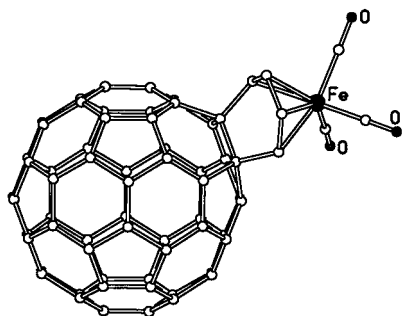


**Figure 14.** The crystallographically determined structure of the metal complex in  $(\eta^4\text{-}1,2\text{-}(3,5\text{-cyclohexadieno})\text{C}_{60})\text{-Fe}(\text{CO})_3 \cdot 2.5\text{CS}_2$  (from data in ref 74).

These  $\eta^2$  complexes have been characterized by  $^{13}\text{C}$  NMR and infrared spectroscopy. The electronic absorption spectrum of  $(\eta^2\text{-C}_{60})\text{Fe}(\text{CO})_4$  has been recorded and assigned by comparison with the results of semiempirical molecular orbital calculations.<sup>72</sup> The increased intensity in the visible range of the spectrum of the complex, when compared to that of free  $\text{C}_{60}$ , was attributed to the lowering of symmetry and relaxation of the selection rules for transitions within the fullerene upon coordination. No evidence for iron 3d to  $\text{C}_{60}$  charge transfer in the visible region was found.

### 3. Other Addition Reactions

There is a brief report that the arc vaporization of graphite in the presence of  $\text{Fe}(\text{CO})_5$  produces a soluble species,  $\text{FeC}_{60}$ , for which both endohedral and exohedral structures were discussed.<sup>73</sup>

$\text{Fe}_3(\text{CO})_{12}$  reacts with the modified fullerene, 1,2-(3,5-cyclohexadieno) $\text{C}_{60}$ , in refluxing benzene according to the reaction in eq 3 to form an air- and light-sensitive  $\text{Fe}(\text{CO})_3$  adduct in which the metal is coordinated to the exterior cyclohexadiene portion rather than to the fullerene itself.<sup>74</sup> The structure

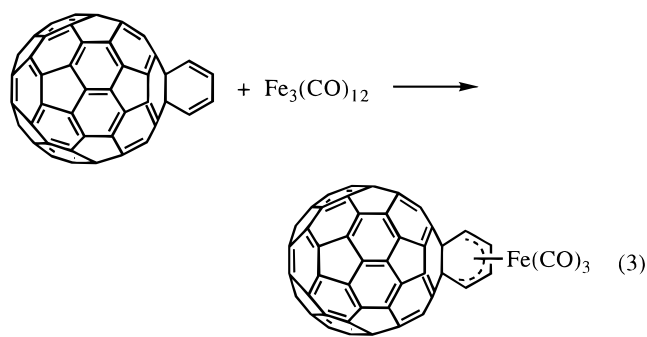


**Figure 15.** A drawing of A,  $\text{C}_{60}\text{Ru}_2(\mu\text{-Cl})(\mu\text{-H})(\eta^5\text{-C}_5\text{Me}_5)_2$ , and B,  $\text{C}_{60}\text{Ru}_2(\mu\text{-Cl})_2(\eta^5\text{-C}_5\text{Me}_5)_2$ , as determined by X-ray crystallography (from data in ref 79).

significance because planar, aromatic hydrocarbons bind strongly to the  $(\eta^5\text{-C}_5\text{Me}_5)\text{Ru}^+$  unit and displace all acetonitrile ligands, whereas electron-deficient olefins displace only one acetonitrile ligand.<sup>77</sup> Thus, the reactivity of  $[(\eta^5\text{-C}_5\text{Me}_5)\text{Ru}(\text{CH}_3\text{CN})_3]^+$  toward  $\text{C}_{60}$  gave one of the first indications that  $\text{C}_{60}$  would not bind metal centers in the way that planar, aromatic hydrocarbons would and that electron-deficient olefins were better models for the reactivity of  $\text{C}_{60}$ . Moreover, the  $\pi$ -orbitals on the faces of  $\text{C}_{60}$  are directed away from the position where  $\eta^6$ -coordination to a six-membered ring would occur and qualitatively the degree of metal–ligand orbital overlap would be diminished relative to a corresponding flat aromatic molecule like benzene. Theoretical calculations (vide infra) have borne out this qualitative argument.<sup>78</sup>

The reaction of  $\text{C}_{60}$  with an equimolar mixture of  $\{(\eta^5\text{-C}_5\text{Me}_5)\text{Ru}(\mu\text{-H})\}_2$  and  $\{(\eta^5\text{-C}_5\text{Me}_5)\text{Ru}(\mu\text{-Cl})\}_2$  in toluene at  $90^\circ\text{C}$  produces green crystals of  $\text{C}_{60}\text{Ru}_2(\mu\text{-Cl})(\mu\text{-H})(\eta^5\text{-C}_5\text{Me}_5)_2$  in 18% yield.<sup>79</sup> The product, whose structure is shown in Figure 15A, has two ruthenium atoms that are coordinated to two adjacent C–C bonds at 6:6 ring junctions of the fullerene and are bridged by both a chloride and a hydride. The Ru–Ru distance of 2.9554(9) Å is indicative of the presence of a bond between the two metal centers. A related complex  $\text{C}_{60}\text{Ru}_2(\mu\text{-Cl})_2(\eta^5\text{-C}_5\text{Me}_5)_2$  was obtained from an analogous reaction of  $\text{C}_{60}$  with a 1:2 molar mixture of  $\{(\eta^5\text{-C}_5\text{Me}_5)\text{Ru}(\mu\text{-H})\}_2$  and  $\{(\eta^5\text{-C}_5\text{Me}_5)\text{Ru}(\mu\text{-Cl})\}_2$ . The structure of the dichloro-bridged complex is also shown in Figure 15B. Again, two ruthenium atoms are bonded to two adjacent C–C bonds at 6:6 ring junctions on a common hexagonal face of the fullerene. The principal difference between the dichloro-bridged complex and the hydrido-chloro-bridged complex involves the Ru–Ru distance. In  $\text{C}_{60}\text{Ru}_2(\mu\text{-Cl})_2(\eta^5\text{-C}_5\text{Me}_5)_2$ , that distance is much

of the product, which is shown in Figure 14, has been determined by X-ray crystallography. The structural parameters reveal that there is a strong steric repulsion between the  $\text{Fe}(\text{CO})_3$  unit and the fullerene that results from the proximity of one of the carbon monoxide ligands to the fullerene surface.

Reaction of excess  $[(\eta^5\text{-C}_5\text{Me}_5)\text{Ru}(\text{CH}_3\text{CN})_3]^+(\text{O}_3\text{SCF}_3^-)$  with  $\text{C}_{60}$  is reported to yield brown  $[(\text{C}_{60})\text{-}\{\text{Ru}(\text{CH}_3\text{CN})_2(\eta^5\text{-C}_5\text{Me}_5)\}_3]^{3+}(\text{O}_3\text{SCF}_3^-)_3$ .<sup>75,76</sup> Unfortunately, this complex has not been obtained in a crystalline form suitable for X-ray diffraction, possibly because of the existence of several different regioisomers. However, this result is of particular

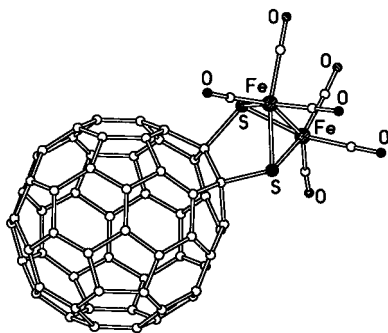
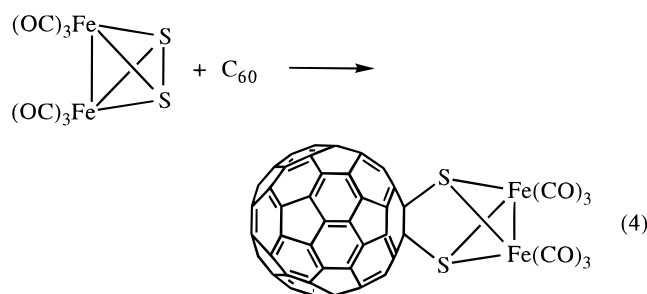


**Figure 16.** A view of  $C_{60}S_2Fe_2(CO)_6$  as determined by X-ray crystallography (from data in ref 80).

longer, 3.461(2) Å, and indicative of the lack of any Ru–Ru bonding. The positive ion FAB mass spectrum of  $C_{60}Ru_2(\mu-H)(\mu-Cl)(\eta^5-C_5Me_5)_2$  shows a peak at  $m/z$  957 which corresponds to  $[(\eta^6-C_{60})Ru(\eta^5-C_5Me_5)]^+$ , and the authors propose that this species utilizes an  $\eta^6$ -mode of coordination of the fullerene to ruthenium, a situation that would be analogous to the bonding in the stable  $[(\eta^6-C_6H_6)Ru(\eta^5-C_5Me_5)]^+$  species. Note that  $[(\eta^6-C_{60})Ru(\eta^5-C_5Me_5)]^+$  could not be prepared via straightforward chemical routes in solution.<sup>75,76</sup>

UV irradiation of toluene solutions of  $C_{60}$  and  $Fe_2S_2(CO)_6$  results in the formation of  $C_{60}S_2Fe_2(CO)_6$ , as well as multiple addition products, according to the reaction in eq 4.<sup>80,81</sup> The mono-addition product



has been characterized by X-ray crystallography. The structure of the product, which is shown in Figure 16, reveals that the S–S bond in the original iron complex has been cleaved and that the two sulfur atoms have added to a 6:6 ring junction of the fullerene. Similar additions of  $S_2Fe_2(CO)_6$  to simple olefins have been known for some time.  $C_{60}S_2Fe_2(CO)_6$  undergoes four reversible, one-electron reductions which are shifted cathodically by 25 mV as is typical for many organometallic  $C_{60}$  adducts.  $C_{70}$  also reacts with  $S_2Fe_2(CO)_6$  to give the series of adducts  $C_{70}\{S_2Fe_2(CO)_6\}_n$  ( $n = 1-4$ ). These addition reactions are particularly interesting for their comparison to the reactivity of sulfur (as  $S_8$ ) with  $C_{60}$  and  $C_{70}$ . Solutions of  $S_8$  and  $C_{60}$  or  $C_{70}$  produce the crystalline solids  $C_{60}\cdot(S_8)\cdot(CS_2)$  or  $C_{70}(S_8)_6$  which are composed of isolated molecules of the fullerene and cyclooctasulfur.<sup>82</sup> Additionally,  $C_{60}$  and  $C_{70}$  can be recrystallized from liquid sulfur without chemical attack on the fullerene.<sup>83</sup>

$[(\eta^5\text{-Cyclohexadienyl})Fe(CO)_3](BF_4)$ ,  $[(\eta^5\text{-cycloheptadienyl})Fe(CO)_3](BF_4)$ ,  $[(\eta^6\text{-}C_5H_4CH_2)Fe(\eta^5\text{-}C_5H_5)](BF_4)$ , and  $[(\eta^5\text{-cyclohexadienyl})Ru(CO)_3](BF_4)$  react with

$C_{60}H^-$  to form adducts  $(\eta^4\text{-}C_6H_7C_{60}H)Fe(CO)_3$ ,  $(\eta^4\text{-}C_7H_9C_{60}H)Fe(CO)_3$ ,  $(\eta^5\text{-}C_5H_4CH_2C_{60}H)Fe(\eta^5\text{-}C_5H_5)$ , and  $(\eta^4\text{-}C_6H_7C_{60}H)Ru(CO)_3$ , respectively (see reaction 2 for a prototypical example).<sup>42</sup>

#### 4. Redox Reactions

The electron-reservoir complex,  $\{(\eta^5\text{-}C_5H_5)Fe^I(\eta^6\text{-}C_6Me_6)\}$ , is a strong reductant ( $E_{1/2} = -1.55$  V vs SCE in dimethylformamide)<sup>84</sup> and is able to reduce  $C_{60}$  to the trianion level. Titration of  $C_{60}$  with  $\{(\eta^5\text{-}C_5H_5)Fe^I(\eta^6\text{-}C_6Me_6)\}$  produces three dark-brown, air-sensitive, paramagnetic salts:  $[(\eta^5\text{-}C_5H_5)Fe^{II}(\eta^6\text{-}C_6Me_6)^+](C_{60}^-)$ ,  $[(\eta^5\text{-}C_5H_5)Fe^{II}(\eta^6\text{-}C_6Me_6)^+]_2(C_{60}^{2-})$ , and  $[(\eta^5\text{-}C_5H_5)Fe^{II}(\eta^6\text{-}C_6Me_6)^+]_3(C_{60}^{3-})$ .<sup>81</sup> The EPR spectrum of  $[(\eta^5\text{-}C_5H_5)Fe^{II}(\eta^6\text{-}C_6Me_6)^+](C_{60}^-)$  consists of a sharp, symmetrical line at  $g = 2.0020$  (line width 2.6 G) at 300 K. For the EPR spectrum of  $[(\eta^5\text{-}C_5H_5)Fe^{II}(\eta^6\text{-}C_6Me_6)^+]_2(C_{60}^{2-})$  a similar line also at  $g = 2.0020$  (line width 4.0 G) is observed at 300 K. However, for  $[(\eta^5\text{-}C_5H_5)Fe^{II}(\eta^6\text{-}C_6Me_6)^+]_3(C_{60}^{3-})$ , the resonance is observed at  $g = 2.0040$  and exhibits a line width that drops markedly with decreasing temperature from 46 G at 300 K to 6 G at 4 K.

Black needles of the salt  $[Ru^{II}(\text{bipyridine})_3](C_{60})_2$  have been obtained through electrocrystallization.<sup>85</sup> The reaction is conducted by reducing  $C_{60}$  in a solution that is saturated with  $[Ru^{II}(\text{bipyridine})_3](PF_6)_2$ . This reaction is possible because reduction of the ruthenium complex has a half-wave potential that is  $\sim 700$  mV more negative than the potential needed for the  $C_{60}$  to  $C_{60}^-$  conversion and 300 mV more negative than that needed for the  $C_{60}^-$  to  $C_{60}^{2-}$  conversion. Two point conductivity measurements on a pressed power sample indicate that  $[Ru^{II}(\text{bipyridine})_3](C_{60})_2$  is a semiconductor with a specific conductivity of  $0.01 \Omega^{-1} \text{ cm}^{-1}$  at 25 °C.

#### 5. Cocrystallizations

The oxidation potential for ferrocene is such that it is not capable of reducing  $C_{60}$  or  $C_{70}$  to their respective anions. However, mixing solutions of  $C_{60}$  or  $C_{70}$  and ferrocene results in crystallization of the solid adducts with similar compositions:  $C_{60}\cdot 2\{(\eta^5\text{-}C_5H_5)_2Fe\}$ <sup>86</sup> and  $C_{70}\cdot 2\{(\eta^5\text{-}C_5H_5)_2Fe\}$ .<sup>87</sup> The structures of both solids consist of isolated molecules which make only van der Waals contact with one another. A view of the packing within the solids are shown in Figures 17 and 18. One of the cyclopentadienyl rings of the ferrocene molecule is involved in  $\pi$ -stacking with  $C_{60}$  or with  $C_{70}$ .

Additionally, a benzene solution of  $C_{60}$  and  $Fe_4(CO)_4(\eta^5\text{-}C_5H_5)_4$  produces crystals of the ternary material,  $C_{60}\cdot\{Fe_4(CO)_4(\eta^5\text{-}C_5H_5)_4\}\cdot 3C_6H_6$ .<sup>88</sup> Figure 19 presents views of the arrangement of components within the solid and gives some dimensions that relate to the structure. The geometrical features of the individual molecules do not show any significant variation from their normal structures, but the fullerene is ordered in this solid. Of the four cyclopentadienyl rings of the organometallic complex, three are involved in face-to-face,  $\pi$ - $\pi$  interactions with neighboring  $C_{60}$  molecules. The infrared spectrum of the solid shows a slight shift in  $\nu(CO)$  for the iron cluster (from  $1626 \text{ cm}^{-1}$  for  $\{Fe_4(CO)_4(\eta^5\text{-}C_5H_5)_4\}$

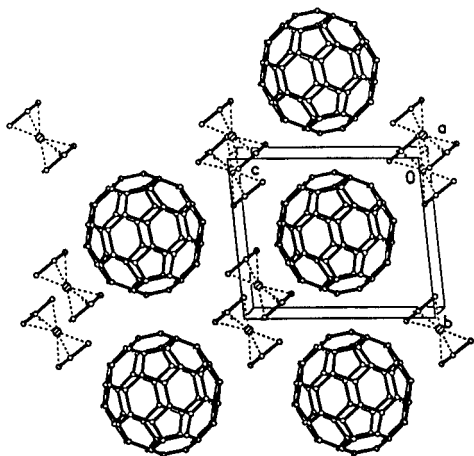


**Figure 17.** A diagram that shows the packing of individual molecules in  $C_{60} \cdot 2\{(\eta^5-C_5H_5)_2Fe\}$  (from data in ref 86).

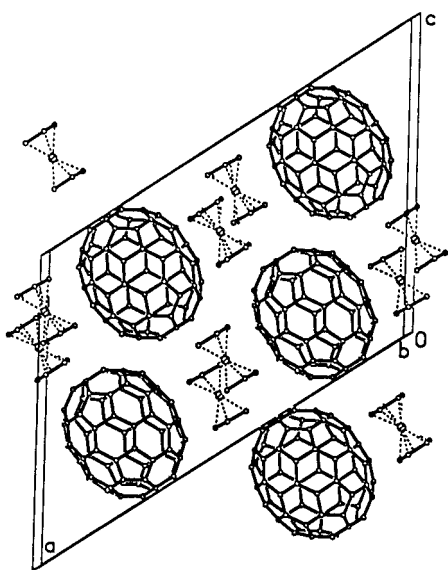


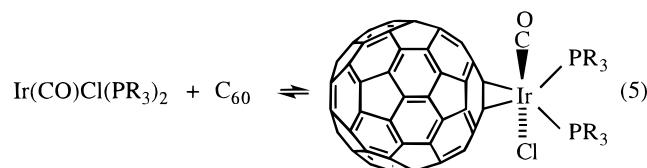
**Figure 18.** A diagram that shows the orientation of individual molecules in  $C_{70} \cdot 2\{(\eta^5-C_5H_5)_2Fe\}$  (from data in ref 87). Note the similarity of the organization to that shown in the related  $C_{60}$  material in Figure 17.

to  $1640\text{ cm}^{-1}$  in the ternary cocrystals). This shift is consistent with the organometallic component functioning as a weak donor.

### G. Iridium, Rhodium, and Cobalt

#### 1. Adduct Formation with Vaska-Type Complexes, $Ir(CO)Cl(PR_3)_2$

$Ir(CO)Cl(PPh_3)_2$  and related complexes with different phosphine ligands react with  $C_{60}$  in benzene as shown in eq 5.<sup>89</sup> Analogous reactions of electron-



deficient olefins with Vaska's complex have been described previously.<sup>90</sup> The reaction shown in eq 5

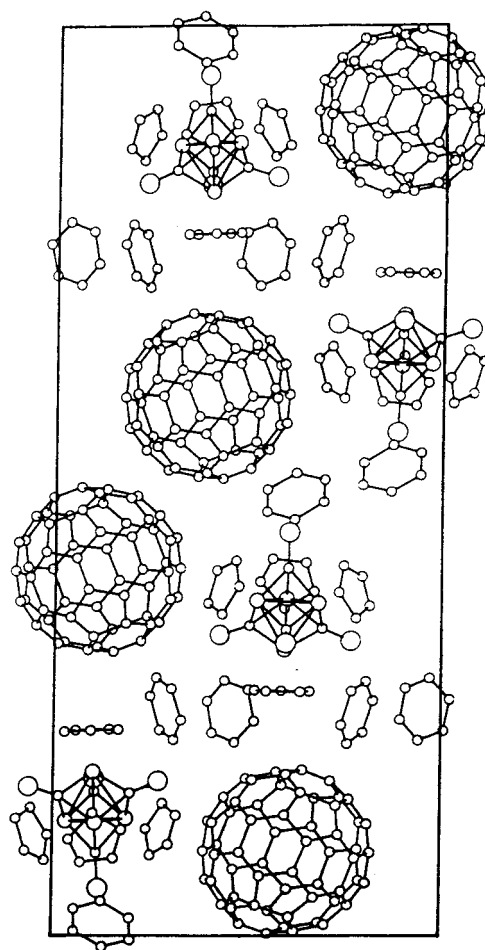


**Figure 19.** Two views of the packing of individual molecular components in  $C_{60} \cdot \{Fe_4(CO)_4(\eta^5-C_5H_5)_4\} \cdot 3C_6H_6$ . (Reprinted with permission from ref 88. Copyright 1993 Royal Society of Chemistry.)

is a case of straightforward adduct formation both from the view of the fullerene and that of the metal complex (i.e., no ligands are displaced from the iridium in the process). Moreover, this is generally a reversible process. However, this ease of dissociation

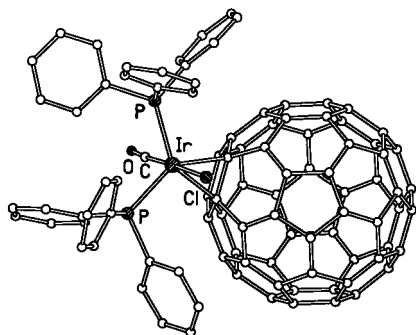


**Figure 20.** The structure of  $(\eta^2\text{-C}_{60})\text{Ir}(\text{CO})\text{Cl}(\text{PPh}_3)_2$  as determined by an X-ray crystallography (from data in ref 89).

tion and reassociation has a great advantage in that it facilitates the preparation of crystalline adducts that are suitable for single-crystal X-ray diffraction. The facile dissociation and reassociation of these adducts allows the selection of a single molecular species from a mixture during the dynamic process of crystal growth. Thus, as seen later in this section, adduct formation with complexes of the type  $\text{Ir}(\text{CO})\text{Cl}(\text{ER}_3)_2$  ( $\text{E} = \text{P}$  or  $\text{As}$ ,  $\text{R} =$  alkyl or various aryl groups) has become a valuable tool to gain useful information about the structure and sites of chemical reactivity in higher fullerenes and in chemically modified fullerenes.

Slow diffusion of a concentrated benzene solution of  $\text{C}_{60}$  into a benzene solution of  $\text{Ir}(\text{CO})\text{Cl}(\text{PPh}_3)_2$  produces dark, nearly black crystals of the adduct,  $(\eta^2\text{-C}_{60})\text{Ir}(\text{CO})\text{Cl}(\text{PPh}_3)_2 \cdot 5\text{C}_6\text{H}_6$ .<sup>89</sup> The structure of the complex is shown in Figure 20. The iridium atom is bound to the fullerene through coordination to a C–C bond at a 6:6 ring junction. The fullerene geometry is perturbed in the vicinity of the addition; since the carbon atoms that are coordinated to the iridium atom are displaced from their normal position in the fullerene core by about 0.3 Å.

Infrared and Mössbauer spectroscopy have been utilized to examine the electronic structure of  $(\eta^2\text{-C}_{60})\text{Ir}(\text{CO})\text{Cl}(\text{PPh}_3)_2$  and related complexes.<sup>89,91</sup> The infrared spectra of the products of oxidative additions to  $\text{Ir}(\text{CO})\text{Cl}(\text{PPh}_3)_2$  show an increase in the CO stretching frequency as compared to the parent. The magnitude of this increase is directly proportional to the reversibility of the addition and to the degree of electron withdrawal from the iridium center.<sup>92</sup> For  $(\eta^2\text{-C}_{60})\text{Ir}(\text{CO})\text{Cl}(\text{PPh}_3)_2$ , the increase in  $\nu(\text{CO})$  (from  $1953\text{ cm}^{-1}$  in the parent to  $2014\text{ cm}^{-1}$  in the fullerene adduct) corresponds to cases of easily reversible additions. Such a change is consistent with the solution behavior of the adduct which is largely dissociated into its components through the reverse of eq 5. The tetracyanoethylene (TCNE) adduct,  $(\eta^2\text{-TCNE})\text{Ir}(\text{CO})\text{Cl}(\text{PPh}_3)_2$ , and the tetrafluoroethylene adduct,  $(\eta^2\text{-C}_2\text{F}_4)\text{Ir}(\text{CO})\text{Cl}(\text{PPh}_3)_2$ , exhibit larger increases in the CO stretching frequencies (to  $2052$  and  $2057\text{ cm}^{-1}$ , respectively).<sup>92</sup> Thus, these highly electron-deficient olefins are more effective than  $\text{C}_{60}$  in their ability to remove electron density from iridium through d-to- $\pi$  back-bonding. The Mössbauer spectra of these compounds have also been reported.<sup>91</sup> The decrease in the quadrupolar splitting on adduct

formation (from  $6.52(3)\text{ mm/s}$  for  $\text{Ir}(\text{CO})\text{Cl}(\text{PPh}_3)_2$  to  $2.714(15)\text{ mm/s}$  for  $(\eta^2\text{-C}_{60})\text{Ir}(\text{CO})\text{Cl}(\text{PPh}_3)_2$  and to  $1.837(15)\text{ mm/s}$  for  $(\eta^2\text{-TCNE})\text{Ir}(\text{CO})\text{Cl}(\text{PPh}_3)_2$ ) has been attributed to an unconventional redistribution of d electrons. In comparison to  $\text{C}_{60}$ , tetracyanoethylene is again found to be a more electron-withdrawing substituent. The alterations of the isomer shifts within the series of compounds— $\text{Ir}(\text{CO})\text{Cl}(\text{PPh}_3)_2$ ,  $+0.022\text{ mm/s}$ ;  $(\eta^2\text{-C}_{60})\text{Ir}(\text{CO})\text{Cl}(\text{PPh}_3)_2$ ,  $-0.259\text{ mm/s}$ ;  $(\eta^2\text{-TCNE})\text{Ir}(\text{CO})\text{Cl}(\text{PPh}_3)_2$ ,  $-0.194\text{ mm/s}$ —were analyzed in terms of a decrease in s electron density in the adducts.

The reactivity of Vaska's complex can be altered by modifying the ligands that are present. For example, alkylphosphines produce Vaska-type complexes that are more prone to oxidative-addition than complexes with aryl phosphine ligands. Thus, the binding constant for oxidative addition to  $\text{Ir}(\text{CO})\text{Cl}(\text{PMe}_2\text{Ph})_2$  is about 200 times larger than it is for  $\text{Ir}(\text{CO})\text{Cl}(\text{PPh}_3)_2$ .<sup>93</sup> Consequently ligand modification has been utilized as a means toward obtaining multiple addition products of  $\text{C}_{60}$ . Reactions of  $\text{C}_{60}$  with excess (2- to 12-fold) of  $\text{Ir}(\text{CO})\text{Cl}(\text{PMe}_2\text{Ph})_2$ ,<sup>94</sup>  $\text{Ir}(\text{CO})\text{Cl}(\text{PEt}_3)_2$ ,<sup>95</sup> or  $\text{Ir}(\text{CO})\text{Cl}(\text{PMe}_3)_2$ <sup>95</sup> has led to the generally selective crystallization of double addition products. In each case the pattern of addition in the isolated, crystalline material is the same; the double-addition product crystallizes as the trans-1 or para isomer shown in Figure 2. Statistically, this is the isomer with the lowest probability of formation, but it is also the isomer with the highest possible symmetry. Thus, it is also likely to have the most compact structure.

The reaction of  $\text{C}_{60}$  with one modified version of Vaska's complex,  $\text{Ir}(\text{CO})\text{Cl}(\text{PMe}_2\text{Ph})_2$ , is complicated by the formation of four different types of solids.<sup>94</sup> These have been identified as the single addition product, two crystalline forms of the double addition product, and an unidentified, apparently amorphous material. The two different forms of the double addition products have been examined by X-ray diffraction, and the structures are compared in Figure 21. The adducts vary in the orientation of the substituents on their phosphine ligands and in the solvate composition, but both have the trans-1 orientation of the two iridium complexes. In the form which crystallizes as obelisks, the four phenyl rings of the phosphine ligands are oriented so that they make face-to-face contact with the fullerene. On the other hand in the plate-forming modification, the phenyl substituents are all positioned away from the fullerene core so that they interact more directly with one another than they do with the  $\text{C}_{60}$  portion. However, this solid has another interesting arene–fullerene contact that is not shown in Figure 21. Two benzene molecules cocrystallize with the adduct molecule. These benzene rings are oriented nearly perpendicular to the fullerene surface so that one hydrogen atom lies only  $3.09\text{ Å}$  away from an electron-rich 6:6 ring junction. Such edge-to-surface interactions are recognized as attractive contributions to the stability of crystalline arenes.<sup>96–99</sup>

Figure 22 shows the structures of two other such adducts with trans-1 geometry,  $\text{C}_{60}\{\text{Ir}(\text{CO})\text{Cl}(\text{PMe}_3)_2\}_2$

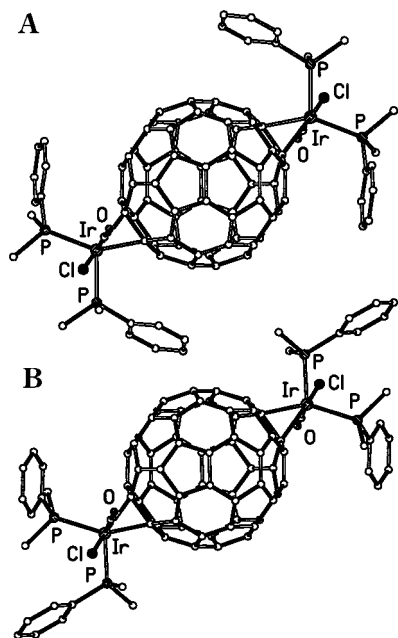


**Figure 21.** The structures of two different conformations of  $C_{60}\{Ir(CO)Cl(PPhMe_2)_2\}_2$  in A,  $C_{60}\{Ir(CO)Cl(PPhMe_2)_2\}_2 \cdot C_6H_6$  and B,  $C_{60}\{Ir(CO)Cl(PPhMe_2)_2\}_2 \cdot 2C_6H_6$  (from data in ref 94). There is a close benzene/ $C_{60}$  contact in the structure of  $C_{60}\{Ir(CO)Cl(PPhMe_2)_2\}_2 \cdot C_6H_6$  that is not shown.

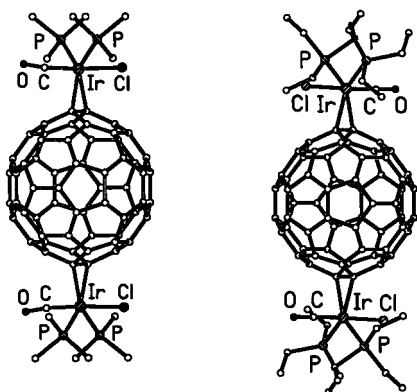


**Figure 22.** The structures of  $C_{60}\{Ir(CO)Cl(PMe_3)_2\}_2$  and  $C_{60}\{Ir(CO)Cl(PEt_3)_2\}_2$  (from data in ref 95).

and  $C_{60}\{Ir(CO)Cl(PEt_3)_2\}_2$ .<sup>95</sup> The frequent occurrence of the trans-1 geometry, in these adducts has been attributed to the low solubility and efficient crystal packing of this type of symmetrical structure.

While many of the adducts of fullerenes with Vaska-type complexes have poor solubility,  $C_{60}\{Ir(CO)Cl(PEt_3)_2\}_2 \cdot C_6H_6$  does dissolve to a significant extent in a 6:4 *o*-dichlorobenzene/toluene mixture to allow examination by  $^{31}P$  NMR spectroscopy.<sup>95</sup> This solvent mixture has a sufficiently large liquid range so that variable temperature studies down to  $-80^\circ C$  are feasible. Relevant  $^{31}P\{^1H\}$  NMR spectra for solutions of  $C_{60}\{Ir(CO)Cl(PEt_3)_2\}_2 \cdot C_6H_6$  are shown in Figure 23. In this solvent mixture, the  $^{31}P\{^1H\}$  NMR spectrum of  $Ir(CO)Cl(PEt_3)_2$  consists of a narrow singlet at 20.2 ppm at  $20^\circ C$ . Trace A shows the spectrum of  $C_{60}\{Ir(CO)Cl(PEt_3)_2\}_2$  at  $20^\circ C$  where two very broad resonances are present with a relative intensity ratio of 1.9. Trace B shows the spectrum of the sample after cooling to  $-30^\circ C$ . The two lines have sharpened considerably, the upfield line shows

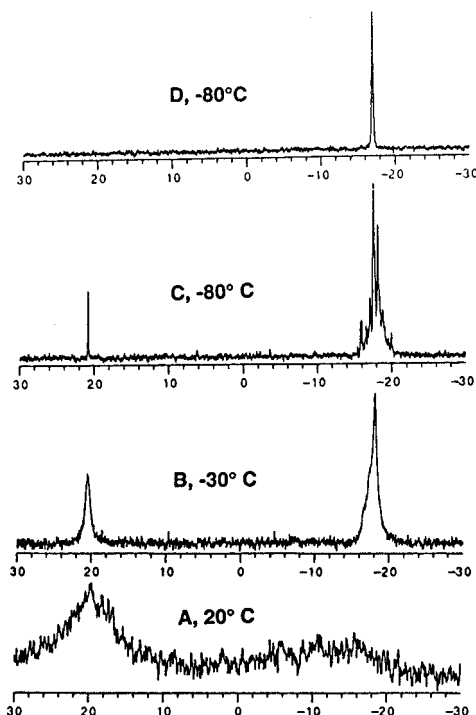
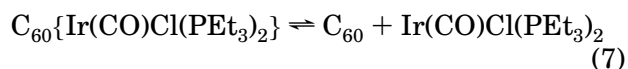
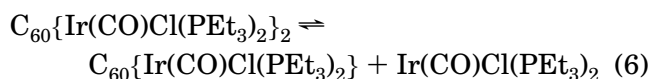


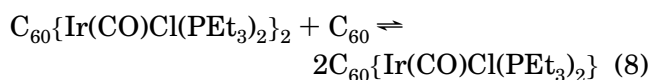
**Figure 23.** The 121-MHz  $^{31}P\{^1H\}$  NMR spectra of  $C_{60}\{Ir(CO)Cl(PEt_3)_2\}_2 \cdot C_6H_6$  dissolved in 6:4 v/v mixture of *o*-dichlorobenzene and toluene at A,  $20^\circ C$ ; B,  $-30^\circ C$ ; C,  $-80^\circ C$ ; D,  $-80^\circ C$  after the addition of excess  $C_{60}$  (Reprinted from ref 95. Copyright 1994 American Chemical Society).

asymmetry, and the ratio of relative intensities between the low-field and the high-field resonances has changed to 0.4. Trace C shows the spectrum that was obtained after cooling the sample to  $-80^\circ C$ . Further narrowing of all resonances has occurred, and the upfield region is now comprised of at least 16 individual components. At this temperature, the ratio of intensities between the resonance at 20.8 ppm and the group of resonances at  $\sim -18$  ppm is 0.15. Addition of an excess of  $C_{60}$  to this sample gives the  $^{31}P\{^1H\}$  NMR spectrum shown in trace D. Only a single resonance is observed.

These data are consistent with extensive dissociation of the adduct in solution as shown in the reactions in eqs 6 and 7.<sup>95</sup>



The resonance at  $\sim 20.8$  ppm is readily assigned to free  $Ir(CO)Cl(PEt_3)_2$ . The broadening seen at  $20^\circ C$  in trace A is readily explained by rapid exchange of the free and fullerene-bound iridium complexes. The single line seen in trace D can be assigned to the single addition product,  $C_{60}\{Ir(CO)Cl(PEt_3)_2\}$ , which forms in the presence of excess  $C_{60}$  through the reverse of eq 7 and also by the reaction in eq 8. The



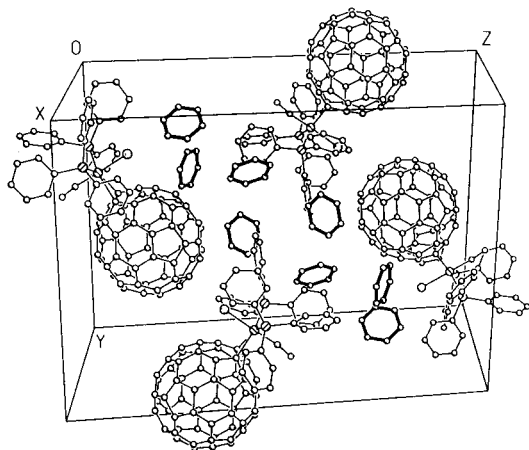


**Figure 24.** A view of the molecular packing in  $(\eta^2\text{-C}_{60})\text{-Ir}(\text{CO})\text{Cl}(\text{PPh}_3)_2 \cdot 5\text{C}_6\text{H}_6$  which emphasizes the location of the benzene rings (from data in ref 89).

multiplicity of lines in the  $-16$  to  $-20$  ppm region have been assigned to the presence of isomeric forms of the double-addition product and possibly some higher addition products. Because of their lower symmetry and the presence of inequivalent phosphorus atoms, each of the seven possible regioisomers for the double-addition products could produce at least two  $^{31}\text{P}$  NMR resonances, and hence the high-field region of the spectrum is expectedly complex.

Cooling the sample results in alteration of the ratio of the amounts of free and fullerene-coordinated  $\text{Ir}(\text{CO})\text{Cl}(\text{PEt}_3)_2$  that are present. At room temperature, free  $\text{Ir}(\text{CO})\text{Cl}(\text{PEt}_3)_2$  is prevalent while at  $-80^\circ\text{C}$ , the fullerene-coordinated form is dominant. This behavior is consistent with thermodynamic considerations in which the entropically driven dissociation reactions shown in eqs 6 and 7 are more significant at higher temperatures.

The structure of  $(\eta^2\text{-C}_{60})\text{Ir}(\text{CO})\text{Cl}(\text{PPh}_3)_2 \cdot 5(\text{C}_6\text{H}_6)$  (Figure 20) shows that two of the phenyl rings of the triphenylphosphine ligands are positioned near the fullerene surface where they can make face-to-face,  $\pi\text{-}\pi$  contact.<sup>89</sup> Additionally, there are five benzene molecules in crystals of this complex as shown in the view of the unit cell in Figure 24. These solvate molecules fill what would otherwise be voids in the structure and make  $\pi\text{-}\pi$  contacts as well as edge-to-face contacts with the fullerene portion and with one another. The presence of such solvate molecules within crystalline metallofullerenes and of fullerenes themselves is extraordinarily common, as has been observed especially well in  $\text{C}_{60} \cdot 4\text{C}_6\text{H}_6$ .<sup>100,101</sup>

The presence of such face-to-face arene/fullerene contacts in many fullerene containing solids suggested that it should be possible to design new phosphine ligands which would enhance such  $\pi\text{-}\pi$  contacts. To accomplish this, it was necessary to design a ligand that would allow flat aromatic portions to be connected in such a flexible manner that they could easily surround the curved exterior of a fullerene. Toward this end, the new ligand  $\text{Ph}_2\text{PCH}_2\text{C}_6\text{H}_4\text{OCH}_2\text{C}_6\text{H}_5$  ( $\text{Ph}_2\text{Pbob}$ ) was synthesized and converted into  $\text{Ir}(\text{CO})\text{Cl}(\text{Ph}_2\text{Pbob})_2$ .<sup>102</sup> This Vaska-type complex reacts with  $\text{C}_{60}$  to form  $(\eta^2\text{-C}_{60})\text{Ir}(\text{CO})\text{Cl}(\text{Ph}_2\text{Pbob})_2$  which precipitates from benzene solu-

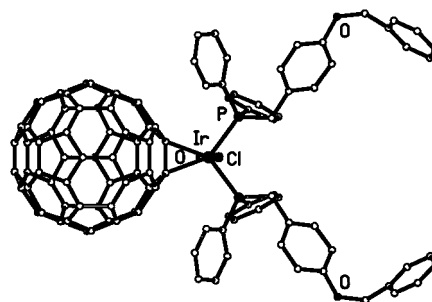


**Figure 25.** A drawing of an individual molecule of  $(\eta^2\text{-C}_{60})\text{Ir}(\text{CO})\text{Cl}(\text{Ph}_2\text{Pbob})_2$  (from data in ref 103).

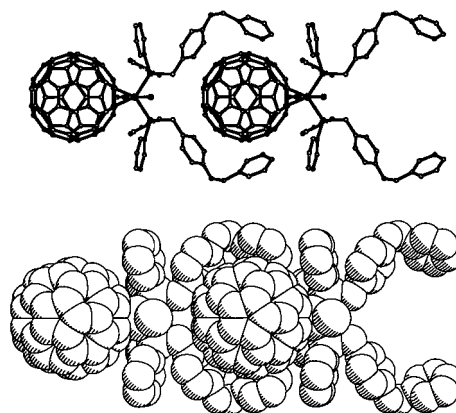


**Figure 26.** A stick drawing and a space filling diagram of two molecules of  $(\eta^2\text{-C}_{60})\text{Ir}(\text{CO})\text{Cl}(\text{Ph}_2\text{Pbob})_2$  which show how the arms of the  $\text{Ph}_2\text{Pbob}$  ligand encircle the fullerene portion of an adjacent molecule. Repetition of this motif creates infinite chains of these molecules in the crystalline solid (from data in ref 102).

tion as black crystals. In this solid the fullerene is bound to iridium in the expected  $\eta^2$ -fashion at a 6:6 ring junction. No benzene is incorporated into the solid; i.e.  $(\eta^2\text{-C}_{60})\text{Ir}(\text{CO})\text{Cl}(\text{Ph}_2\text{Pbob})_2$  crystallizes as a solvate-free species. The two benzyloxybenzyl groups of one molecule of the complex cradle the  $\text{C}_{60}$  portion of the adjacent molecule in a van der Waals embrace. Figure 25 shows a drawing of an isolated molecule, while Figure 26 shows how one molecule embraces the next. The result is a linear array of molecules that extends throughout the crystal. The packing efficiency in this solid is remarkable. Two of the phenyl rings of each benzyloxybenzyl group make face-to-face  $\pi$ -contact with an adjacent fullerene, while another phenyl ring makes face-to-face contact with the fullerene within the molecule. The remaining phenyl ring of each phosphine ligand fits snugly between two columns of the complexes. While  $\text{Ir}(\text{CO})\text{Cl}(\text{Ph}_2\text{Pbob})_2$  readily forms a crystalline solid with  $\text{C}_{60}$ , it does not react with  $\text{C}_{70}$  to yield crystalline material under similar conditions. The failure to form such an adduct with  $\text{C}_{70}$  may result from the larger size of this fullerene and its inability to form as compact a structure as that shown in Figure 25.

The dendrimeric ligands,  $\text{Ph}_2\text{P}$  (3,5-bis(benzyloxy)benzyl) ( $\text{PPh}_2(\text{G}-1)$ ) and  $\text{Ph}_2\text{P}$  (3,5-bis(3,5-bis(benzyloxy)oxybenzyl)) ( $\text{PPh}_2(\text{G}-2)$ ) which incorporate five and nine benzene rings into each phosphine, have been prepared and utilized to study the reversibility of  $\text{C}_{60}$  binding to the complexes,  $\text{Ir}(\text{CO})\text{Cl}(\text{PPh}_2\text{G}-1)_2$  and  $\text{Ir}(\text{CO})\text{Cl}(\text{PPh}_2\text{G}-2)_2$ .<sup>103</sup> Analysis of the  $^{31}\text{P}$  NMR



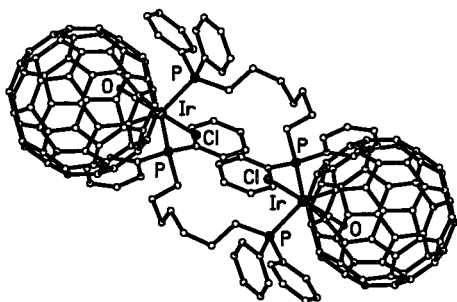


**Figure 27.** A molecule with two fullerene units connected by a dimetallomacrocyclic. The structure of  $(C_{60})_2Ir_2(CO)_2Cl_2(\mu-Ph_2P(CH_2)_7PPh_2)_2$  as determined by X-ray crystallography (from data in ref 105).

spectra of the reaction of these complexes with  $C_{60}$  produced the first thermodynamic data for fullerene binding to a transition metal. In chlorobenzene solution, it was concluded that the dendrimeric arms of the phosphine ligands did not play a major role in stabilization of the fullerene adducts. Unfortunately, solubility considerations precluded examination of the equilibrium in nonaromatic solvents where the dendrimeric ligands might have played a greater role in adduct stabilization.

Metallomacrocycles<sup>104</sup> of the type  $Ir_2(CO)_2Cl_2\{Ph_2P(CH_2)_n PPh_2\}_2$ , which have varying spacing between the two iridium centers, have been prepared and their ability to coordinate to fullerenes has been examined. These dimetallic complexes are unable to make two connections to the same fullerene, but they are able to form bridges between two fullerene units. As shown in eq 9,  $C_{60}$  and  $Ir_2(CO)_2Cl_2\{Ph_2P(CH_2)_7PPh_2\}_2$  combine to form a stable adduct in which two fullerenes are chemically connected through the metallomacrocyclic.<sup>105</sup> The structure of the product

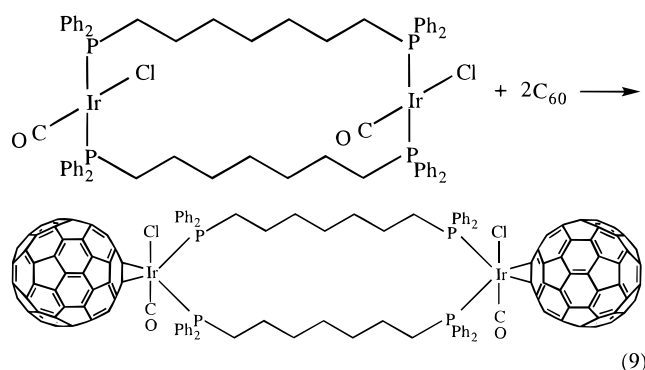


**Figure 28.** The structure of  $(\eta^2-C_{70})Ir(CO)Cl(PPh_3)_2 \cdot 2.5C_6H_6$  as determined by X-ray crystallography (from data in ref 106).

It possesses an ellipsoidal shape with a 6.82 Å diameter and a 7.90 Å distance along the (former) 5-fold axis. The curvature of the fullerene portion is highest at the poles, while the hexagons about the waist of the molecule are somewhat concave. In Table 2, the fullerene dimensions obtained from the structure of  $(\eta^2-C_{70})Ir(CO)Cl(PPh_3)_2 \cdot 2.5C_6H_6$  are compared to those obtained from crystalline  $C_{70} \cdot 6(S_8)$ ,<sup>107</sup> from a related double-addition product,<sup>108</sup> from a theoretical calculation,<sup>109</sup> and from an electron diffraction study of  $C_{70}$  (at much higher temperature, 810–835 °C).<sup>110,111</sup> These data are largely consistent with one another. However, the electron diffraction study does give an equatorial  $C_e-C_e$  bond length that is 0.06 Å longer than the other studies. Consequently, in the gas phase at high temperature, the equatorial hexagons of  $C_{70}$  are not pinched inward as they are in all other structures that are compared in Table 2. Complex formation causes only a local structural deformation of the carbon cage.

In  $C_{70}$  there are eight types of C–C bonds, four of which occur at 6:6 ring junctions. Thus, the potential for the formation of isomeric addition products is considerable. The isolation of only a single isomer of  $(\eta^2-C_{70})Ir(CO)Cl(PPh_3)_2$  can be attributed in part to the reversibility of the addition reaction that is utilized in its formation and crystallization as discussed above. The isolation of this particular isomer, with the iridium complex bound to a  $C_a-C_b$  bond,<sup>18</sup> and the fact that the molecule is most curved near the poles. In contrast, the molecule is flattened at the equator (as seen in Figures 4 and 28). Because of the curvature at the poles, the carbon atoms of types  $C_a$  and  $C_b$  are the most pyramidalized.<sup>58,112</sup> Coordination of metal centers to olefins results a distortion of the olefin so that the substituents are bent away from the added metal center (i.e. the carbon atoms of the olefin become pyramidalized). In the  $C_{70}$  the carbon atoms at the poles are already somewhat pyramidalized, but even further pyramidalization occurs upon coordination of a metal center. The pyramidalization of  $C_a$  and  $C_b$  increases from 11.96° and 11.96° in  $C_{70}$  itself to 14.4° and 17.0° in  $(\eta^2-C_{70})Ir(CO)Cl(PPh_3)_2$ .<sup>58</sup> Thus, in  $C_{70}$  the most pyramidalized carbon atoms ( $C_a, C_b$ ) are the prime sites for attachment of organometallic reagents such as  $Ir(CO)Cl(PPh_3)_2$  and  $Pt(PPh_3)_2$  (vide infra).

is shown in Figure 27. In this case, the bifunctional metallomacrocyclic serves to keep the two fullerene moieties in the molecule rather far apart. Both the fullerene center-to-center separation of 16,559 Å and the nonbonded  $Ir \cdots Ir$  distance of 8.104 Å are long.

Higher fullerenes also yield adducts with Vaska-type complexes. The adduct,  $(\eta^2-C_{70})Ir(CO)Cl(PPh_3)_2 \cdot 2.5C_6H_6$ , is readily formed from the reaction of  $C_{70}$  with  $Ir(CO)Cl(PPh_3)_2$  in benzene solution.<sup>106</sup> Figure 28 shows the structure of the molecule as determined in a single-crystal X-ray diffraction study. In it, the iridium atom is coordinated to a  $C_a-C_b$  bond at a 6:6 ring junction at one pole of the  $C_{70}$  moiety. The structure of the fullerene moiety conforms to expect-

**Table 2. Dimensions within Free and Complexed C<sub>70</sub>**

| bond                           | average bond length (Å) |                                     |   |   |            |
|--------------------------------|-------------------------|-------------------------------------|---|---|------------|
|                                | ab initio calculation   | C <sub>70</sub> ·6(S <sub>8</sub> ) | ( $\eta^2$ -C <sub>70</sub> )Ir(CO)Cl(PPh <sub>3</sub> ) <sub>2</sub> | ( $\eta^2$ -C <sub>70</sub> ){Ir(CO)Cl(PMe <sub>2</sub> Ph) <sub>2</sub> } <sub>2</sub> | gas phase  |
| C <sub>a</sub> –C <sub>a</sub> | 1.451                   | 1.453 (3)                           | 1.46 (3)  | 1.440 (6)   | 1.461 (8)  |
| C <sub>a</sub> –C <sub>b</sub> | 1.375                   | 1.387 (4)                           | 1.38 (1) <sup>a</sup>   | 1.386 (19) <sup>a</sup>   | 1.388 (16) |
| C <sub>b</sub> –C <sub>c</sub> | 1.446                   | 1.445 (3)                           | 1.45 (3)  | 1.455 (11)  | 1.453 (11) |
| C <sub>c</sub> –C <sub>c</sub> | 1.361                   | 1.378 (3)                           | 1.37 (2)  | 1.374 (13)  | 1.386 (25) |
| C <sub>c</sub> –C <sub>d</sub> | 1.457                   | 1.447 (2)                           | 1.43 (2)  | 1.444 (14)  | 1.405 (13) |
| C <sub>d</sub> –C <sub>d</sub> | 1.415                   | 1.426 (3)                           | 1.44 (1)  | 1.427 (8)   | 1.425 (14) |
| C <sub>d</sub> –C <sub>e</sub> | 1.407                   | 1.414 (2)                           | 1.42 (3)  | 1.420 (7)   | 1.405 (13) |
| C <sub>e</sub> –C <sub>e</sub> | 1.475                   | 1.462 (4)                           | 1.46 (2)  | 1.458 (7)   | 1.538 (19) |
| ref                            | 109                     | 107                                 | 106   | 108   | 111        |

<sup>a</sup> The bonds that are coordinated to iridium are excluded from the average.

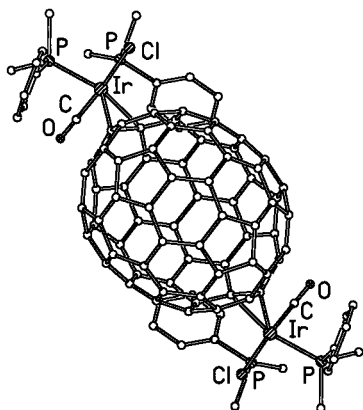
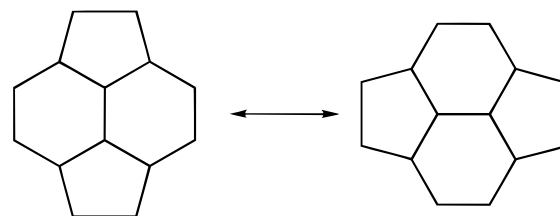


**Figure 29.** The structure of C<sub>70</sub>{Ir(CO)Cl(PPhMe<sub>2</sub>)<sub>2</sub>}<sub>2</sub> as determined by X-ray crystallography (from data in ref 108).

The addition of multiple numbers of Vaska-type complexes to C<sub>70</sub> has also been explored. So far, multiple addition has been limited to the formation of products with two iridium complexes appended to C<sub>70</sub>. Figure 5 shows the possible sites for double addition when the reactivity of C<sub>70</sub> is confined to the C<sub>a</sub>–C<sub>b</sub> bonds at its opposite poles. Three double-addition products can result: addition at site A brings the two added groups closest to one another, addition at site C positions the two groups furthest apart, while addition at site B places them at an intermediate distance. With the more reactive complex, Ir(CO)Cl(PMe<sub>2</sub>Ph)<sub>2</sub>, both single- and double-addition products have been obtained as crystalline solids.<sup>108</sup> The yield of the two products is controlled by the stoichiometry of the reaction. The structure of the single-addition product resembles that of the triphenylphosphine analogue, and again, addition to a C<sub>a</sub>–C<sub>b</sub> bond occurs. The reaction of C<sub>70</sub> with a 6- to 12-fold excess of Ir(CO)Cl(PMe<sub>2</sub>Ph)<sub>2</sub> produces crystalline ( $\eta^2$ -C<sub>70</sub>){Ir(CO)Cl(PMe<sub>2</sub>Ph)<sub>2</sub>}<sub>2</sub>·3C<sub>6</sub>H<sub>6</sub>, exclusively.<sup>108</sup> The structure of this double-addition product is shown in Figure 29. This product results from an addition to site B in C<sub>70</sub> (Figure 5). That is the site which places the two added groups at an intermediate distance apart. Steric effects are not responsible for guiding this reaction; since there are no unfavorable contacts between the added moieties when they are artificially placed in sites A, B, or C. In this double-addition product, all of the four phenyl rings make close  $\pi$ – $\pi$  contacts with the fullerene portion, while the methyl substituents on the phosphine ligands are directed away from the fullerene.

This orientation of the phenyl rings resembles that seen for one of the forms of ( $\eta^2$ -C<sub>60</sub>){Ir(CO)Cl(PMe<sub>2</sub>Ph)<sub>2</sub>}<sub>2</sub> which is shown in Figure 21.<sup>94</sup>

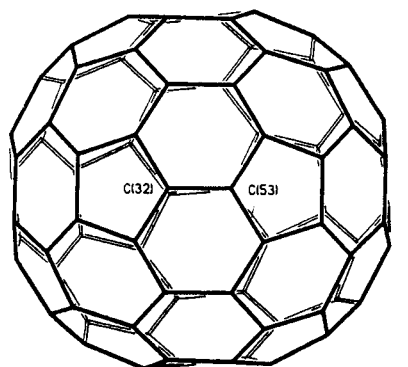
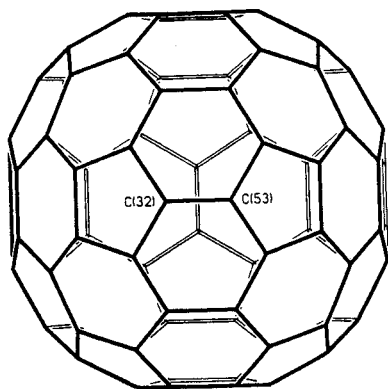
The structure of C<sub>84</sub> has also been investigated through the formation of an adduct with Vaska's complex. With C<sub>84</sub> there are 24 isomeric structures that obey the isolated pentagon rule. Thus, its structure is more complex than C<sub>60</sub> or C<sub>70</sub> where only one isolated pentagon structure exists. These 24 structures for C<sub>84</sub> are divided into two disjoint families.<sup>113</sup> The isomers within each family can be converted into one another through the pycrolyene or Stone–Wales transformation.<sup>114</sup> Within the group



Stone–Wales Transformation

of 24 isolated pentagon isomers, there are four  $D_2$  and two  $D_{2d}$  isomers, as well as other isomers with symmetries as high as  $D_{5h}$  and even  $T_d$ . Calculations indicate that the  $D_2$  (22) and  $D_{2d}$  (23) isomers shown in Figure 30 have the lowest energies.<sup>115</sup> Initial <sup>13</sup>C NMR studies on C<sub>84</sub> have indicated that the 32-line pattern can be explained by the presence of a 2:1 mixture of these  $D_2$  (22) and  $D_{2d}$  (23) isomers.<sup>116,117</sup> However, only recently has an effective chromatographic separation of these isomers has been reported.<sup>118</sup> Further studies of the C<sub>84</sub> fullerene, particularly those examining endohedral He@C<sub>84</sub> via <sup>3</sup>He NMR spectroscopy, indicate that several other isomers are present.<sup>119,120</sup>

The addition of an excess of Ir(CO)Cl(PPh<sub>3</sub>)<sub>2</sub> to a saturated benzene solution of the mixture of isomers of C<sub>84</sub> formed in the arc process produces black crystals of ( $\eta^2$ -C<sub>84</sub>)Ir(CO)Cl(PPh<sub>3</sub>)<sub>2</sub>·4C<sub>6</sub>H<sub>6</sub>.<sup>121</sup> The results of a single-crystal X-ray diffraction study are shown in Figure 31. While the complex itself has no crystallographically imposed symmetry, the geometry of the fullerene portion corresponds to the  $D_{2d}$  (23) isomer of C<sub>84</sub>. The distance along the (former) C<sub>2</sub> axis that bisects the C(32)–C(53) and C(42)–C(43) bonds is 8.61 Å, while the distance across the two (former) 2-fold axes that are perpendicular to this is 8.34 Å.

**D<sub>2</sub> (22)****D<sub>2d</sub> (23)**

**Figure 30.** The  $D_2$  (22) and  $D_{2d}$  (23) isomers of  $C_{84}$  which calculations indicate are the most stable of the 24 isolated pentagon isomers of  $C_{84}$ .

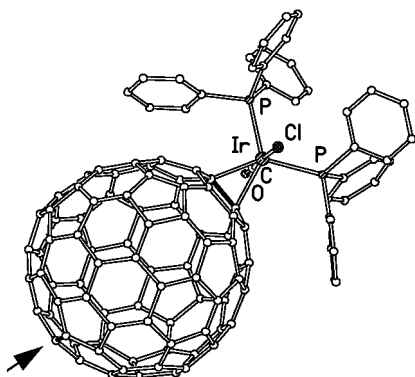


**Figure 31.** The crystallographically determined structure of  $(\eta^2-C_{84})\text{Ir}(\text{CO})\text{Cl}(\text{PPh}_3)_2 \cdot 4\text{C}_6\text{H}_6$  (from data in ref 121). The  $D_{2d}$  isomer of  $C_{84}$  is the prevalent form that separates upon crystallization. The arrow points to the C(42)–C(43) bond directly opposite the C–C bond to which the iridium atom is coordinated.

The iridium ion is coordinated to the C(32)–C(53) bond, which is one of the 19 different types of C–C bonds in  $C_{84}$ . Hückel calculations indicate that this is the bond in  $C_{84}$  that has the highest  $\pi$ -bond order, and therefore it should be the most reactive.<sup>18</sup> As a consequence of coordination, the length of the C(32)–C(53) bond (1.455 (6) Å) is considerably greater than that of its unreacted counterpart, the C(42)–C(43) bond (1.332 (11) Å) at the opposite side of the fullerene.

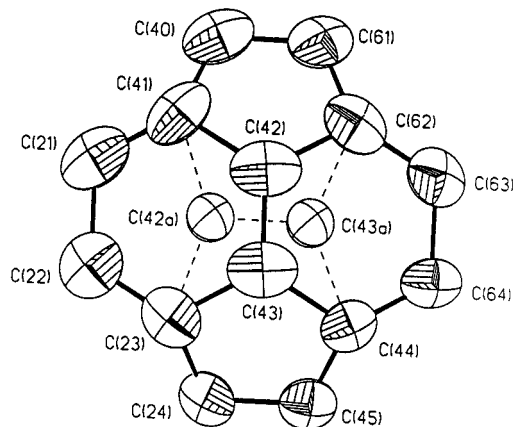


**Figure 32.** A region of additional electron density on the  $C_{84}$  surface in the structure of  $(\eta^2-C_{84})\text{Ir}(\text{CO})\text{Cl}(\text{PPh}_3)_2 \cdot 4\text{C}_6\text{H}_6$  (from data in ref 121). This is the region noted by the arrow in Figure 31.

The selective crystallization of the less abundant  $D_{2d}$  (23) isomer into the adduct,  $(\eta^2-C_{84})\text{Ir}(\text{CO})\text{Cl}(\text{PPh}_3)_2 \cdot 4\text{C}_6\text{H}_6$ , may be a consequence of the higher reactivity of this isomer. Hückel molecular orbital calculations show that the  $D_{2d}$  (23) isomer of  $C_{84}$  has the most localized  $\pi$ -bonds in the group of fullerenes that includes  $C_{60}$ ,  $C_{70}$ ,  $C_{76}$ ,  $C_{78}$ , and other isomers of  $C_{84}$ .<sup>18</sup> Consequently, it has been suggested that this  $D_{2d}$  (23) isomer will be the most reactive toward addition reactions.<sup>18</sup>

However, the separation of  $C_{84}$  isomers that is achieved through crystallization of the adduct,  $(\eta^2-C_{84})\text{Ir}(\text{CO})\text{Cl}(\text{PPh}_3)_2 \cdot 4\text{C}_6\text{H}_6$ , is not complete. Examination of residual electron density within the fullerene portion of the adduct indicates that another isomer of  $C_{84}$  is probably present. Difference maps reveal the presence of electron density near the centers of six hexagons that are adjacent to three specific bonds. Figure 32 shows the location of one set of such sites of electron density, which have been treated as additional carbon atoms with fractional occupancy. The observed pattern is a superposition of the two local structures that are related by a Stone–Wales transformation.<sup>114</sup> No other orientation of the  $D_{2d}$  (23) isomer of  $C_{84}$  would produce the observed pattern of additional electron density. It is possible that the presence of small amounts of other isomers could produce these features. However, with the limited amount of data available, an unambiguous identification of the isomer (or isomers) of  $C_{84}$  which is responsible for these features is not possible. Nevertheless, through adduct formation and crystallization, a partial separation of the  $C_{84}$  isomers has been achieved for the first time.

Adduct formation with Vaska's complex has produced the first set of structures where the three most common fullerenes,  $C_{60}$ ,  $C_{70}$ , and  $C_{84}$ , can be directly compared. Figure 33 presents drawings of  $(\eta^2-C_{60})\text{Ir}(\text{CO})\text{Cl}(\text{PPh}_3)_2$ ,  $(\eta^2-C_{70})\text{Ir}(\text{CO})\text{Cl}(\text{PPh}_3)_2$ , and  $(\eta^2-C_{84})\text{Ir}(\text{CO})\text{Cl}(\text{PPh}_3)_2$  on the same scale so that the differences in sizes and shapes of the three fullerenes are apparent.

The reaction of chemically modified fullerenes with Vaska's compound can also produce crystalline materials that give information about their structure

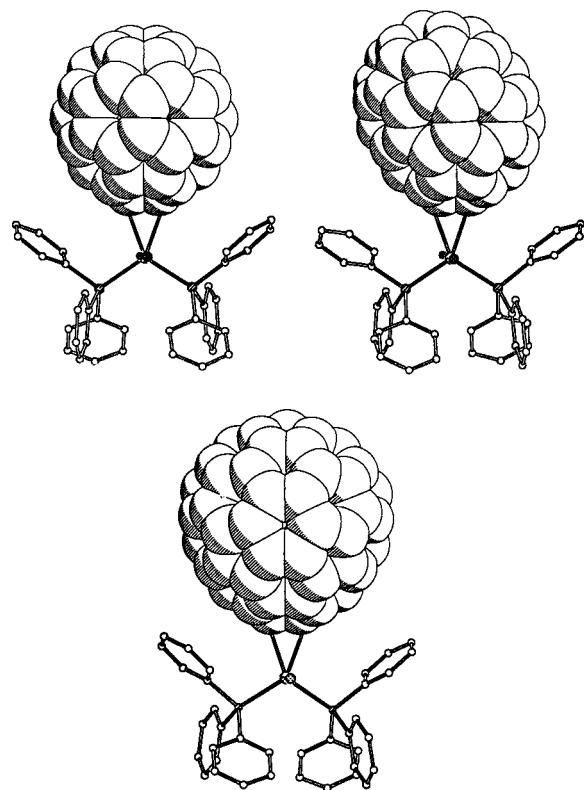


**Figure 33.** A comparison of the structures of  $(\eta^2\text{-C}_{60})\text{Ir}(\text{CO})\text{Cl}(\text{PPh}_3)_2$ ,  $(\eta^2\text{-C}_{70})\text{Ir}(\text{CO})\text{Cl}(\text{PPh}_3)_2$ , and  $(\eta^2\text{-C}_{84})\text{Ir}(\text{CO})\text{Cl}(\text{PPh}_3)_2$ . The three drawings were made to the same scale. van der Waals contours are represented.

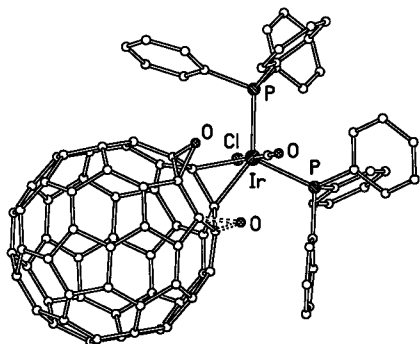


**Figure 34.** A view of  $(\eta^2\text{-C}_{60}\text{O})\text{Ir}(\text{CO})\text{Cl}(\text{PPh}_3)_2$  as determined by X-ray crystallography (from data in ref 125). The epoxide oxygen is disordered over two sites.

and reactivity. Several fullerene oxidation products have been examined and characterized using this methodology. The simplest fullerene oxide,  $\text{C}_{60}\text{O}$ , has the epoxide structure,<sup>122,123</sup> but crystallizes with the oxygen atom disordered over the entire fullerene surface.<sup>124</sup> However,  $\text{C}_{60}\text{O}$  reacts with  $\text{Ir}(\text{CO})\text{Cl}(\text{PPh}_3)_2$  to form black crystals of  $(\eta^2\text{-C}_{60}\text{O})\text{Ir}(\text{CO})\text{Cl}(\text{PPh}_3)_2 \cdot 5\text{C}_6\text{H}_6$  which show much more limited disorder.<sup>125</sup> The structure of the adduct, as determined by X-ray diffraction, is shown in Figure 34. The epoxide functionality is clearly present. The  $\text{O}(1)\text{-C}(3)\text{-C}(4)$  unit forms a nearly equilateral triangle; the  $\text{C-O}$  distances (1.445(12), 1.462(12) Å) and the  $\text{C-C}$  distance (1.480(11) Å) are within the range expected for an epoxide unit. Surprisingly, in the context of examples of multiple addition of metal complexes to  $\text{C}_{60}$ , the addition occurs so that the

iridium center binds to a 6:6 ring junction that shares a common hexagonal face with the epoxide unit. The nonbonded  $\text{Ir-O}(1)$  separation is large (3.463(7) Å), and it is clear that there is no direct interaction between the iridium and oxygen atoms. This observation is particularly significant since there are cases known where low-valent metal complexes do insert into the  $\text{C-O}$  bonds of epoxides.<sup>126</sup> In the solid-state structure of  $(\eta^2\text{-C}_{60}\text{O})\text{Ir}(\text{CO})\text{Cl}(\text{PPh}_3)_2 \cdot 5\text{C}_6\text{H}_6$ , the epoxide oxygen atom occupies two sites ( $\text{O}(1)$  and  $\text{O}(1')$ ) with different occupancies, but both sites are similarly situated with regard to the placement of the iridium atom.

Some loss of oxygen from  $\text{C}_{60}\text{O}$  is observed during the growth of crystals of  $(\eta^2\text{-C}_{60}\text{O})\text{Ir}(\text{CO})\text{Cl}(\text{PPh}_3)_2 \cdot 5\text{C}_6\text{H}_6$ .<sup>125</sup> This deoxygenation may result from a small degree of phosphine dissociation from the parent complex, since free triphenylphosphine reacts with  $\text{C}_{60}\text{O}$  to form  $\text{C}_{60}$  and triphenylphosphine oxide.<sup>127</sup> The use of  $\text{Ir}(\text{CO})\text{Cl}(\text{AsPh}_3)_2$  for adduct formation avoids these problems, because triphenylarsine is less reactive than triphenylphosphine toward deoxygenation of  $\text{C}_{60}\text{O}$ .<sup>127</sup> Crystallographic analysis of the resulting adduct,  $(\eta^2\text{-C}_{60}\text{O})\text{Ir}(\text{CO})\text{Cl}(\text{AsPh}_3)_2 \cdot 4.82\text{C}_6\text{H}_6 \cdot 0.18\text{CHCl}_3$ , shows that the epoxide function is again present and that the organometallic group binds in the immediate proximity of the epoxide. However, the degree of disorder in the location of the epoxide oxygen atom found in this compound is greater than that found in the triphenylphosphine analogue; since there are four sites which are occupied by oxygen atoms in the solid-state structure of  $(\eta^2\text{-C}_{60}\text{O})\text{Ir}(\text{CO})\text{Cl}(\text{AsPh}_3)_2 \cdot 4.82\text{C}_6\text{H}_6 \cdot 0.18\text{CHCl}_3$ .

Oxidation of  $\text{C}_{60}$  with *m*-chloroperoxybenzoic acid produces  $\text{C}_{60}\text{O}$ , two separable isomers of  $\text{C}_{60}\text{O}_2$ , and three separable isomers of  $\text{C}_{60}\text{O}_3$ .<sup>128</sup> All of these oxides react with triphenylphosphine to form  $\text{C}_{60}$ , and hence all contain epoxide functionalities.<sup>129</sup>  $^{13}\text{C}$  NMR spectroscopy has shown that the most abundant isomer of  $\text{C}_{60}\text{O}_2$  has  $C_s$  symmetry, and is one of the three isomers shown in Figure 35.<sup>128</sup> Reaction of this isomer with  $\text{Ir}(\text{CO})\text{Cl}(\text{PPh}_3)_2$  yields a crystalline adduct,  $(\eta^2\text{-C}_{60}\text{O}_2)\text{Ir}(\text{CO})\text{Cl}(\text{PPh}_3)_2 \cdot 5\text{C}_6\text{H}_6$ . This compound has been studied by single-crystal X-ray diffraction, but again there is a significant degree of disorder in the locations of the oxygen atoms. These oxygen atoms are found at seven partially occupied sites over 6:6 ring junctions on the fullerene surface. Analysis of the relative populations of these sites indicates that the  $\text{C}_{60}\text{O}_2$  isomer that is present is the *cis*-1 isomer (see Figure 2). This isomer has the two epoxide groups on a common hexagonal face of the fullerene. Figure 36 shows the structure of the prevalent form of the adduct that is present. This figure also includes a drawing of the fullerene surface which shows the locations of the seven sites where oxygen atoms are found, as well as the relative populations of these sites. In the predominant form of the adduct, the iridium atom is coordinated to two carbon atoms that are immediately adjacent to both of the epoxide groups. Thus, despite the disorder, crystallographic analysis of the adduct has allowed differentiation among the three possible  $\text{C}_{60}\text{O}_2$  isomers whose structures are consistent with the ob-

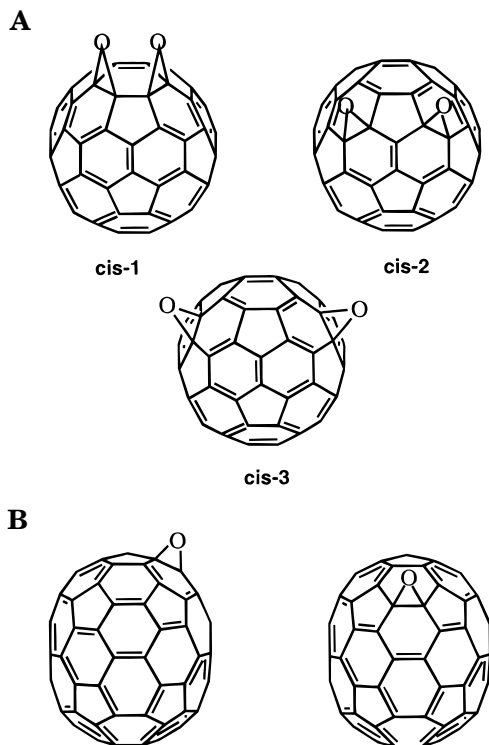


**Figure 35.** (A) Drawings of the three C<sub>s</sub> isomers of C<sub>60</sub> diepoxide with C<sub>s</sub> symmetry that are consistent with the observed <sup>13</sup>C NMR spectrum and (B) drawings of the two known isomers of C<sub>70</sub>O.

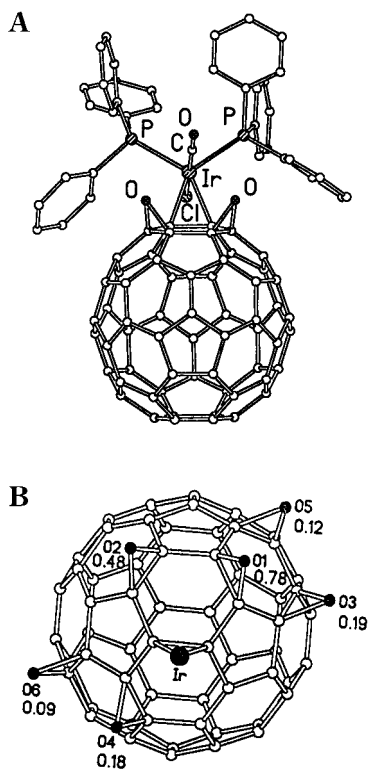


**Figure 36.** (A) A view of the predominant form of (η<sup>2</sup>-C<sub>60</sub>O<sub>2</sub>)Ir(CO)Cl(PPh<sub>3</sub>)<sub>2</sub> that is present in the crystalline adduct. (B) A drawing of the fullerene portion which shows the relative location of the iridium center, the seven sites that are occupied by epoxide oxygen atoms, and the relative populations of these seven sites (from data in ref 128).

served pattern of <sup>13</sup>C NMR resonances for the diepoxide.

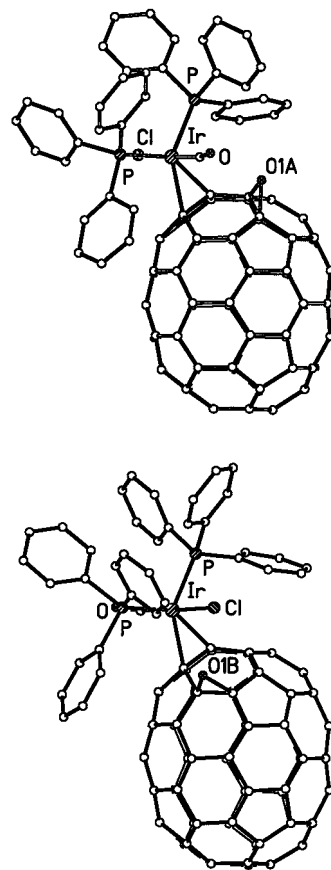


**Figure 37.** Drawings of the two forms of (η<sup>2</sup>-C<sub>70</sub>O)Ir(CO)Cl(PPh<sub>3</sub>)<sub>2</sub> that share a common site in crystalline (η<sup>2</sup>-C<sub>70</sub>O)Ir(CO)Cl(PPh<sub>3</sub>)<sub>2</sub>·5C<sub>6</sub>H<sub>6</sub> (from data in ref 131).

Oxidation of C<sub>70</sub> yields C<sub>70</sub>O, which has been found to exist in two isomeric forms.<sup>130</sup> Both isomers are epoxides: one has the oxygen atom located above a C<sub>a</sub>-C<sub>b</sub> bond of the fullerene, while the other has the oxygen atom located over a C<sub>c</sub>-C<sub>c</sub> bond of fullerene as shown in Figure 35. Reaction of a mixture of the two C<sub>70</sub>O isomers with Ir(CO)Cl(PPh<sub>3</sub>)<sub>2</sub> yields (η<sup>2</sup>-C<sub>70</sub>O)Ir(CO)Cl(PPh<sub>3</sub>)<sub>2</sub>·5C<sub>6</sub>H<sub>6</sub>.<sup>131</sup> As shown in Figure 37, X-ray crystallography of the adduct shows that C<sub>70</sub>O has the epoxide structure and that the iridium complex is bound to a C-C bond that is immediately adjacent to the epoxide. However, as with the other fullerene oxide adduct structures, there is a significant degree of disorder in this structure as well. Thus as with crystalline (η<sup>2</sup>-C<sub>60</sub>)Ir(CO)(PPh<sub>3</sub>)<sub>3</sub>·5C<sub>6</sub>H<sub>6</sub>,<sup>121</sup> there are two sites for the oxygen atoms. Remarkably, there are also two different orientations of the C<sub>70</sub> unit. These two orientations occupy a common site. Figure 38 shows the relationship between these two orientations. In this drawing one C<sub>70</sub> molecule is shown with solid lines connecting the atoms while the other C<sub>70</sub> molecule has open lines connecting the atoms. The locations of the 5-fold rotation axes of the fullerenes are shown by the arrows. Note the similarity of the immediate environment surrounding the iridium centers in both orientations and the similarity in the local C<sub>70</sub> structures near the poles. The crystal structure of (η<sup>2</sup>-C<sub>70</sub>O)Ir(CO)Cl(PPh<sub>3</sub>)<sub>2</sub>·5C<sub>6</sub>H<sub>6</sub> is consistent with the presence of two C<sub>70</sub>O isomers in the solid. After the structural analysis, a

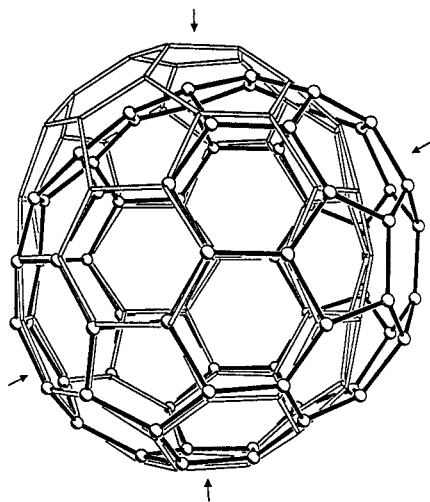


**Figure 38.** A view of two superimposed molecules of  $C_{70}$ . The molecules are oriented so that the  $C_5$  ring at the pole of one molecule (shown with solid lines) overlaps with one of the five  $C_5$  rings that is immediately adjacent to the pole of the other  $C_{70}$  molecule (shown with hollow lines). The arrows show the locations of the 5-fold rotation axes in the two molecules.

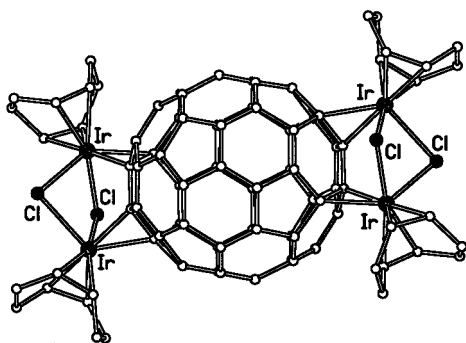


**Figure 39.** The crystallographically determined structure of  $C_{60}\{\text{Ir}_2\text{Cl}_2(\eta^4\text{-C}_8\text{H}_{12})_2\}_2 \cdot 2\text{C}_6\text{H}_6$  with a diagram that expands the coordination geometry in the vicinity of the two iridium atoms (from data in ref 132).

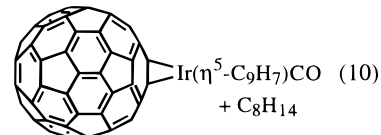
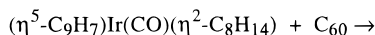
chromatographic means of separation of the two isomers of  $C_{70}\text{O}$  was devised.

## 2. Addition of $\text{Ir}_2(\mu\text{-Cl})_2(\eta^4\text{-C}_8\text{H}_{12})_2$ to $C_{60}$

Mixing benzene solutions of  $C_{60}$  and  $\text{Ir}_2(\mu\text{-Cl})_2(\eta^4\text{-C}_8\text{H}_{12})_2$  produces black crystals of  $C_{60}\{\text{Ir}_2\text{Cl}_2(\eta^4\text{-C}_8\text{H}_{12})_2\}_2 \cdot 2\text{C}_6\text{H}_6$ . The structure of the adduct is shown in Figure 39.<sup>132</sup> Two of the dimeric iridium complexes are bound to the opposite ends of the  $C_{60}$  moiety. Each iridium is  $\eta^2$ -coordinated to a single C–C bond at a 6:6 ring junction of the fullerene. The two iridium atoms of each binuclear, chloro-bridged unit coordinate to C–C bonds on a common hexagonal face of the fullerene. The presence of the chlorobridges constrains the location of the two iridium centers to one hexagon of the fullerene. The Ir–C distances are similar to those found for the Vaska-type adducts that were described in Section G. Addition of  $\text{Ir}_2(\mu\text{-Cl})_2(\eta^4\text{-C}_8\text{H}_{12})_2$  to  $C_{60}$  results in a decrease in the isomer shift in the  $^{193}\text{Ir}$  Mössbauer spectrum of the adduct.<sup>133,134</sup> Little else is known about addition reactions of the inorganic component,  $\text{Ir}_2(\mu\text{-Cl})_2(\eta^4\text{-C}_8\text{H}_{12})_2$ .

## 3. Reaction of $(\eta^5\text{-C}_9\text{H}_7)\text{Ir}(\text{CO})(\eta^2\text{-C}_8\text{H}_{12})$ with $C_{60}$

Heating a benzene solution of the indenyl iridium complex,  $(\eta^5\text{-C}_9\text{H}_7)\text{Ir}(\text{CO})(\eta^2\text{-C}_8\text{H}_{14})$ , with  $C_{60}$  for 8 h produces the new complex  $(\eta^2\text{-C}_{60})\text{Ir}(\text{CO})(\eta^5\text{-C}_9\text{H}_7)$  as shown in eq 10.<sup>135</sup> Black  $(\eta^2\text{-C}_{60})\text{Ir}(\text{CO})(\eta^5\text{-C}_9\text{H}_7)$



dissolves in aromatic and chlorinated solvents to give stable solutions. The infrared spectrum of  $(\eta^2\text{-C}_{60})\text{Ir}(\text{CO})(\eta^5\text{-C}_9\text{H}_7)$  shows a carbon monoxide stretching vibration at  $1998\text{ cm}^{-1}$  that is shifted to higher energy than that of the parent olefin complex,  $(\eta^2\text{-C}_{60})\text{Ir}(\text{CO})(\eta^5\text{-C}_9\text{H}_7)$  at  $1954\text{ cm}^{-1}$ . This shift is consistent with the withdrawal of electrons from the iridium center onto the fullerene through the d-to- $\pi^*$  type of back-bonding.

$(\eta^2\text{-C}_{60})\text{Ir}(\text{CO})(\eta^5\text{-C}_9\text{H}_7)$  is reduced electrochemically in two reversible, one-electron processes.<sup>136</sup> The potentials for these processes are shifted by  $\sim 0.1\text{ V}$  to more negative values relative to those of  $C_{60}$ . Such cathodic shifts are consistent with the effects seen for the addition of other metal complexes to  $C_{60}$ .<sup>24</sup> The reduction of  $(\eta^2\text{-C}_{60})\text{Ir}(\text{CO})(\eta^5\text{-C}_9\text{H}_7)$  has been followed by infrared spectroelectrochemistry. During reduction to form the monoanion, the carbon monoxide stretching frequency is lowered by  $12\text{ cm}^{-1}$ . Further reduction to the dianion produces an additional shift in  $\nu(\text{CO})$  by  $23\text{ cm}^{-1}$ . Since these shifts are relatively small, the reductions are largely centered on the fullerene portion of the molecule.

Thin films of  $(\eta^2\text{-C}_{60})\text{Ir}(\text{CO})(\eta^5\text{-C}_9\text{H}_7)$  on gold electrodes show surface-enhanced Raman spectra with added complexity (compared to  $C_{60}$  itself) that is due to the lower symmetry of the adducts.<sup>137</sup>

The electronic absorption spectrum of  $(\eta^2\text{-C}_{60})\text{Ir}(\text{CO})(\eta^5\text{-C}_9\text{H}_7)$  is similar to that of  $C_{60}$ , with the exception of a new band at  $436\text{ nm}$ . This new feature has been assigned to a  $C_{60}$ -based transition that gains intensity through the lower symmetry of the adduct.<sup>138</sup> Photolysis of a toluene solution  $(\eta^2\text{-C}_{60})\text{Ir}(\text{CO})(\eta^5\text{-C}_9\text{H}_7)$  at  $388\text{ nm}$  produces a transient absorption spectrum with maxima at  $420$ ,  $490$ , and  $720\text{ nm}$ . This spectrum is similar to the transient absorption spectrum obtained after photolysis of a solution of uncomplexed  $C_{60}$ . The excited-state lifetime for this transient form of  $(\eta^2\text{-C}_{60})\text{Ir}(\text{CO})(\eta^5\text{-C}_9\text{H}_7)$  is  $100\text{ ns}$  under  $\text{O}_2$ -free conditions. Thus, its lifetime is 500 times shorter than that of free  $C_{60}$ . Addition of dioxygen reduces the lifetime of the excited state of  $(\eta^2\text{-C}_{60})\text{Ir}(\text{CO})(\eta^5\text{-C}_9\text{H}_7)$ . In the presence of tetramethylethylene, energy transfer from the excited state of  $(\eta^2\text{-C}_{60})\text{Ir}(\text{CO})(\eta^5\text{-C}_9\text{H}_7)$  results in the formation of singlet oxygen and subsequent production of a hydroperoxide.

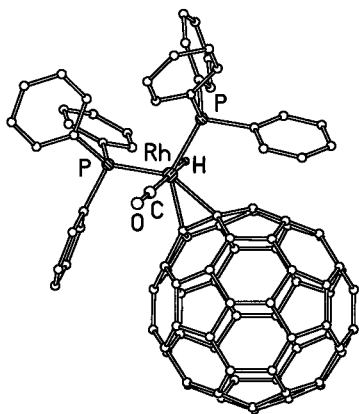
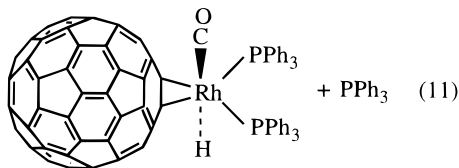
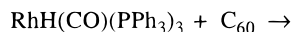


**Figure 40.** A drawing of the structure of one of the two independent molecules of  $(\eta^2\text{-C}_{60})\text{RhH}(\text{CO})(\text{PPh}_3)_2$ . The location of the hydrogen atom is presumed to be trans to the carbon monoxide ligand but it was not located in the crystal structure analysis (from data in ref 140).

#### 4. Reaction of $\text{C}_{60}$ with the Hydrogenation Catalyst, $\text{RhH}(\text{CO})(\text{PPh}_3)_3$

$\text{RhH}(\text{CO})(\text{PPh}_3)_3$  is a useful catalyst for the homogeneous hydrogenation of olefins.<sup>139</sup> However, efforts to use  $\text{Rh}(\text{CO})\text{H}(\text{PPh}_3)_3$  to catalyze the hydrogenation of  $\text{C}_{60}$  have not been successful. Nevertheless,  $\text{RhH}(\text{CO})(\text{PPh}_3)_3$  does react with  $\text{C}_{60}$  as shown in eq 11.



The deep green complex,  $(\eta^2\text{-C}_{60})\text{RhH}(\text{CO})(\text{PPh}_3)_2$ , has been isolated as crystals suitable for X-ray diffraction.<sup>140</sup> Figure 40 shows a view of the two independent, but structurally similar, molecules within the solid. The arrangement within the  $(\eta^2\text{-C}_{60})\text{Rh}(\text{PPh}_3)_2$  unit is very similar to the analogous portion of  $(\eta^2\text{-C}_{60})\text{Ir}(\text{CO})\text{Cl}(\text{PPh}_3)_2$  (Figure 20). Electron density in the hydride position was not directly observed by the crystallographic study, as is frequently the case for metal hydrides. However, there is little doubt that the hydride ligand resides in the space trans to the carbon monoxide ligand. Green  $(\eta^2\text{-C}_{60})\text{Rh}(\text{CO})\text{H}(\text{PPh}_3)_2$  is stable in solution with respect to dissociation of the fullerene. The spectroscopic data for this complex indicate that the hydride ligand is bound to rhodium and not to the fullerene. The  $^1\text{H}$  NMR resonance for the hydride appears as a triplet at  $-9.33$  ppm with  $^2J_{\text{PH}} = 8.4$  Hz. The value of  $^1J_{\text{RhH}}$  is too small to be observed for both the  $\text{C}_{60}$  adduct and the parent complex,  $\text{Rh}(\text{CO})\text{H}(\text{PPh}_3)_3$ .<sup>139</sup>

Although  $(\eta^2\text{-C}_{60})\text{Rh}(\text{CO})\text{H}(\text{PPh}_3)_2$  is not effective in stoichiometric or catalytic hydrogenation of  $\text{C}_{60}$ , it is a hydroformylation catalyst for ethylene and propylene.<sup>31,140</sup> However, hydrogenation of  $\text{C}_{60}$  to form  $\text{C}_{60}\text{H}_2$  has been achieved using a heterogeneous rhodium-catalyzed process.<sup>141</sup>

Electrochemical studies of  $(\eta^2\text{-C}_{60})\text{Rh}(\text{CO})\text{H}(\text{PPh}_3)_2$  reveal that the complex undergoes extensive dis-

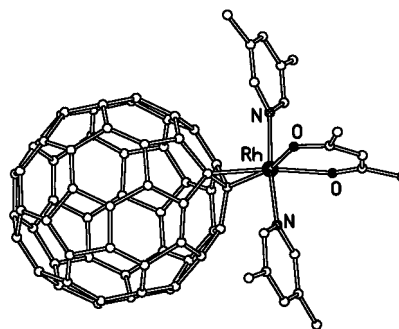


**Figure 41.** The structure of  $(\eta^2\text{-C}_{60})\text{Rh}(\text{acac})(3,5\text{-dimethylpyridine})_2$  as determined by X-ray crystallography (from data in ref 147).

sociation of the fullerene upon either oxidation or reduction.<sup>142</sup>

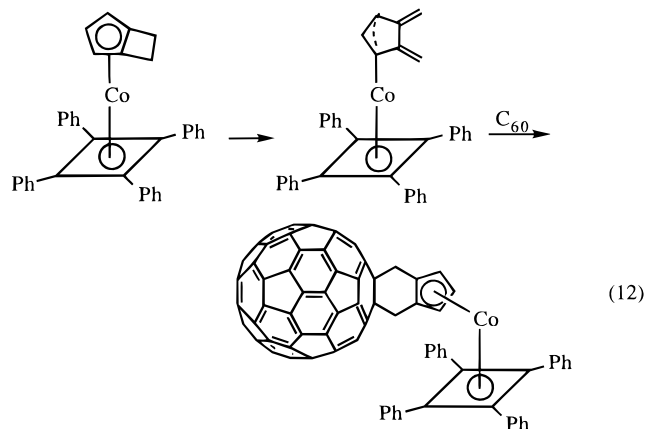
An analogous complex of  $\text{C}_{70}$ ,  $(\eta^2\text{-C}_{70})\text{Rh}(\text{CO})\text{H}(\text{PPh}_3)_2$ , has also been prepared.<sup>143-145</sup> The iridium analogue of  $(\eta^2\text{-C}_{60})\text{Rh}(\text{CO})\text{H}(\text{PPh}_3)_2$ , i.e.  $(\eta^2\text{-C}_{60})\text{Ir}(\text{CO})\text{H}(\text{PPh}_3)_2$ , has been prepared from the reaction of  $\text{C}_{60}$  with  $\text{Ir}(\text{CO})\text{H}_2\text{Cl}(\text{PPh}_3)_2$  in the presence of potassium hydroxide.<sup>146</sup>

#### 5. Other Additions

A benzene solution of  $\text{C}_{60}$  and  $\text{Rh}(\text{acac})(\text{C}_2\text{H}_4)_2$  produces a brown precipitate with poor solubility that is presumed to be polymeric.<sup>147</sup> The polymer dissolves in 3,5-dimethylpyridine, and dilution with benzene yields the five-coordinate Rh(I) complex  $(\eta^2\text{-C}_{60})\text{Rh}(\text{acac})(3,5\text{-dimethylpyridine})_2$  whose structure, as determined by X-ray crystallography, is shown in Figure 41.

Fluxional processes within  $(\eta^2\text{-C}_{60})\text{M}(\text{NO})(\text{PPh}_3)_2$  ( $\text{M} = \text{Rh}$  or  $\text{Ir}$ ) and  $(\eta^2\text{-C}_{60})\text{Rh}(\text{CO})\text{H}(\text{PPh}_3)_2$  have been examined by  $^{13}\text{C}$  NMR spectroscopy.<sup>148</sup> At low temperatures the spectra are consistent with simple  $\eta^2$ -fullerene coordination, but warming the THF solution produces spectral changes that have been interpreted in terms of fluxional processes that involve rotation about the metal-fullerene bond and subsequent metal-fragment migration over the fullerene surface. For sorting out the fullerene resonances in molecules of this type, the 2D EXSY measurements are particularly useful.

The reaction of  $\text{C}_{60}$  with  $(\eta^5\text{-bicyclo}[3.2.0]\text{hepta-1,3-dienyl})(\eta^4\text{-tetraphenylcyclobutadiene})\text{cobalt}(\text{I})$  proceeds via a ring slippage reaction through an  $\eta^3$ -



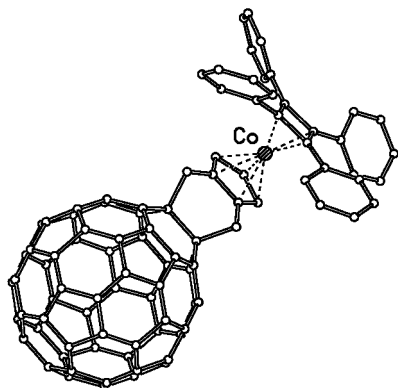
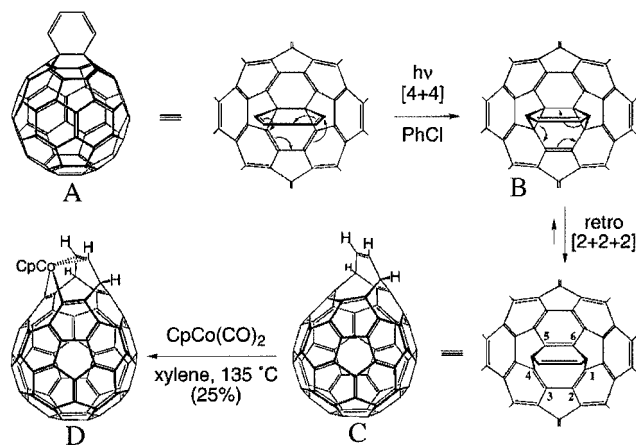


**Figure 42.** The structure of the [4+2] cycloadduct ( $\eta^4$ -Ph<sub>4</sub>C<sub>4</sub>)Co( $\eta^5$ -C<sub>5</sub>H<sub>3</sub>(CH<sub>2</sub>)<sub>2</sub>C<sub>60</sub>) as determined crystallographically (from data in ref 149).

**Scheme 5. Ring Opening Reactions of C<sub>60</sub> (ref 151)**



intermediate that undergoes a [4+2] cycloaddition to the fullerene, as shown in eq 12.<sup>149</sup>

Similar [4+2] cycloadditions of this cobalt complex to simple olefins have been reported previously.<sup>150</sup> The cycloadduct has been unambiguously characterized by X-ray crystallography. The structure of the cycloadduct is shown in Figure 42.

One of the most remarkable transformations in transition metal–fullerene chemistry involves the ring-opening reactions outlined in Scheme 5.<sup>151,152</sup> The 1,2-(3,5-cyclohexadieno)C<sub>60</sub> (**A**, Scheme 5) undergoes [4+4] photoaddition to produce **B** transiently. Intermediate **B** is rapidly converted by a retro [2+2+2] cycloreversion to form the isolable bis-methano[12]annulene **C**. Purple **C** reacts with ( $\eta^5$ -C<sub>5</sub>H<sub>5</sub>)Co(CO)<sub>2</sub> to form **D**, in which the cobalt center is coordinated in an  $\eta^2$ -fashion to the nonfullerene double bond that was present in **C** and in an  $\eta^1$ -fashion to two of the carbon atoms of the fullerene portion. The structure of **D**, which is shown in Figure 43, has been elucidated by X-ray crystallography. The separations between the cobalt center and these two carbon atoms are 1.923(8) and 1.902(8) Å. The distance between the two carbon atoms is 2.41(1) Å, which is no longer a bonded distance. Thus, the chemistry outlined in Scheme 5 offers an interesting instance in which the fullerene cage is somewhat disrupted during chemical transformations. An imaginative article by Rubin that describes a variety of

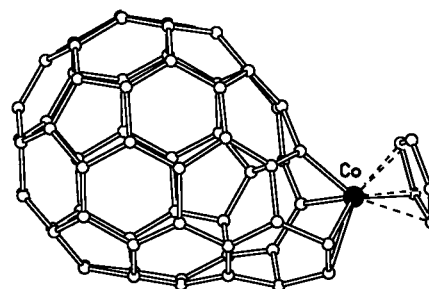


**Figure 43.** The structure of ( $\eta^5$ -C<sub>5</sub>H<sub>5</sub>)Co( $\eta^1, \eta^1, \eta^2$ -C<sub>64</sub>H<sub>4</sub>) as determined by X-ray crystallography (from data in ref 151).

approaches to the opening of the fullerenes has been published.<sup>152</sup>

### 6. Redox Reactions

The reduction potential of cobaltocene (−0.9 V vs SCE) is such that it is capable of reducing C<sub>60</sub> by one or two electrons.<sup>40,153</sup> Addition of cobaltocene to C<sub>60</sub> in a 1:1 ratio in benzonitrile solution yields brown [( $\eta^5$ -C<sub>5</sub>H<sub>5</sub>)<sub>2</sub>Co<sup>+</sup>](C<sub>60</sub><sup>−</sup>)·PhCN.<sup>40</sup> Addition of excess cobaltocene is reported to generate the dianion, (C<sub>60</sub><sup>2−</sup>).<sup>40</sup> The EPR spectrum of [( $\eta^5$ -C<sub>5</sub>H<sub>5</sub>)<sub>2</sub>Co<sup>+</sup>](C<sub>60</sub><sup>−</sup>)·PhCN in tetrahydrofuran shows a resonance at  $g = 1.9969$  with a temperature-dependent line width (7 G at 4.5 K, 24 G at 130 K). Additionally, the material shows a sharp spike of low intensity at  $g = 2.000$ . Reed and co-workers suggest that the spike arises from thermal population of an excited state that could result from splitting of the degeneracy of the <sup>2</sup>T<sub>u</sub> state. Reduction was suggested to cause a distortion from *I<sub>h</sub>* to *D<sub>5d</sub>* symmetry that would split the <sup>2</sup>T<sub>u</sub> state into <sup>2</sup>A<sub>2u</sub> and <sup>2</sup>E<sub>1u</sub> states.<sup>40</sup> However, the absence of this spike in other salts raises the possibility that the spike results from species other than (C<sub>60</sub><sup>−</sup>).

Treatment of C<sub>60</sub> with excess cobaltocene in carbon disulfide produces black crystals of [( $\eta^5$ -C<sub>5</sub>H<sub>5</sub>)<sub>2</sub>Co<sup>+</sup>](C<sub>60</sub><sup>−</sup>)·CS<sub>2</sub> that are barely suitable for X-ray diffraction.<sup>153</sup> A view of molecular packing of the components is given in Figure 44. The C<sub>60</sub><sup>−</sup> anion shows orientational disorder with two different orientations resolved. Unfortunately, the poor crystal quality and the disorder do not allow a meaningful analysis of the effect of reduction on the geometry of the fulleride component. The dimensions of the cobalt complex, however, are consistent with the presence of the cobaltocenium ion rather than neutral cobaltocene. The EPR spectrum, with a narrow line at  $g = 1.998$  which broadens on warming, is indicative of electron transfer to give the fulleride ion. The EPR spectrum at 4 K does not show the known features of neutral cobaltocene, nor does it show evidence of a narrow spike at higher temperatures.

The anionic carbonyl compound, Na[Co(CO)<sub>4</sub>], reacts with C<sub>60</sub> with a total loss of carbon monoxide to produce an amorphous black solid with the composition NaCoC<sub>60</sub>·3THF.<sup>154</sup> The infrared spectrum of the solid contains broader C<sub>60</sub> bands at 1428, 1181, 575, and 526 cm<sup>−1</sup> but no bands due to carbon monoxide ligands. The Raman spectrum of the powder is very similar to that of ( $\eta^2$ -C<sub>60</sub>)Pt(PPh<sub>3</sub>)<sub>2</sub> (see Figure 49). Magnetic susceptibility and EPR studies indicate that the material is paramagnetic with approxi-



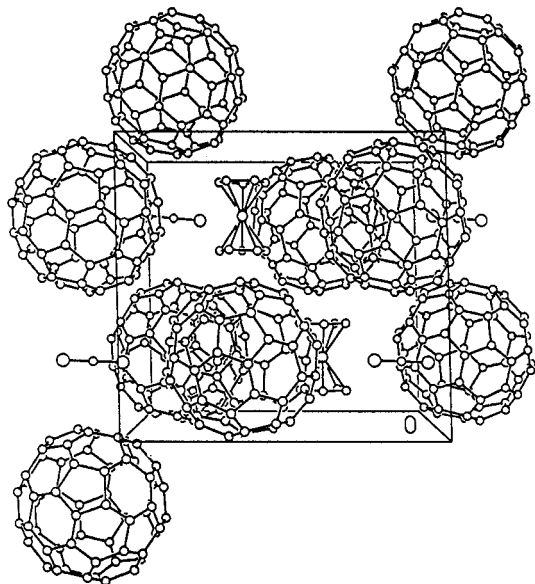


**Figure 44.** A view of the structure of  $[(\eta^5\text{-C}_5\text{H}_5)_2\text{Co}^+][\text{C}_{60}]^-\cdot\text{CS}_2$  down the  $c$  axis showing the relative orientations of the three components (from data in ref 153).

mately two unpaired electrons per formula unit with an EPR line at  $g = 1.991$ . A polymeric structure with a  $(\eta^3\text{-C}_{60})(\mu\text{-Co})(\eta^4\text{-C}_{60})$  unit that has alkylic or dienic coordination between the metal and the fullerene has been proposed. This material may be structurally related to other metal– $\text{C}_{60}$  polymers such as  $\text{C}_{60}\text{Pd}_n$  (vide infra).

### 7. Cocrystallizations

Solutions of  $\text{C}_{60}$ ,  $\text{C}_{70}$ , and  $\text{C}_{60}\text{O}$  and cobalt(II) octaethylporphyrin ( $\text{Co}^{\text{II}}(\text{OEP})$ ) produce crystalline precipitates with the compositions  $\text{C}_{60}\cdot 2\{\text{Co}^{\text{II}}(\text{OEP})\}\cdot\text{CHCl}_3$ ,  $\text{C}_{70}\cdot\text{Co}^{\text{II}}(\text{OEP})\cdot\text{C}_6\text{H}_6\cdot\text{CHCl}_3$  and  $\text{C}_{60}\text{O}\cdot 2\{\text{Co}^{\text{II}}(\text{OEP})\}\cdot\text{CHCl}_3$ .<sup>155</sup> X-ray crystallographic studies reveal that there is no direct covalent link between the cobalt porphyrin and the fullerene and that the cobalt is not coordinated to any part of the fullerene (or to the epoxide function in  $\text{C}_{60}\text{O}$ ). The fullerenes do closely approach the porphyrin planes as shown in Figure 45 for  $\text{C}_{60}\cdot 2\{\text{Co}^{\text{II}}(\text{OEP})_2\}\cdot\text{CHCl}_3$ . Part A shows the arrangement of the two porphyrin units about the fullerene. The distances between the cobalt atoms and adjacent carbon atoms are in the range 2.7–2.9 Å, which is short for van der Waals contacts but too long to represent any chemical bonding between the units. However, it is likely that there is some degree of charge transfer between the individual components. Such interactions may also be involved in the use of porphyrin-modified materials for the chromatographic separation of fullerenes.<sup>156</sup> In addition to the close but asymmetrical fullerene/porphyrin contact, these compounds also show back-to-back  $\text{Co}^{\text{II}}(\text{OEP})/\text{Co}^{\text{II}}(\text{OEP})$  interactions. The fullerenes/ $\text{Co}^{\text{II}}(\text{OEP})$  and  $\text{Co}^{\text{II}}(\text{OEP})/\text{Co}^{\text{II}}(\text{OEP})$  interactions produce continuous chains of molecules in the solid state as shown in Part B of Figure 45.

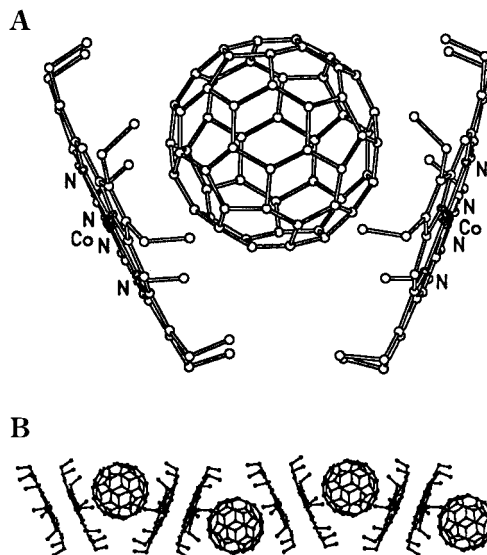
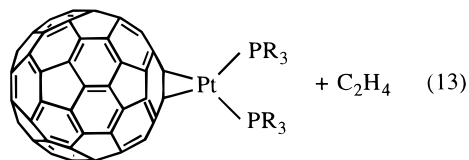
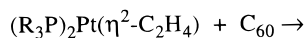


**Figure 45.** (A) A drawing of the interaction of the two porphyrins with  $\text{C}_{60}$  in  $\text{C}_{60}\cdot 2\{\text{Co}^{\text{II}}(\text{OEP})\}\cdot\text{CHCl}_3$ . (B) A chain of molecules connected by  $\text{C}_{60}/2\text{Co}^{\text{II}}(\text{OEP})$  and  $\text{Co}^{\text{II}}(\text{OEP})/\text{Co}^{\text{II}}(\text{OEP})$  interactions (from ref 155).

## H. Platinum, Palladium, and Nickel

### 1. Addition of $M(\text{PR}_3)_2$ Units to Fullerenes

Mixing solutions of  $\text{C}_{60}$  and  $(\text{Ph}_3\text{P})_2\text{Pt}(\eta^2\text{-C}_2\text{H}_4)$  produces black  $(\eta^2\text{-C}_{60})\text{Pt}(\text{PPh}_3)_2$  according to eq 13.<sup>75,76,157,158</sup> At the platinum site, this is a substitu-



tion reaction in which one olefin,  $\text{C}_{60}$ , replaces another, ethylene. The structure of the product has been determined by single-crystal X-ray diffraction and is shown in Figure 46.<sup>75</sup> This was the first compound in which  $\eta^2$ -coordination of a fullerene to a metal was demonstrated. The overall coordination geometry at the platinum atom resembles that of the precursor  $(\text{Ph}_3\text{P})_2\text{Pt}(\eta^2\text{-C}_2\text{H}_4)$ .<sup>159</sup> For the fullerene, the C–C bond (with a bond length of 1.502(30) Å) where the platinum atom is bound is considerably longer than the average C–C distances (1.388(30) Å) at the other 6:6 ring junctions. The platinum–carbon distances, 2.145(24) and 2.115(23) Å, are similar to the corresponding distances, 2.106(4) and 2.116(9) Å, in the parent ethylene adduct. To accommodate the pyramidalization that occurs upon olefin-like coordination, the carbon atoms that are coordinated to the platinum atom are pulled away from the surface of the fullerene as is also observed in related complexes such as  $(\eta^2\text{-C}_{60})\text{Ir}(\text{CO})\text{Cl}(\text{PPh}_3)_2$  (see Section G.1). Thus the pyramidalization of the two platinum-bound carbon atoms is 15.4° versus 11.64° for the carbon atoms in  $\text{C}_{60}$ .<sup>58</sup>

The  $^{31}\text{P}$  NMR spectrum of  $(\text{Ph}_3\text{P})_2\text{Pt}(\eta^2\text{-C}_{60})$  in tetrahydrofuran solution consists of a singlet at 27.0

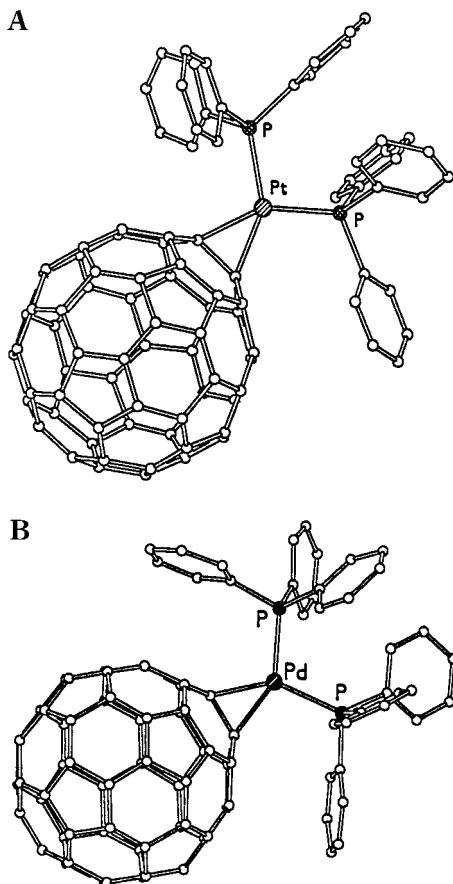
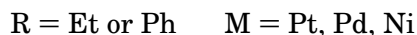
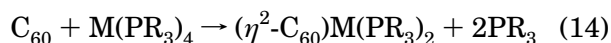


**Figure 46.** Drawing of the structures of (A)  $(\eta^2\text{-C}_{60})\text{Pt}(\text{PPh}_3)_2$  and (B)  $(\eta^2\text{-C}_{60})\text{Pd}(\text{PPh}_3)_2$  as determined by X-ray crystallography from refs 75 and 160, respectively.

ppm with satellites due to coupling to  $^{195}\text{Pt}$  with  $^1J_{\text{PtP}}$  of 3936 Hz.<sup>75</sup> For comparison, the  $^{31}\text{P}$  NMR spectrum of  $(\text{Ph}_3\text{P})_2\text{Pt}(\eta^2\text{-C}_2\text{H}_4)$  consists of a similar resonance at 38.4 ppm with  $J_{\text{PtP}}$  of 3738 Hz.

Related complexes with nickel, palladium, and platinum can also be obtained by treatment of  $\text{C}_{60}$  with  $\text{M}(\text{PR}_3)_4$  via eq 14.<sup>76,157,160</sup> Other adducts have



also been prepared from the reaction of  $\text{M}\{\text{P}(\text{OR})_3\}_4$  with  $\text{C}_{60}$ .<sup>161</sup> Figure 46 shows the structure of the palladium complex,  $(\eta^2\text{-C}_{60})\text{Pd}(\text{PPh}_3)_2$ , as determined by single-crystal X-ray diffraction.<sup>160</sup> The overall structure is similar to that of the platinum analogue as comparison of the two structures in Figure 46 shows. However, the phenyl ring locations are different in the two structures. Two phenyl rings lie over the  $\text{C}_{60}$  moiety in the palladium complex where they make  $\pi\text{-}\pi$  contacts with the cluster. In the analogous platinum compound that sort of contact is lacking. Remarkably, the phenyl ring orientation seen in the palladium complex is also seen in a number of other organometallic adducts of the fullerenes. For example the structure of the  $(\eta^2\text{-C}_{60})\text{-Ir}(\text{PPh}_3)_2$  portion of  $(\eta^2\text{-C}_{60})\text{IrCl}(\text{CO})(\text{PPh}_3)_2$  closely resembles the structure of  $(\eta^2\text{-C}_{60})\text{Pd}(\text{PPh}_3)_2$  (compare Figures 20 and 46B). The reaction between  $\text{Ph}_2\text{-}$

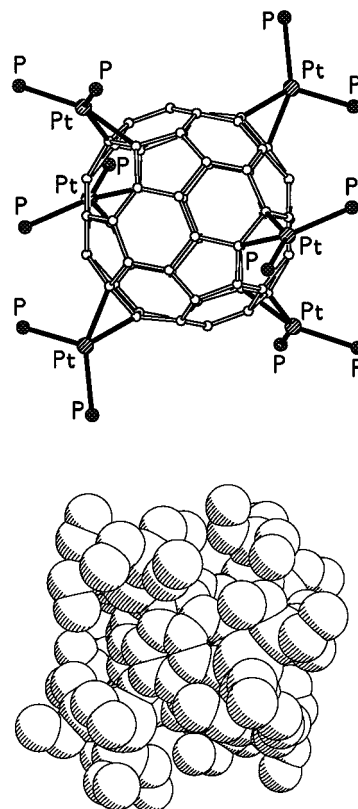


**Figure 47.** Two views of the structure of  $\text{C}_{60}\{\text{Pt}(\text{PEt}_3)_2\}_6$  as determined crystallographically (from data in ref 165). The top view shows the  $\text{C}_{60}\{\text{PtP}_2\}_6$  core while the lower drawing shows space-filling van der Waals contours that show how effectively the surface of the fullerene is covered by the  $\text{Pt}(\text{PEt}_3)_2$  groups.

$\text{CHCH}_2\text{HgPt}(\text{PPh}_3)_2\text{Br}$  and  $\text{C}_{60}$  also yields  $(\eta^2\text{-C}_{60})\text{-Pt}(\text{PPh}_3)_2$ .<sup>162</sup>

An optically active fullerene complex has been obtained through the reaction of  $(\eta^2\text{-C}_{60})\text{Pt}(\text{PPh}_3)_2$  with the optically active, chelating diphosphine, +DIOP (2,3-*O,O'*-isopropylidene-2,3-dihydroxy-1,4-bis(diphenylphosphino)butane).<sup>163</sup> The product,  $(\eta^2\text{-C}_{60})\text{Pt}(\text{+DIOP})$ , has been characterized by X-ray crystallography. The structure is similar to that of  $(\eta^2\text{-C}_{60})\text{Pd}(\text{PPh}_3)_2$ <sup>160</sup> with two of the phenyl rings of the DIOP ligand making close face-to-face contact with the fullerene.

The complex,  $(\eta^2\text{-C}_{60})\text{Pd}(\text{PPh}_3)_2$ , has been used as both a homogeneous and heterogeneous catalyst in the conversion of a substituted acetylene to an olefin.<sup>164</sup>

Multiple addition to  $\text{C}_{60}$  has been examined through the reactions of  $\text{M}(\text{PEt}_3)_4$  ( $\text{M} = \text{Pt or Pd}$ ) with this fullerene. With an excess of  $\text{M}(\text{PEt}_3)_4$ , a stable hexaaddition product is obtained as shown in eq 15.<sup>165</sup> The product,  $\text{C}_{60}\{\text{M}(\text{PEt}_3)_2\}_6$ , has been isolated



and crystallized as a single isomer. The structure of the platinum adduct, as determined by X-ray crystallography, is shown in Figure 47.<sup>165</sup> The six platinum atoms are arranged in an octahedral array about the fullerene core with each platinum atom coordinated to a C-C bond at a 6:6 ring junction. The

arrangement of the phosphorus atoms lowers the symmetry of the array so that the  $C_{60}Pt_6P_{12}$  core has nearly ideal  $T_h$  symmetry, which in and by itself is an unusual geometric arrangement. The placement of the  $Pt(PEt_3)_2$  groups at the six octahedral sites on the fullerene surface positions these groups as far apart as possible and consequently minimizes steric interaction between them. As a result of the size of the phosphine ligands, the surface of the fullerene is nearly completely surrounded by the added groups.

The formation of  $C_{60}\{Pt(PEt_3)_2\}_6$  occurs in a stepwise manner, and some spectroscopic information is available on the intermediates,  $C_{60}\{Pt(PEt_3)_2\}_n$  (with  $n = 2, 3, 4,$  and  $5$ ) that are produced.<sup>165</sup> It has been suggested that the lability of the assembly increases as the addition process proceeds through the addition of more and more  $Pt(PEt_3)_2$  groups to the fullerene. Moreover, the stepwise addition may not always occur at the sites required to form the final product with its octahedral array of the  $C_{60}Pt_6$  core.

The  $Pt(PEt_3)_2$  groups can be plucked from  $(C_{60})\{Pt(PEt_3)_2\}_6$  by supplying appropriate ligands to coordinate to platinum in place of the fullerene. Thus, addition of diphenylacetylene to  $(C_{60})\{Pt(PEt_3)_2\}_6$  rapidly produces  $C_{60}\{Pt(PEt_3)_2\}_5$  and  $(\eta^2-C_2Ph_2)Pt(PEt_3)_2$ . The facile occurrence of this type of reaction gives credence to the notion that the  $Pt(PEt_3)_2$  groups in  $(C_{60})\{Pt(PEt_3)_2\}_6$  are labile with respect to dissociation.

The regiochemistry of addition of the six  $Pt(PEt_3)_2$  groups to  $C_{60}$  provided an early insight into multiple addition patterns to  $C_{60}$ . Subsequent work on multiple additions of organic substituents to  $C_{60}$  has shown that the pattern of addition which places groups in an octahedral arrangement about the fullerene core is preferred in part because this arrangement leaves six isolated hexagons with benzenoid character in the product.<sup>166</sup>

Electrochemical studies on these platinum adducts are more complex than the behavior observed with some fullerene complexes such as  $(\eta^2-C_{60})W(CO)_3(Ph_2PCH_2CH_2PPh_2)$  (see Figure 7),<sup>32</sup> where simple reversible reductions are observed. For these platinum complexes, cyclic voltammetry reveals fullerene based reductions with enhanced lability of the anionic forms.<sup>157</sup> The electrochemical behaviors of  $(\eta^2-C_{60})Pt(PPh_3)_2$  and  $C_{60}$  are compared in the cyclic voltammograms shown in Figure 48. The three reduction waves (M1c, M2c, and M3c) are assigned to the electrochemically reversible formation of  $[(\eta^2-C_{60})Pt(PPh_3)_2]^-$ ,  $[(\eta^2-C_{60})Pt(PPh_3)_2]^{2-}$ , and  $[(\eta^2-C_{60})Pt(PPh_3)_2]^{3-}$ , respectively. The reduction potentials for the platinum adducts are shifted by  $\sim 0.3$  V to more negative values than those of  $C_{60}$  for each of the three reduction steps. The voltammogram in Figure 48 indicates that some free  $C_{60}$  is present at the beginning of the experiment. Moreover, the concentration of free  $C_{60}$  grows as the sample is cycled through the reduction process. Thus, the reduced forms are susceptible to dissociation of the  $Pt(PPh_3)_2$  unit and the fulleride ion. The rates of dissociation have been examined for a variety of related  $(\eta^2-C_{60})M(PR_3)_2$  complexes. The rate of dissociation is faster for  $PPh_3$  rather than  $PEt_3$  as the ligand. The rate of dissociation

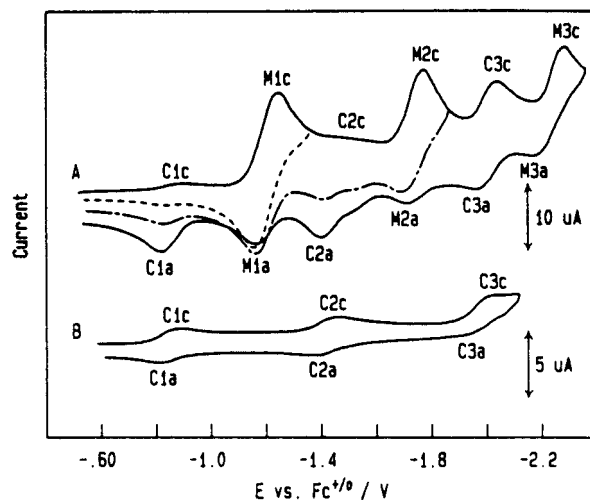
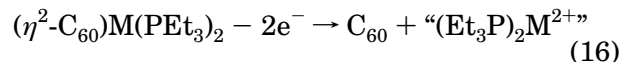


**Figure 48.** Cyclic voltammograms of (A)  $(\eta^2-C_{60})Pt(PPh_3)_2$  and (B)  $C_{60}$  in tetrahydrofuran solution with  $(n-Bu_4N)(PF_6)$  as supporting electrolyte and a platinum disk electrode. (Reprinted from ref 157. Copyright 1992 American Chemical Society.)

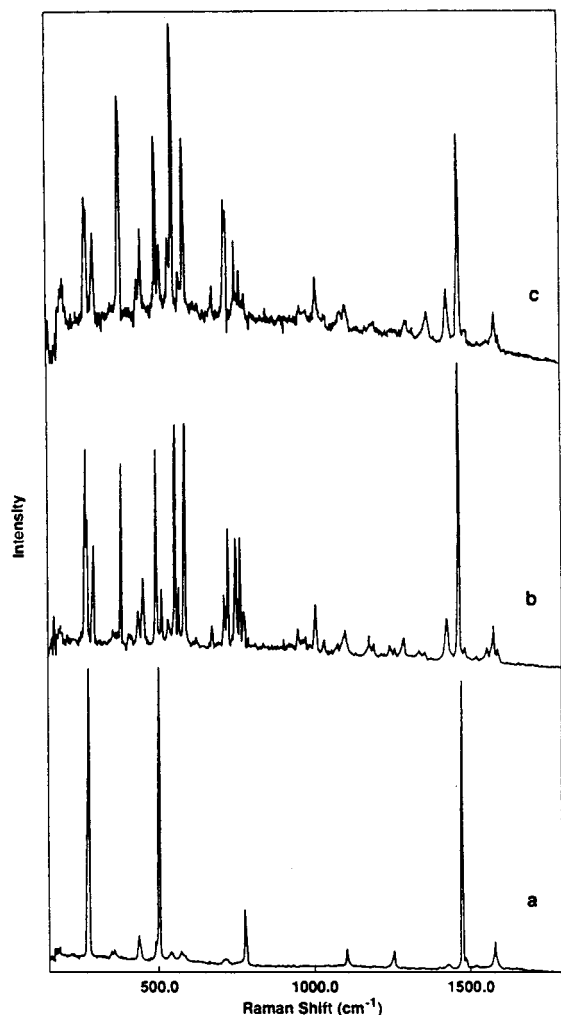
tion is faster for Ni than Pd and faster for Pd than for Pt. Dissociation is faster from the trianion than from the dianion or from the monoanion. The reduction potentials for the series of adducts  $(C_{60})\{Pt(PEt_3)_2\}_n$ , with  $n = 1-4$ , show a 0.36 V cathodic shift for each added metal for the initial reduction to form the corresponding monoanions. Since the three adducts,  $(\eta^2-C_{60})M(PEt_3)_2$  with  $M = Ni, Pd,$  and  $Pt$ , are reduced at similar potentials, the reduction process is largely localized on the fullerene and there is little difference in the degree of electron donation from metal to fullerene among these three metal complexes. Related electrochemical studies on  $(\eta^2-C_{60})Pd(PPh_3)_2$  alone and mixed with  $Pd(PPh_3)_4$  confirm that a complex set of equilibria occur that involve  $(\eta^2-C_{60})Pd(PPh_3)_2$ , polymetalated complexes,  $C_{60}\{Pd(PPh_3)_2\}_n$ , and free  $C_{60}$ .<sup>167</sup>

The oxidative behavior of these complexes has also been examined electrochemically.<sup>168</sup> The monoaddition products,  $(\eta^2-C_{60})M(PEt_3)_2$  with  $M = Ni, Pd,$  and  $Pt$ , undergo irreversible two-electron oxidations which are tentatively described by eq 16. The potentials



for these processes increase in the order  $Ni < Pd < Pt$ , so the reactions are viewed as metal-centered. Within the series,  $C_{60}\{Pt(PEt_3)_2\}_n$  ( $n = 1-4$ ), the ease of oxidation increases as additional  $Pt(PEt_3)_2$  groups are added to the fullerene, but again oxidation results in the stepwise loss of  $Pt(PEt_3)_2$  groups.

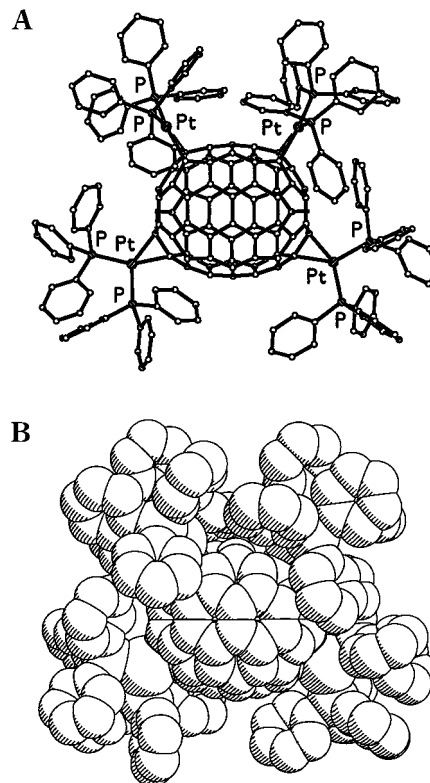
The Raman spectra of these platinum and palladium compounds show clear evidence of the lower symmetry of  $C_{60}$  when it is bound to a metal atom.<sup>169</sup> While  $C_{60}$  itself has only 10 vibrations (of the possible 174 modes) that are Raman-active, the adducts show additional Raman active, fullerene-derived bands. The FT-Raman spectra of  $C_{60}$ ,  $(\eta^2-C_{60})Pd(PPh_3)_2$ , and  $(\eta^2-C_{60})Pt(PPh_3)_2$  are shown in Figure 49. With excitation at  $1.064 \mu m$ , the vibrational bands from the fullerene dominate the spectrum, while the vibrational bands of the phosphine ligands have low



**Figure 49.** FT-Raman spectra of (a)  $C_{60}$ , (b)  $(\eta^2-C_{60})Pd(PPh_3)_2$ , and (c)  $(\eta^2-C_{60})Pt(PPh_3)_2$ . (Reprinted from ref 169. Copyright 1992 American Chemical Society.)

intensity. Thus, effects of the lowered symmetry of the fullerene portion are readily apparent. For example in Figure 49, the nondegenerate  $A_g$  band at  $1468\text{ cm}^{-1}$  is a sharp, single band in all three spectra, while the degenerate  $H_g$  band at  $772\text{ cm}^{-1}$  in  $C_{60}$  is split into five components in the adducts. Additionally, bands that were Raman-inactive in the spectrum of  $C_{60}$  itself appear in the spectra of the adducts. The C–C bonds of the fullerene appear to be weakened by metal-to-fullerene, d-to- $\pi$ , back-bonding; since the high-frequency  $C_{60}$  modes are shifted to slightly lower frequencies in the adducts. Similarly, symmetry-lowering effects were also seen in the Raman spectra of the hexaaddition products,  $C_{60}\{M(PEt_3)_2\}_6$ . Analogous effects have also been observed in the Raman spectrum of  $(\eta^2-C_{60})Ir(CO)(\eta^5-C_9H_7)$ .<sup>137</sup>

The absorption spectrum of photoexcited  $(\eta^2-C_{60})Pd(PPh_3)_2$  has been observed to produce bands at 870 and 1010 nm through picosecond and nanosecond laser spectroscopy.<sup>170</sup> The photoexcited state of this complex has been interpreted as a superposition of the charge-transfer ( $C_{60}^-$ ) and  $S_1$  states of  $C_{60}$ . The photoreactivity of  $(\eta^2-C_{60})Pt\{P(OPh)_3\}_2$  has been examined. Metal-to-ligand charge-transfer excitation leads to dissociation to form free  $C_{60}$  and Pt-

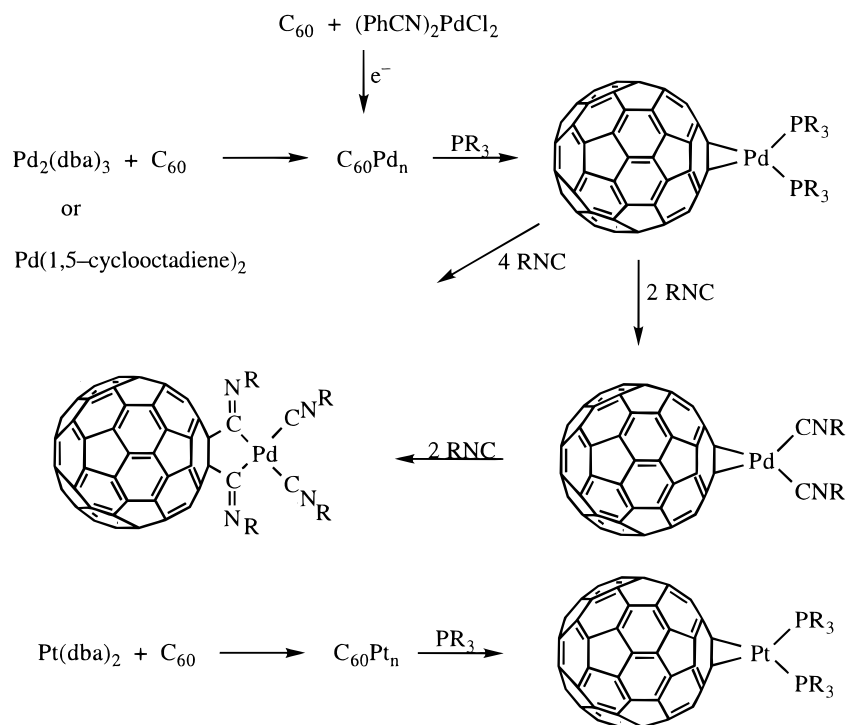


**Figure 50.** The crystallographically determined structure of  $(C_{70})\{Pt(PPh_3)_2\}_4$  (from data in ref 173). In A, the substituents on the phosphine ligands are omitted. In B, space-filling van der Waals contours are shown which reveal that the mid-section of the  $C_{70}$  moiety is left bare even with the four bulky platinum complexes attached.

$\{P(OPh)_3\}_2$ , which is trapped through reaction with chloroform or dioxygen.<sup>171</sup>

The reactivity of the phosphoryl radicals,  $\cdot P(O)(OPr^i)_2$  with  $(\eta^2-C_{60})M(PPh_3)_2$  ( $M = Pd, Pt$ ) has been examined by EPR spectroscopy. Evidence for the existence of unstable spin adducts is available, but these undergo dissociation of the  $M(PPh_3)_2$  unit.<sup>172</sup>

The reaction of  $C_{70}$  with  $(\eta^2-C_2H_4)Pt(PPh_3)_2$  produces four adducts,  $(C_{70})\{Pt(PPh_3)_2\}_n$  where  $n = 1-4$ .<sup>173</sup> The products show  $^{31}P$  NMR spectra that indicate the first two additions occur at the  $C_a-C_b$  bonds at opposite ends of the fullerene, while the next two additions occur at the  $C_c-C_c$  bonds also at opposite ends of the  $C_{70}$  moiety. Only the tetra-addition product has been obtained in crystalline form that is suitable for X-ray crystallography. The structure is shown in Figure 50. The product has the  $C_{70}(PtP_2)_4$  core arranged so that it has idealized  $C_{2v}$  symmetry. The pattern of addition differs from what one might expect on the basis of the known structure of  $C_{70}\{Ir(CO)Cl(PMe_2Ph)_2\}_2$ , which occurs as isomer B (see Figure 5), and also on the basis of studies of the cyclopropanation of  $C_{70}$ , which show that the B isomer is the most prevalent product. In the  $C_{70}\{PtP_2\}_4$  core, the two  $PtP_2$  groups that are bonded to the  $C_a-C_b$  bonds of the fullerene have a relative orientation that corresponds to the double addition product with isomeric structure A (Figure 5). Hence, it is not possible at this stage to predict the geometry of  $C_{70}$  adducts on the basis of the

**Scheme 6. Formation and Reactions of Fullerene/Pd<sup>0</sup> (or Pt<sup>0</sup>) Polymers**

limited knowledge that we have of simple single- and double-addition products.

**2. Formation of Pd(0) and Pt(0) Polymers**

Addition of the labile complex, Pd<sub>2</sub>(dba)<sub>3</sub>·CHCl<sub>3</sub> (dba is dibenzylideneacetone), to a benzene solution of C<sub>60</sub> yields a black, amorphous, air-stable solid, as shown in Scheme 6.<sup>174,175</sup> This material is insoluble in common organic solvents and, consequently, is believed to have a polymeric structure. The product's composition, C<sub>60</sub>Pd<sub>n</sub> (with  $n = 1-7$ ), depends on the reaction conditions. When excess C<sub>60</sub> is present, a material with composition C<sub>60</sub>Pd<sub>1</sub> is obtained. This material has infrared bands at 1429, 1182.5, 576.5, and 527 cm<sup>-1</sup> that are similar to, but broader, than those of C<sub>60</sub>. The C<sub>60</sub>Pd<sub>1</sub> material is believed to be a one-dimensional polymer with alternating palladium atoms and C<sub>60</sub> units in the chain. Materials with higher Pd/C<sub>60</sub> ratios are believed to have palladium atoms that cross-link two chains. A second type of palladium atom that merely sits on the fullerene surface may also be present. Heating solid C<sub>60</sub>Pd<sub>1</sub> in toluene results in the partial dissolution of C<sub>60</sub>, and the formation of a solid with a Pd/C<sub>60</sub> ratio between 2 and 3. Magnetic susceptibility studies of C<sub>60</sub>Pd<sub>n</sub> indicate that these materials may be paramagnetic.<sup>176</sup> These polymers have also been examined by electron microscopy.<sup>177</sup> For C<sub>60</sub>Pd<sub>3</sub>, one-fourth of the sample consisted of small crystals of Pd in an amorphous matrix. The rest of the sample was free of Pd crystals and showed local crystallinity. Ten percent of the material gave an electron diffraction pattern that was interpreted in terms of a model of a C<sub>60</sub>Pd<sub>6</sub> octahedral unit with each palladium center bridging two fullerene units. The local structure proposed is analogous to that observed crystallographically for C<sub>60</sub>{Pt(PEt<sub>3</sub>)<sub>2</sub>}<sub>6</sub>.<sup>165</sup> Treatment of black

polymeric C<sub>60</sub>Pd<sub>n</sub> with phosphine or phosphite ligands results in the dissolution of the solid, and the known complexes, (η<sup>2</sup>-C<sub>60</sub>)Pd(PR<sub>3</sub>)<sub>2</sub>, can be isolated from these solutions.<sup>178</sup>

A related platinum polymer, C<sub>60</sub>Pt<sub>n</sub>, has also been made through the reaction of C<sub>60</sub> with Pt(dba)<sub>2</sub><sup>179</sup> or with Pt(1,5-cyclooctadiene)<sub>2</sub>.<sup>180</sup> Black C<sub>60</sub>Pt reacts with chelating diphosphines to yield (η<sup>2</sup>-C<sub>60</sub>)Pt-(Ph<sub>2</sub>P(CH<sub>2</sub>)<sub>n</sub>PPh<sub>2</sub>) ( $n = 2$  or  $3$ ).<sup>180</sup> C<sub>60</sub>Pd<sub>n</sub> and C<sub>60</sub>Pt<sub>n</sub> also dissolve in toluene in the presence of isocyanide ligands to produce either one of two types of complexes: (1) (η<sup>2</sup>-C<sub>60</sub>)M(CNR)<sub>2</sub> (M = Pd, Pt), which is analogous to (η<sup>2</sup>-C<sub>60</sub>)M(PPh<sub>3</sub>)<sub>2</sub> (see Figure 46) but where isocyanide ligands have replaced the triphenylphosphine ligands, or (2) C<sub>60</sub>(CNR)<sub>2</sub>Pd(CNR)<sub>2</sub> with the unusual structure shown in Scheme 6.<sup>181</sup>

Black, polymeric C<sub>60</sub>Pd<sub>n</sub> can also be made electrochemically.<sup>182</sup> Figure 51 shows multiple-scan cyclic voltammograms of a mixture of C<sub>60</sub> and (PhCN)<sub>2</sub>PdCl<sub>2</sub> in a 4:1 toluene/acetonitrile mixture with tetra-(*n*-butylammonium)hexafluorophosphate as the supporting electrolyte and a gold electrode. Note that successive scans result in an increase in the current due to the growth of the electrode surface as a result of the deposition of the black material on the gold electrode. The deposit is not palladium metal which has markedly different electrochemical characteristics. Analysis by energy-dispersive X-ray spectroscopy shows that both carbon and palladium are present in the deposit but that chlorine is not. Measurements of the resistivity of the deposit suggest that it develops a window of increased conductivity at potentials below -0.7 V.

C<sub>60</sub>Pd<sub>n</sub> with  $n > 2.8$  is a catalyst for hydrogenation of acetylenes and olefins at room temperature.<sup>175</sup> Because polymers with lower Pd/C<sub>60</sub> ratios are inactive as catalysts, it has been suggested that the

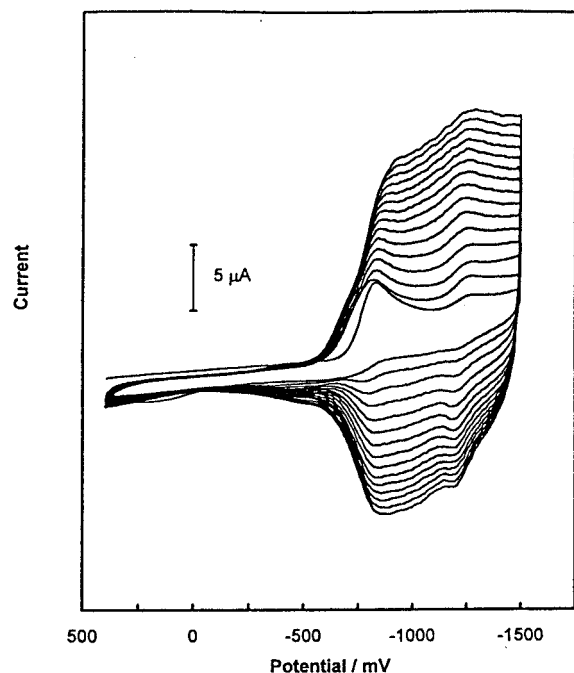


**Figure 51.** Multiscan cyclic voltammograms of a mixture of  $C_{60}$  and  $(PhCN)_2PdCl_2$  in 4:1 toluene/acetonitrile with 0.1 M  $(Bu_4N)PF_6$  as supporting electrolyte and a gold electrode. The reference electrode is a SCE (from ref 182).

exposed, surface palladium atoms, rather than the buried, cross-linking palladium atoms, are involved in this process. Further physical and structural characterization of this polymer appears warranted. This compound may be related to a few other materials such as  $NaCoC_{60} \cdot 3(\text{tetrahydrofuran})^{154}$  and  $C_{60} \cdot Eu_n$  ( $n = 1-6$ )<sup>183</sup> which appear to have polymeric structures with some degree of covalent metal–fullerene bonding.

### 3. Redox Reactions

Mixing carbon disulfide solutions of  $(\eta^5-C_5Me_5)_2Ni$  and  $C_{60}$  produces dark red  $[(\eta^5-C_5Me_5)_2Ni^+][C_{60}^-] \cdot CS_2$ .<sup>184</sup> The structure, as determined by an X-ray crystallographic study, shows that the  $(C_{60})^-$  unit has undergone a distortion due to axial compression so that there is a short axis dimension, 6.878(6) Å (from the midpoint of a C–C bond at a 6:6 ring junction to the opposite midpoint), and two corresponding longer orthogonal distances, 6.965(5) Å and 6.976(5) Å. This structural change may result from the expected Jahn–Teller distortion but the interaction with the  $[(\eta^5-C_5Me_5)_2Ni]^+$  ions, as shown in Figure 52, may also be responsible for the reshaping of the fulleride ion.

### 4. Cocrystallizations

Attempts to coordinate  $PdCl_2$  units onto  $C_{60}$  through reaction with the extremely labile complex,  $(PhCN)_2PdCl_2$ , which is a known precursor to olefin complexes, have resulted in the formation of the ternary material  $C_{60} \cdot 2(Pd_6Cl_{12}) \cdot 2.5C_6H_6$  that crystallizes from benzene solution.<sup>185</sup> A view of the unit cell of this compound is shown in Figure 53. The  $Pd_6Cl_{12}$  cluster, which has dimensions similar to that of  $C_{60}$  (trans Cl...Cl distance, 6.54 Å; trans Pd...Pd distance,

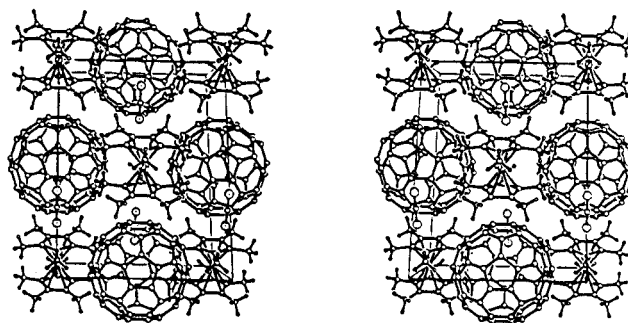


**Figure 52.** Stereoscopic view of the packing in  $[(\eta^5-C_5Me_5)_2Ni^+][C_{60}^-] \cdot CS_2$ . (Reprinted from ref 184. Copyright 1995 American Chemical Society.)

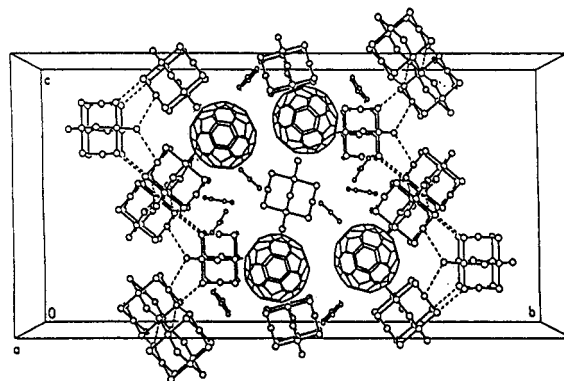


**Figure 53.** A section through the structure of  $C_{60} \cdot 2(Pd_6Cl_{12}) \cdot 2.5C_6H_6$  which shows the relative locations of the three molecular components. The  $C_{60}$  molecules, which are disordered, are represented at their experimentally determined locations by idealized drawings of the molecule. (Reprinted from ref 185. Copyright 1996 American Chemical Society.)

4.67 Å), forms by a spontaneous, self-association process. Benzene rings are interspersed between the fullerene and the  $Pd_6Cl_{12}$  clusters. There is significant attraction between  $Pd_6Cl_{12}$  and aromatic molecules, since a variety of binary and ternary cocrystals of  $Pd_6Cl_{12}$  with aromatic molecules (benzene, mesitylene, durene, and hexamethylbenzene) have been prepared.<sup>185</sup>

## I. Gold, Silver, and Copper

$C_{60}$  and  $Ph_3PAuCl$  cocrystallize from toluene solution to form  $C_{60} \cdot 4\{(Ph_3P)AuCl\} \cdot 0.1C_6H_5CH_3$ .<sup>186</sup> As shown in Figure 54, the solid consists of isolated  $C_{60}$  and  $Ph_3PAuCl$  units without any covalent interaction between the two components. In solution,  $Ag(CF_3SO_3)$  is reported to produce small perturbation of the absorption spectrum of  $C_{60}$  which has been chemically modified through the addition of a potentially coordinating amino–polyether side chain.<sup>187</sup> The spectral changes are attributed to  $Ag^+ - \pi$  interactions.

The reaction of  $C_{60}$  with the organocuprate,  $[Ph_2Cu]^-$ , that is generated from  $PhMgBr$  and  $Me_3SCuBr$ , produces both a novel addition pattern in the product,  $C_{60}Ph_5H$ , that is obtained after hydrolysis, and a modified fullerene that is able to function as an  $\eta^5$ -ligand.<sup>188</sup> The relevant chemistry is summarized in Scheme 7. The authors speculate that the  $C_{60}/[Ph_2Cu]^-$  reaction occurs by two successive 1,4 additions

## Scheme 7. Formation of Pentaphenyl and Pentahapto Chemically Modified Fullerenes (ref 187)

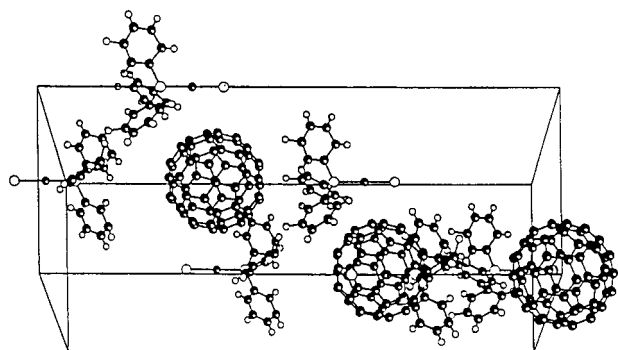
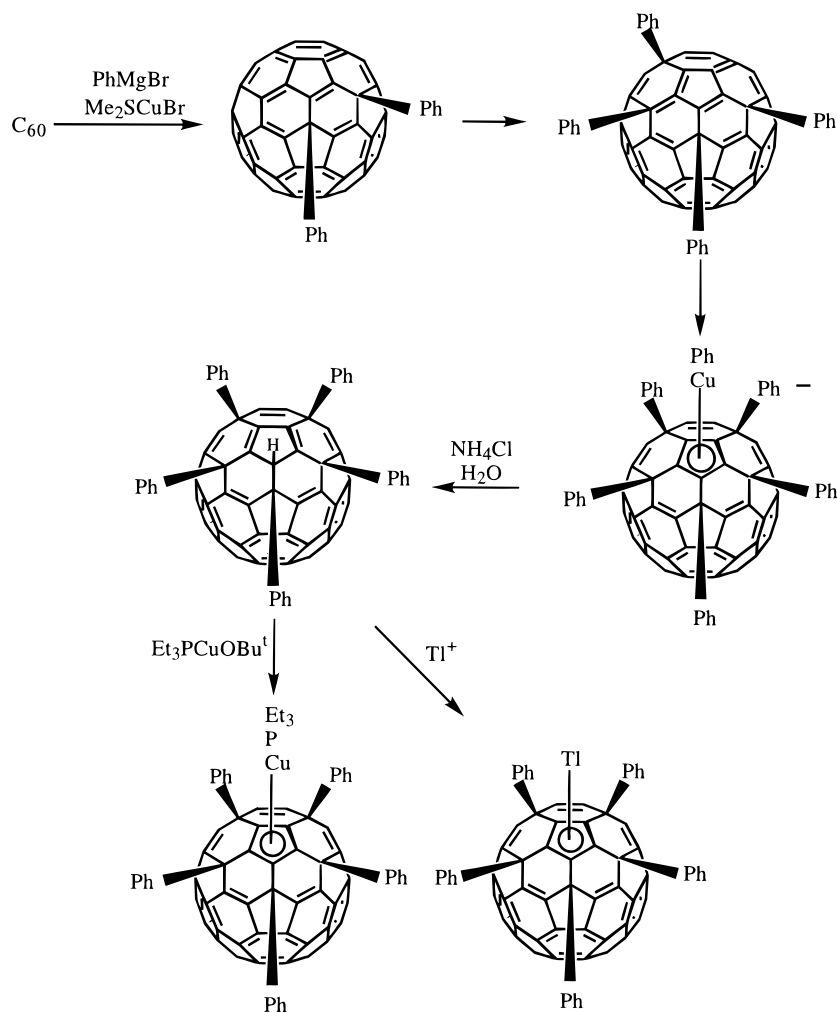


**Figure 54.** The array of molecular components in  $C_{60} \cdot 2\{(Ph_3PAuCl)_4 \cdot 0.1C_6H_5CH_3\}$ . (Reprinted with permission from ref 186. Copyright 1996 John Wiley & Sons Limited.)

of the phenyl groups to the fullerene in a reaction that contrasts with the general monoaddition reactions of Grignard and organolithium reagents with  $C_{60}$ . The addition pattern in  $C_{60}Ph_5H$ , which can also be made from  $C_{60}Cl_6$ ,<sup>189a</sup> effectively isolates one pentagonal face of the fullerene and produces an anion with  $C_5$  symmetry,<sup>189b</sup> that is capable of forming adducts with  $Et_3PCu^+$  and  $Tl^+$ . These adducts appear to utilize  $\eta^5$ -coordination of the modified fullerene. This sort of bonding has been confirmed by X-ray crystallography for the thallium complex, as shown in Figure 55. The thallium atom is located

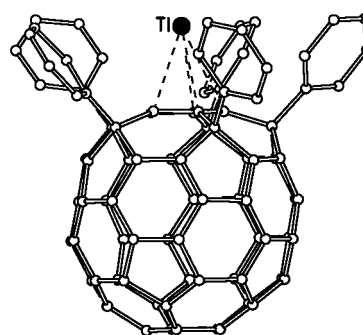


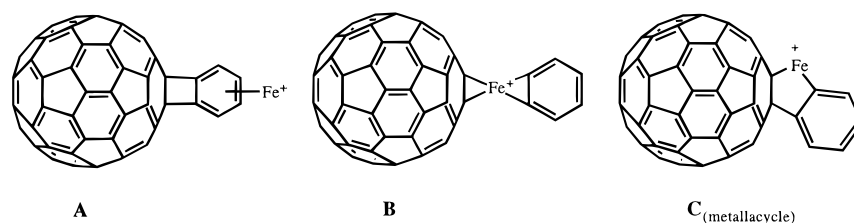
**Figure 55.** A view of  $(\eta^5-Ph_5C_{60})Tl$  as determined by X-ray crystallography (from data in ref 187).

2.60 Å above the center of the adjacent pentagonal face of the modified fullerene. The Tl–C bond lengths fall in a narrow range, 2.85(1) to 2.90(1) Å, and are comparable to the corresponding distances in  $Tl(\eta^5-C_5Bz_5)$ .<sup>190</sup> The eventual coordination of a variety of transition metal centers to this uniquely modified fullerene has been anticipated.<sup>187</sup>

#### IV. Gas-Phase Studies of Fullerene Interactions with Transition Metal Ions

The interplay of gas-phase observations and eventual condensed-phase isolation has been particularly important to the development of fullerene chemis-

## Scheme 8



try.<sup>1,2</sup> Mass spectrometric observations were among the first studies to demonstrate that fullerenes are capable of binding transition metal ions. Such studies continue to provide interesting targets for the synthetic chemist to isolate in solid form. This section reviews gas-phase formation of fullerene metal adducts rather than mass spectrometric studies which are used to provide compositional information on isolated fullerene complexes.

A multistep process involving the generation of  $\text{Fe}^+$  by laser desorption from an iron target, reaction of  $\text{Fe}^+$  with gaseous pentane to form  $\text{Fe}(\text{C}_n\text{H}_{2n})^+$  ( $n = 2-5$ ) and subsequent ligand exchange with gaseous  $\text{C}_{60}$  or  $\text{C}_{70}$ , produces  $\text{FeC}_{60}^+$  and  $\text{FeC}_{70}^+$  which were isolated by ion cyclotron resonance techniques.<sup>191</sup> Collision-induced dissociation (CID) of  $\text{FeC}_{60}^+$  results in the formation of  $\text{C}_{60}^+$  and requires relatively small activation energies. The fragmentation to form  $\text{C}_{60}^+$ , rather than the loss of  $\text{C}_2$  units, and the low energies (0.6–11.8 eV in centers of mass energy) of this process were interpreted to indicate that the iron was bound to the exterior of the fullerene.

The bis- $\text{C}_{60}$  metal adduct,  $\text{Ni}(\text{C}_{60})_2^+$ , was observed in a related reaction in which  $\text{Ni}^+$  was prepared by laser desorption,  $^{58}\text{Ni}^+$  was isolated by double resonance ejection of the other Ni isotopes, and  $\text{C}_{60}$  vapor was reacted with  $^{58}\text{Ni}^+$  to generate  $^{58}\text{NiC}_{60}$  and subsequently  $^{51}\text{Ni}(\text{C}_{60})_2^+$ .<sup>192</sup> This work led to the suggestion that a family of bis-fullerene “dumbbell” complexes that are analogous to the metallocenes should be isolable. However, to date, with the exception of the polymeric materials such as  $\text{C}_{60}\text{-Pd}_n$ <sup>174,175</sup> and  $\text{NaCoC}_{60}\cdot 3\text{THF}$ ,<sup>154</sup> discrete bis-fullerene/metal complexes have not been isolated by wet chemical techniques.

Subsequent studies reveal that a range of externally bound complexes,  $\text{M}(\text{C}_{60})^+$  where M is Fe, Co, Ni, Cu, Rh, La, and VO, can be formed and that the Fe, Co, Ni, and Cu complexes dissociate to form  $\text{C}_{60}^+$  while  $\text{LaC}_{60}^+$  and  $\text{VOC}_{60}^+$  dissociate to form  $\text{La}^+$  and  $\text{VO}^+$ . The pattern of dissociations is in accord with the relative ionization potentials involved.<sup>193</sup>

The gas-phase reactions between an array of carbon cluster ions,  $\text{C}_n^+$ , and  $\text{Fe}(\text{CO})_5$  demonstrated that  $\text{C}_{60}^+$  and  $\text{C}_{70}^+$  display unique reactivities which has led to the formation of the highly abundant ions,  $\text{C}_{60}\text{Fe}(\text{CO})_4^+$  and  $\text{C}_{70}\text{Fe}(\text{CO})_4^+$ .<sup>194</sup> Collisionally induced dissociation of  $\text{C}_{60}\text{Fe}(\text{CO})_4^+$  forms  $\text{C}_{60}\text{Fe}(\text{CO})_n^+$  ( $n = 3, 2, 1, 0$ ) while secondary reactions of  $\text{C}_{60}\text{Fe}(\text{CO})_4^+$  with  $\text{Fe}(\text{CO})_5$  forms  $\text{C}_{60}\text{Fe}_2(\text{CO})_8^+$ ,  $\text{C}_{60}\text{Fe}_3(\text{CO})_8^+$ ,  $\text{C}_{60}\text{Fe}_3(\text{CO})_9^+$ , and  $\text{C}_{60}\text{Fe}_4(\text{CO})_{11}^+$ .

These gas-phase ions,  $\text{MC}_{60}^+$ , have been demonstrated to undergo further chemical modifications through gas-phase reactions. Thus,  $\text{Co}(\text{C}_{60})^+$  reacts

with  $\text{C}_{60}$  and with olefins (ethylene, propene, 1-butene, isobutene) to form  $\text{Co}(\text{C}_{60})_2^+$  and  $\text{Co}(\text{C}_{60})\text{olefin}^+$  in which dissociation data suggests that the added ligands are bound to the metal.<sup>195</sup> However, cyclopropane reacts with  $\text{Co}(\text{C}_{60})^+$  to form both  $\text{Co}(\text{C}_{60})\text{-}(\text{CH}_2)_{1-4}^+$  and  $\text{C}_{60}(\text{CH}_2)_{1-3}^+$ . CID of  $\text{Co}(\text{C}_{60})_n^+$  produces  $\text{C}_{60}(\text{CH}_2)_n$  ( $n = 1$  or  $2$ ) with low activation energies. Reaction of  $\text{C}_{60}$  with  $\text{Co}(\text{C}_{60})(\text{CH}_2)_n$  yields  $\text{C}_{60}\text{Co}(\text{C}_{60})(\text{CH}_2)_n$  rather than a simple ligand displacement.<sup>195</sup> As a consequence of these observed reactions,  $\text{Co}(\text{C}_{60})(\text{CH}_2)_n$  is proposed to have a metallacyclic structure with four- or five-membered rings that incorporate the fullerene, cobalt, and the methylene groups.

Related metallacycles have also been observed in gas-phase reactions of  $\text{Fe}(\text{benzynes})^+$  and  $\text{Fe}(\text{biphenylene})^+$  with  $\text{C}_{60}$ .<sup>196</sup> Thus  $\text{Fe}(\text{benzynes})^+$  and  $\text{C}_{60}$  react to form  $\text{Fe}(\text{C}_{60})(\text{C}_6\text{H}_4)^+$ . The ion  $\text{Fe}(\text{C}_{60})(\text{C}_6\text{H}_4)^+$  fragments by two routes upon collisionally induced dissociation to form  $\text{C}_{60}(\text{C}_6\text{H}_4)^+$  and Fe, and  $\text{Fe}(\text{C}_6\text{H}_4)^+$  and  $\text{C}_{60}$ , respectively. Of the three structures shown in Scheme 8 for  $\text{Fe}(\text{C}_{60})(\text{C}_6\text{H}_4)^+$ , it is suggested that the metallacyclic structure C is most consistent with the observed fragmentation pattern.

The gas-phase reaction of  $\text{Rh}(\text{C}_{60})^+$  with methyl iodide produces  $\text{C}_{60}\text{Rh}(\text{CH}_2)_n^+$  ( $n = 2$  or  $3$ ) for which metallacyclic structures that may or may not involve the fullerene have been considered.<sup>197</sup>

The gas-phase reactions of  $\text{Mn}^+$  and  $\text{Mn}_2^+$  with  $\text{C}_{60}$  in a guided-ion beam mass spectrometer have produced evidence for the existence of two forms of  $\text{Mn}(\text{C}_{60})^+$ .<sup>198</sup> In one form the manganese ion is weakly bound and this form is formulated as an exohedral adduct. The other form is more difficult to obtain yet is more stable toward decomposition. The latter form may be an endohedral complex with manganese trapped within the fullerene or it may be an exohedral adduct with the metal multiply bonded to the fullerene framework.

Transition metal atom coated fullerenes with much higher coverages of the exterior with metal centers have also been observed. Metal vapors were obtained by laser desorption of the metal inside a condensation cell and combined with fullerene vapor from a resistively heated oven.<sup>199,200</sup> The mixture is quenched by low-pressure helium and analyzed by time-of-flight mass spectrometry. Clusters of the types  $\text{C}_{60}\text{V}_x^+$ ,  $\text{C}_{60}\text{Ti}_x^+$ , and  $\text{C}_{60}\text{Zr}_x^+$  have been examined.<sup>199</sup> For Ti strong features in the mass spectra suggest special stability of  $\text{C}_{60}\text{Ti}_{80}^+$ ,  $\text{C}_{60}\text{Ti}_{72}^+$ , and  $\text{C}_{60}\text{Ti}_{62}^+$ . With  $\text{Ti}^+$  and  $\text{C}_{70}$ , the spectral features of ions with composition,  $\text{C}_{70}\text{Ti}_{86}^+$ ,  $\text{C}_{70}\text{Ti}_{73}^+$ , and  $\text{C}_{70}\text{Ti}_{62}^+$ , are especially intense. For vanadium and  $\text{C}_{60}$ , the magic numbers correspond to compositions  $\text{C}_{60}\text{V}_{86}^+$ ,  $\text{C}_{60}\text{V}_{73}^+$ , and  $\text{C}_{60}\text{V}_{62}^+$ . Photodissociation of these highly coated



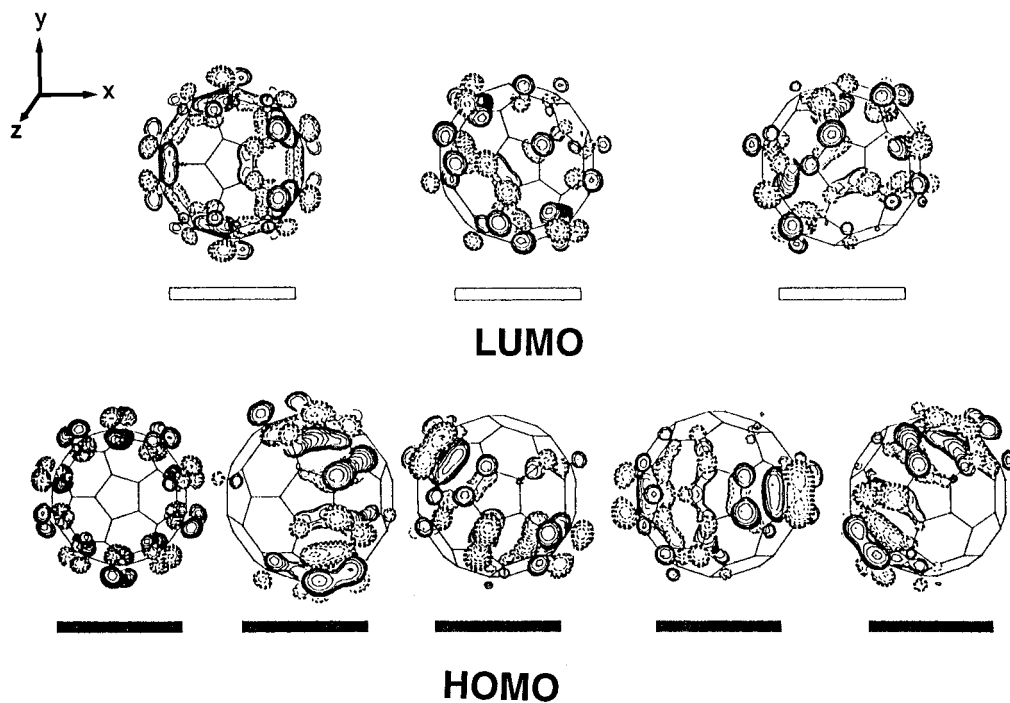


**Figure 56.** Orbital surface plots of the five  $h_u$  (HOMO) and three  $t_{1u}$  (LUMO) orbitals of  $C_{60}$  (Reprinted with permission from ref 209. Copyright 1994 Elsevier Science.)

clusters can yield either loss of single metal atoms or formation of metal-carbon clusters such as  $V_8C_{12}$ .<sup>201</sup> Related fullerenes with alkali and alkaline earth metal ions as outer coatings have also been observed.<sup>202-204</sup>

### V. Theoretical Studies of the Electronic Structures of Metal Fullerene Complexes

A number of theoretical analyses of the electronic structures of transition metal fullerene complexes have appeared. Several of these have focused on complexes of the type  $(\eta^2-C_{60})M(PR_3)_2$  with  $M = Pd$  or  $Pt$ .<sup>205-210</sup>

The symmetrical structure of  $C_{60}$  produces a set of degenerate HOMO and LUMO orbitals (see Figure 3) that are distributed over the surface of the molecule. Figure 56 shows the spatial distribution of the five degenerate  $h_u$  orbitals which constitute the HOMO and the three  $t_{1u}$  orbitals that are the LUMO.<sup>209</sup> These orbitals have been analyzed by fragment analysis which focuses on the 12 pentagonal faces of the fullerene.<sup>208,209</sup> Within the pentagons the frontier orbitals of  $C_{60}$  resemble the well-known  $e''$ -orbital of the cyclopentadienyl group with a single node perpendicular to the plane of the pentagon. The total electron density provided by filling of the set of five  $h_u$  orbitals (the HOMO's) is shown as **A** in Figure 57 while filling of the three  $t_{1u}$  orbitals produces the distribution shown as **B** in Figure 57.<sup>209</sup> The filled  $h_u$  orbitals provide net  $\pi$ -bonding that is localized over the 6:6 ring junctions of the fullerene and net  $\pi$ -antibonding between the carbon atoms at the 6:5 ring junctions. Thus the HOMO is set up to be an electron donor and the sites above the 6:6 ring junctions are optimal for  $\sigma$ -donation.

Lichtenberger and co-workers have systematically examined the bonding between a palladium atom or

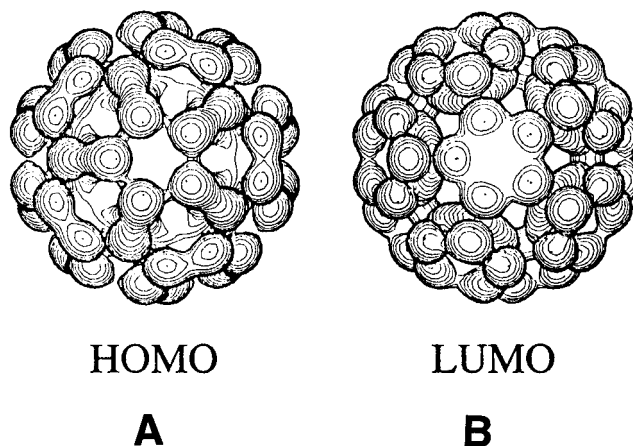


**Figure 57.** Surface electron density plots for a fully occupied  $h_u$  (HOMO), **A**, and  $t_{1u}$  (LUMO), **B**, orbitals of  $C_{60}$ . (Reprinted with permission from ref 209. Copyright 1994 Elsevier Science.)

a silver(I) ion and  $C_{60}$  at five different sites on the fullerene surface.<sup>205,209</sup> These sites are (1) directly over a single carbon atom (representing  $\eta^1$ -coordination), (2) above the midpoint of a 6:6 ring junction (representing  $\eta^2$ -coordination), (3) above the midpoint of a 6:5 ring junction, (4) above the center of a pentagonal face (representing  $\eta^5$ -coordination), and (5) above the center of a hexagonal face (representing  $\eta^6$ -coordination). Only two of these sites, the site above a 6:6 ring junction ( $\eta^2$ -bonding) and the site above a pentagonal face ( $\eta^5$ -bonding), lead to an attractive interaction; the others produced net repulsive interactions. The  $\eta^2$ -bonding site is favored over the  $\eta^5$ -bonding site, and the differentiation between these sites increases as the electron density on the metal increases. In general, the binding of  $C_{60}$  to a metal center is weaker than that to a smaller molecule such as ethylene.

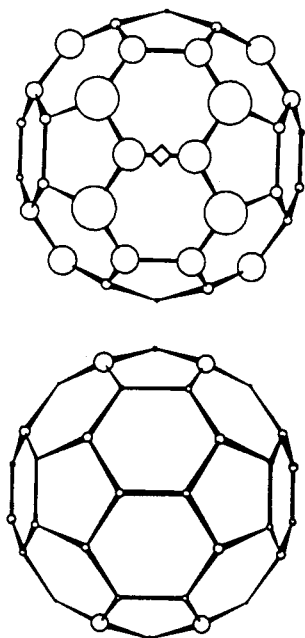


**Figure 58.** Sites of negative charge within  $(\eta^2\text{-C}_{60})\text{Pt}(\text{PH}_3)_2$ . The location of the platinum atom is designated by the small diamond. (Reprinted with permission from ref 205. Copyright 1993 Elsevier Science.)

The effects of multiple addition to  $\text{C}_{60}$  have also been probed. Calculations on  $(\eta^2\text{-C}_{60})\text{Pt}(\text{PH}_3)_2$  show that the negative charge transferred from platinum to the fullerene is delocalized to a greater extent in  $\text{C}_{60}$  than it is in the corresponding ethylene complex.<sup>205,209</sup> The effect is localized in the hemisphere closest to the metal as seen in Figure 58.<sup>205</sup> There is nearly negligible perturbation of the more remote hemisphere. Consequently, it is difficult to predict the pattern of multiple additions to  $\text{C}_{60}$ . Calculations on the equatorial and trans-1 isomers (see Figure 2) of  $(\eta^2\text{-C}_{60})\text{Ni}(\text{PH}_3)_2$  reveal a negligible energetic difference between the isomers.<sup>206</sup> However, another extended Hückel analysis of  $(\eta^2\text{-C}_{60})\text{Pt}(\text{PH}_3)_2$  revealed a slight preference for the second addition occurring at the trans-1 site as is experimentally observed for the double addition of iridium compounds (see Figures 21 and 22).<sup>208</sup> The metal- $\text{C}_{60}$   $\pi^*$ -antibonding orbital which should be the third LUMO could be responsible for stabilization of the trans-1 site. Analyses of the electronic structure of the hexa-addition product,  $\text{C}_{60}\{\text{Pt}(\text{PEt}_3)_2\}_6$ , (Figure 47) have also been made.<sup>206,208</sup>

The electronic structure of  $\text{C}_{60}\text{O}_2\text{OsO}_2(\text{py})_2$  has also been examined by molecular orbital calculations.<sup>52</sup> These calculations show that the molecular orbitals near the frontier portion are not strongly affected by the addition of the osmyl group and that the orbitals that are involved in the formation of the adduct lie lower in energy. In the osmylation product, the HOMO-LUMO gap is narrowed relative to that in unreacted  $\text{C}_{60}$ .

Electronic structure calculations have also been used to probe the differences between  $(\eta^5\text{-C}_5\text{H}_5)$  and  $(\eta^5\text{-C}_{60})$  coordination as well as those between  $(\eta^6\text{-C}_6\text{H}_6)$  and  $(\eta^6\text{-C}_{60})$  coordination.<sup>78,208-211</sup> The  $[\text{M}(\eta^5\text{-C}_5\text{H}_5)]^+$  ( $\text{M} = \text{Fe}, \text{Ru}, \text{Os}$ ) moiety bonds more strongly to a  $(\eta^5\text{-C}_5\text{H}_5)^-$  unit than to a pentagonal fullerene

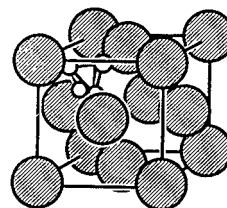


**Figure 59.** A schematic drawing showing the hypothetical bonding of one  $\text{M}_4$  ( $\text{M} = \text{Co}$  or  $\text{Rh}$ ) unit within the fcc lattice of  $\text{C}_{60}$ . (Reprinted from ref 213. Copyright 1996 American Chemical Society.)

face. The overlap population is greater for bonding to the cyclopentadienyl group than it is for the fullerene.<sup>211</sup> Additionally, the cyclopentadienyl anion is a better donor of electron density than is the fullerene. The effects are accentuated when the six-membered rings of benzene and those of  $\text{C}_{60}$  are compared. Overlap populations are greater for coordination of a  $\text{M}(\eta^6\text{-C}_6\text{H}_6)$  ( $\text{M} = \text{Cr}, \text{Mo}, \text{W}$ ) unit to another benzene molecule than for coordination to a hexagonal face of  $\text{C}_{60}$ .

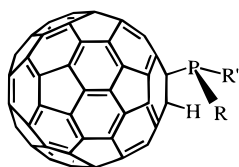
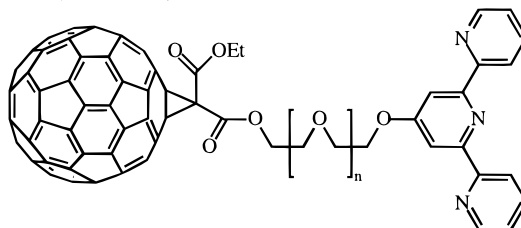
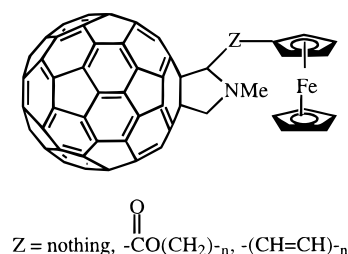
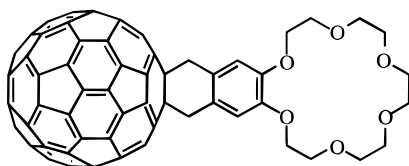
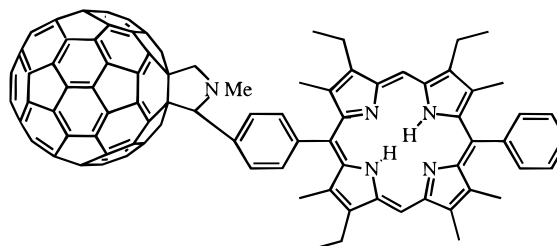
The natures of metal-fullerene interactions have also been explored in terms of the pyramidalization of the fullerene carbon atoms, the strain present within these curved clusters, and the strain release that accompanies adduct formation.<sup>212</sup> The analysis of the orientation of the surface  $\pi$ -orbitals suggests that while  $\eta^5$ - and  $\eta^6$ -coordination on the exterior faces of fullerenes is unfavorable, the interior surface presents  $\pi$ -orbitals that are well disposed for overlap with metal centers.

Calculations have also been performed on hypothetical metal cluster fullerides with composition  $\text{C}_{60}\text{-}(\text{M}_4)_2$  where  $\text{M}$  is either cobalt or rhodium.<sup>213,214</sup> Goldberg and Hoffmann have found that it is geometrically feasible to utilize the tetrahedral and octahedral holes in the face-centered cubic structure of solid  $\text{C}_{60}$  to bind tetrahedral  $\text{M}_4$  units and octahedral  $\text{M}_6$  units, respectively. A schematic drawing that shows the location of one such tetrahedral unit in the  $\text{C}_{60}$  lattice is shown in Figure 59. Molecular orbital and band structure calculations indicate that the bonding within this sort of fulleride has a significant covalent component and thus differs from the alkali metal fullerides.<sup>10</sup> The  $\text{C}_{60}(\text{M}_4)_2$  materials are predicted to be metallic but there is no way of predicting whether they will be superconducting.<sup>214</sup> It remains to be seen whether known, isolated, but amorphous, materials such as  $\text{C}_{60}\text{Pd}_n$  contain metal cluster units within their structures.

## VI. Fullerenes with Ligating Centers Attached

With the development of an extensive organic chemistry of fullerenes, it is now possible to construct a variety of modified fullerenes that incorporate metal-binding groups into their structure. The synthesis of such fullerene-containing ligands offers the potential to exploit the chemical reactivity, redox and electron-acceptor characteristics, photochemical behavior, electron-withdrawing properties, and novel structural features that a fullerene group provides. The molecules in this class of fullerene-containing

## Scheme 9. Selected Examples of Fullerenes Bearing Ligating Substituents

Fullerene-Phosphines  
(ref. 215,216)Fullerene-Polypyridines  
(ref. 217-220)Fullerene-Metalloenes  
(ref. 221,222)Fullerene-Crown Ethers  
(ref. 223-225)Fullerene-Porphyrins  
(ref. 226-234)

ligands have metal-binding sites that are generally remote from the fullerene.

A survey of some selected examples of these ligands is shown in Scheme 9.<sup>215-234</sup> These fullerene-containing ligands include relatively simple molecules such as the fullerene phosphines,<sup>215,216</sup> along with more complex structures that include polypyridine groups,<sup>217-220</sup> metallocenes,<sup>221,222</sup> crown ethers,<sup>223-225</sup> and porphyrins.<sup>226-234</sup> The attachment of the more complex structures is generally accomplished through cyclopropanation with a diazomethane or through addition of an azomethine ylide.

The fullerene phosphines, however, have been made through the direct addition of phosphide or borane-protected phosphide nucleophiles to  $C_{60}$  and subsequent protonation of the resulting anion.<sup>215,216</sup> Some palladium and platinum complexes of these fullerene phosphines have been made. These complexes, of the type (fullerene phosphine)<sub>2</sub>MCl<sub>2</sub>, show both multielectron redox behavior and catalytic activity in Grignard reagent/styrene cross coupling reactions.<sup>216</sup>

The fullerene-ferrocene compounds have been utilized to probe intramolecular electron transfer.<sup>221,222</sup> Steady-state fluorescence and time-resolved flash photolysis studies have been utilized to examine the effect of a variety of spacers on the electron-transfer kinetics between the two components.<sup>221</sup> With saturated spacers between the ferrocene and fullerene moieties, long-lived charge separated states with  $\tau_{1/2} = 2 \mu\text{s}$  have been observed.<sup>221</sup> Related studies of intramolecular charge transfer in fullerene-porphyrin diads and related fullerene-porphyrin-carotene triads have been conducted.<sup>234</sup>

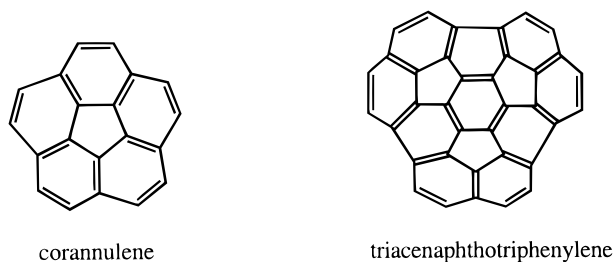
Chemically modified fullerenes that bear additional olefinic groups or acetylene functions can also act as ligands through these added units. In part, that is the case with the modified fullerene shown in Scheme

5.<sup>151</sup> Alkynyl(hydride) adducts of  $C_{60}$  have these substituents placed at 1,2-positions on the cage.<sup>235</sup> 2-H,1-(Me<sub>3</sub>SiC≡C) $C_{60}$  reacts with  $\text{Co}_2(\text{CO})_8$  to form {2-H,1-(Me<sub>3</sub>SiC≡C) $C_{60}$ }Co<sub>2</sub>(CO)<sub>6</sub> and with  $(\eta^5\text{-C}_5\text{H}_5)_2\text{Ni}_2(\text{CO})_2$  to form {2-H,1-(Me<sub>3</sub>SiC≡C) $C_{60}$ }Ni<sub>2</sub>( $\eta^5\text{-C}_5\text{H}_5$ )<sub>2</sub>.<sup>235</sup> The structure of the latter complex has been determined by X-ray crystallography and shown to involve coordination of both nickel atoms to the acetylenic portion of the molecule. There is no direct interaction of the nickel atoms and the fullerene portion of the compound.

Polyhydroxylated fullerenes, fullerlenols- $C_{60}(\text{OH})_x$ , which are available through a variety of chemical routes,<sup>236,237</sup> have been converted into polydentate phosphine ligands.<sup>238</sup> Thus chloro diphenylphosphine reacts with  $C_{60}(\text{OH})_{12}$  to produce the highly air-sensitive  $C_{60}(\text{OPPh}_2)_{12}$ , which forms complexes with transition metals.<sup>238</sup> For example, reaction with {RhCl(CO)<sub>2</sub>}<sub>2</sub> produces a brown material formulated as  $C_{60}(\text{OPPh}_2)_{12}\{\text{RhCl}(\text{CO})_2\}_6\{\text{RhCl}(\text{CO})\}_3$ . Similarly, an orange brown compound which analyzed as  $C_{60}(\text{OPPh}_2)_{12}\text{Mo}_9(\text{CO})_{31}\cdot 2\text{PPh}_3\cdot 5\text{H}_2\text{O}$  was obtained from the reaction of  $\text{Mo}(\text{CO})_2(\text{MeCN})_2(\text{PPh}_3)_2$  and  $C_{60}(\text{OPPh}_2)_{12}$ .

## VII. Coordination Chemistry of Fullerene Fragments

A number of polyaromatic hydrocarbons (PAH's) with nonplanar structures that are related to the fullerenes are known, and the number of these curved hydrocarbons is growing.<sup>239-241</sup> The simplest fullerene fragment is corannulene,  $C_{20}\text{H}_{10}$ , which has a central five-membered ring that is surrounded by five hexagonal rings.<sup>242</sup> At present, the largest fullerene-like fragment which has been isolated and characterized is triacenaphthotriphenylene,  $C_{36}\text{H}_{12}$ .<sup>243</sup> This compound has a hexagonal base that is surrounded by,



and part of, three corannulene-like units. Figure 60 shows the crystallographically determined structures of the bowl-shaped hydrocarbons  $C_{20}H_{10}$ <sup>244</sup> and  $C_{36}H_{12}$ <sup>245</sup> and compares these to the structure of  $C_{60}$ .<sup>246</sup> While corannulene is flatter than the corresponding portion of  $C_{60}$ , the base of  $C_{36}H_{12}$  is very similar to the corresponding part of  $C_{60}$  but splays outward at its rim. The pyramidalization (as defined by the  $\pi$ -orbital axis vector, POAV)<sup>112</sup> of the five base carbon atoms in  $C_{20}H_{10}$  ( $98.72^\circ$ ) is significantly less than that of  $C_{60}$  ( $101.64^\circ$ ), but the pyramidalization ( $101.91$  and  $102.38^\circ$  for the two types of carbon atoms) for the six carbon atoms in the base of  $C_{36}H_{12}$  is actually greater than that in  $C_{60}$ . The availability of these novel hydrocarbons allows the study not only of the exterior surfaces of curved, fullerene-like molecules, but also of the interior surfaces and the edges.

It is likely that the chemistry of these curved fullerene fragments will develop rapidly in the near future, but so far only two studies of their reactivity toward a transition metal complexes have been reported. The reaction of corannulene with  $[(\eta^5-C_5Me_5)Ru(CH_3CN)_3^+](O_3SCF_3^-)$ , known for its ability to react with a variety of hydrocarbons through replacement of the three acetonitrile ligands, produces  $[(\eta^6-C_{10}H_{20})Ru(\eta^5-C_5Me_5)^+](O_3SCF_3^-)$  which has been characterized spectroscopically in solution.<sup>247</sup> Analysis of the variable-temperature  $^1H$  NMR spectra of the complex indicates that the ruthenium atoms is coordinated to one hexagonal ring of the corannulene moiety and that the ruthenium center remains on that one ring on the NMR time scale. It is not presently known whether the metal is bound to the concave or the convex surface of corannulene, but the NMR spectral data are consistent with either rapid concave/convex interconversion or slow concave/convex interconversion with only one isomer being detectable.  $[(\eta^6-C_{10}H_{20})Ru(\eta^5-C_5Me_5)^+](O_3SCF_3^-)$  is sensitive to atmospheric conditions and readily undergoes exchange of the corannulene portion for either three acetonitrile molecules or one benzene molecule.

The reaction of semibuckminsterfullerene,  $C_{30}H_{12}$ , with  $Pt(C_2H_4)(PPh_3)_2$  does not result in simple coordination of a  $Pt(PPh_3)_2$  unit to a 6:6 ring junction but rather to insertion of the platinum into one of the C–C bonds on the edge of the hydrocarbon as shown in eq 18.<sup>248</sup> The structure of the product, which retains considerable curvature in the hydrocarbon portion, is shown in Figure 61. The unusual C–C bond breaking seen in eq 18 has been attributed to relief of the strain present in the five-membered rings at the edge of the parent hydrocarbon. Related reactivity at the edge of another fullerene fragment,

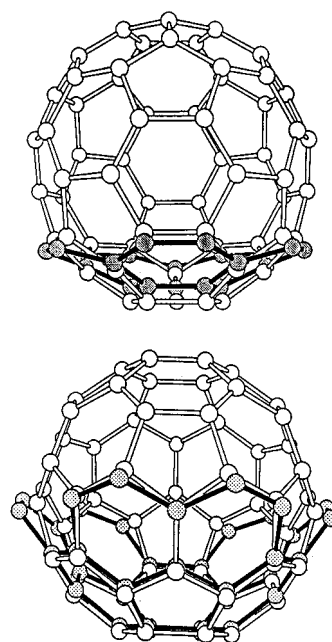


**Figure 60.** A comparison of the carbon atom positions of  $C_{20}H_{10}$  (corannulene) and  $C_{60}$ , and  $C_{36}H_{12}$  and  $C_{60}$  (from data in refs 244 and 245). The  $C_{60}$  structure is shown with hollow lines between the atomic positions.

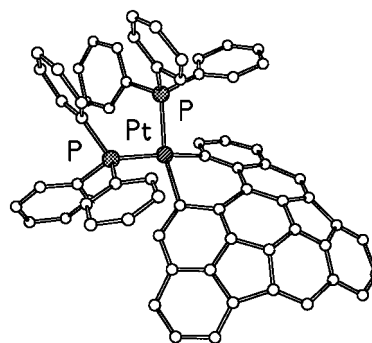
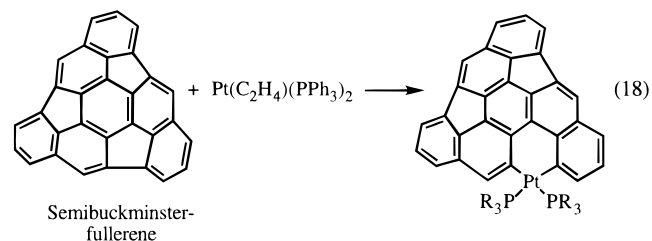


**Figure 61.** The structure of  $(C_{36}H_{12})Pt(PPh_3)_2$  (from data in ref 248).

$C_{36}H_{14}$ , has been observed to result in facile oxidation, with cleavage of a C–C bond within a six-membered ring, to produce the nearly planar dione,  $C_{36}H_{14}O_2$ .<sup>249</sup>



## VIII. Transition Metals and Carbon Nanotubes and Other Nanostructures

Carbon nanotubes are hollow tubules that are made up of cylindrical graphitic shells with diameters of 10 to 25 Å.<sup>250,251</sup> The nanotubes, which may be as long as several microns, can be single-walled or nested inside one another. For the nested, multi-walled tubes the spacing between the layers is  $\sim 3.4$  Å, which is the typical spacing also seen in graphite sheets. The structural features of these tubes are

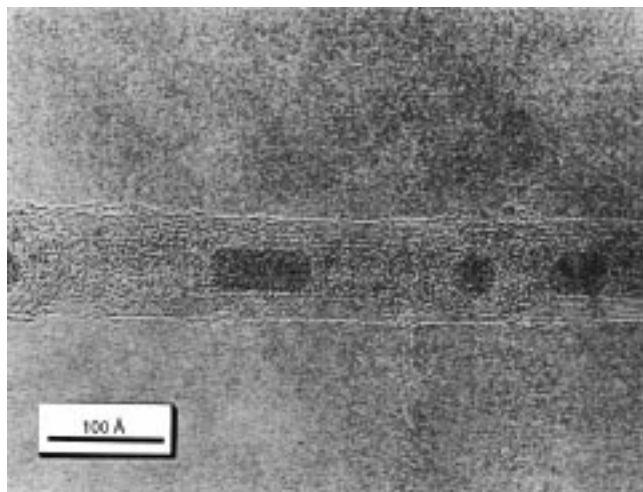


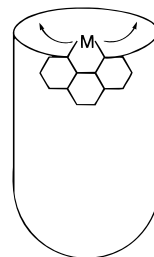
**Figure 62.** A high-resolution transmission electron micrograph of a carbon nanotube which is partially filled with spherical nanoparticles of silver. (Reprinted from ref 252a. Copyright 1996 American Chemical Society.)

generally probed by electron microscopy. Figure 62 shows an high-resolution transmission electron micrograph of a multiwalled carbon nanotube.<sup>252</sup> In this case the hollow space in the center of the tube is partially filled with spherical nanocrystals of silver (vide infra), but completely hollow tubes exist as well. Many potential applications of filled and empty nanotubes have been suggested based on the unique electronic, mechanical and magnetic properties of these nanostructures. Transition metals have been observed to influence the growth patterns in nanotube formation and serve as catalysts for their preparation. Additionally, transition metals or their compounds have also been incorporated on the interior (as seen in Figure 62) and exterior of the nanostructures themselves.

Carbon nanotubes are formed by several processes. The arc discharge process utilizing graphite rods in a low-pressure helium atmosphere that was initially developed for the preparation of fullerenes also can produce carbon nanotubes.<sup>253</sup> When transition metals are also present during the arc discharge process, the formation of threadlike filaments of single-walled nanotubes is frequently enhanced.<sup>254–259</sup> The initial preparations used graphite rods with small amounts of iron and an argon/methane atmosphere or graphite rods with a cobalt metal insert and a helium atmosphere.<sup>255,256</sup> In the case of iron, the formation of round particles of  $\text{Fe}_3\text{C}$  accompanied the formation of the nanotubes while in the cobalt case, cobalt clusters formed along with the nanotubes. Other metals used include iron, cobalt, nickel, copper, platinum, silver, lanthanum, tungsten, and yttrium. Of these, silver, lanthanum, tungsten, and copper were not effective in producing single-walled nanotubes, while the other metals did enhance single-walled nanotube formation.

Carbon nanotubes can also be obtained through catalytic decomposition of acetylene and other hydrocarbons.<sup>260–263</sup> Transition metal catalysts including cobalt on silica and iron on silica and zeolites have been utilized. Both straight and coiled nanotubes can be obtained from these procedures.

Laser vaporization of composite rods of graphite with nickel and cobalt in an oven at 1200 °C results in a high yield (50% of vaporized carbon) of single-walled nanotubes.<sup>264–266</sup> This method is reported to give greater control over the preparation. It has been utilized to give single-walled nanotubes with metallic conductivity which are organized in “ropes” that involve 100–500 nanotubes packed together in a triangular fashion.<sup>265</sup> The role of the cobalt or nickel “catalysts” in these preparations has been suggested to involve a metal ion chemisorbed at an open edge of the carbon net as shown below:



Notice that the structure suggested for this intermediate is modeled by the platinum complex shown in Figure 61 where a platinum atom is situated on the edge of a fullerene fragment.<sup>248</sup> Mobility of the metal atom about the edge of the growing tube is postulated to keep the tube structure intact by annealing any pentagonal units or other high energy defects in the (10,10) single-walled nanotube.<sup>265</sup>

Isolated single-walled carbon nanotubes can also be obtained from the disproportionation of carbon monoxide at 1200 °C with a molybdenum catalyst.<sup>267</sup> The catalyst is prepared from bis(acetylacetonato)-dioxomolybdenum(VI) and fused alumina nanoparticles. The diameter of the tube that forms is related to the size of the catalyst particle which is found attached at the end of the tube.

The growth of carbon nanotubes with a variety of different metal catalysts and procedures has spawned speculation on the mechanisms of tube growth.<sup>265,267–269</sup> In addition to the scooting of metal atoms about the edge of a growing tubule as shown in the diagram above, other proposals have emerged. For the case of catalysis by molybdenum particles, a “yarmulke mechanism” is proposed by which nanotubes are nucleated by a catalytic particle that protects the tube from having a vulnerable open edge during growth. Molecular dynamics calculations have provided a theoretical framework for the growth of single-walled nanotubes from metal carbide particles through a root-growth mechanism.<sup>268</sup> The possibility that  $\text{C}_{60}$  acts as a template during single-walled nanotube growth has been suggested.<sup>269</sup> A schematic drawing of this concept is shown in Figure 63. In this proposed process, the metal atoms (cobalt or nickel in the case of 10,10 nanotube formation) are  $\pi$ -bound to the outside of the fullerene as well as to the inside of the nanotube. The geometric factors for such a model closely predict the outer circumference of the nanotube to be 13.6–13.8 Å, which agrees with the experimental data, and the model has been used to make a set of predictions about nanotube growth.<sup>269</sup>

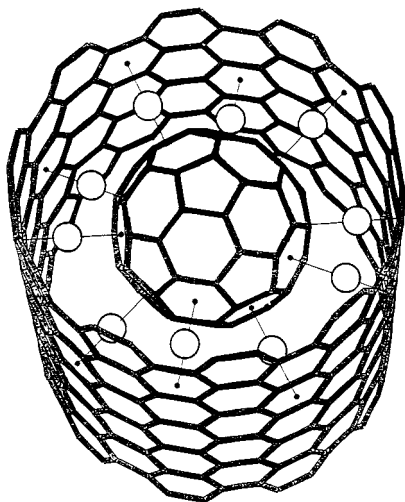


**Figure 63.** A drawing of the proposed role of  $C_{60}$  as a template for carbon-nanotube formation in which metal atoms are simultaneously bound to the fullerene and the nanotube (Reprinted with permission from ref 269. Copyright 1997 Elsevier Science.)

Carbon particles containing transition metals or compounds are found not only at the ends of nanotubes but also encased within graphitic networks. For example, crystalline gold clusters have been found to be enclosed within graphitic carbon onion-like units which are produced by the arc discharge with gold-impregnated graphite rods.<sup>270</sup> In an intense electron beam, these gold clusters migrate out of the graphitic cages, presumably through a process of opening and subsequent closing of the fullerene-like cages.

Polyhedral carbon particles with diameters of 20–40 nm have been found to encapsulate microcrystalline  $LaC_2$ .<sup>271</sup> These particles were obtained via the arc discharge method with  $La_2O_3$ -doped graphite rods. The carbon framework was found to protect the  $LaC_2$  core from hydrolysis. Carbon nanocapsules containing platinum group metals have also been obtained via arc discharge techniques<sup>272</sup> as have capsules containing hafnium.<sup>273</sup>

The arc discharge method has also been used to form carbon nanotubes filled with a variety of metals or metal carbides including those of the transition metals: Ti, Cr, Fe, Co, Ni, Cu, Zn, Mo, Pd, Ta, and W.<sup>272</sup> Continuous “nanowires” are observed in many cases to completely fill the interior of these tubes.<sup>272</sup>

Preformed carbon nanotubes have been found to bind transition metals on either their interior or exterior surfaces.<sup>275–285</sup> Open carbon nanotubes tubes can be filled with molten materials such as  $V_2O_5$  and  $MoO_3$  through capillary action.<sup>278,279</sup> Oxidation can open the curved, closed ends of nanotubes, and allow chemicals access to the interior space within a tube.<sup>275–277</sup> However, oxidation can also introduce acidic surface groups ( $-CO_2H$  and  $-OH$ ) on the nanotubes, and these acidic groups offer another favorable site for binding metal complexes on the nanotube outer surface.<sup>277,283</sup> Treatment of such oxidized, opened nanotubes with aqueous solutions of palladium nitrate followed by drying, and reduction under  $H_2$  at 250 °C results in crystallites of metallic palladium on the inside and the outside of

the nanotubes.<sup>275</sup> Solid metal carbide nanorods have been obtained by treating empty carbon nanotubes with volatile oxide or halide species ( $TiO$  or  $Ti + I_2$ ).<sup>280</sup>

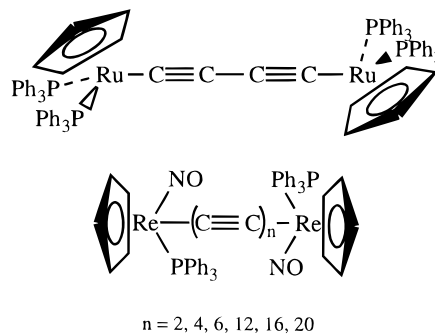
Carbon nanotubes have been utilized as supports for heterogeneous catalysts by treating a suspension of the tubes with tris(2,5-pentanedionate)ruthenium(III), evaporation and reduction under hydrogen.<sup>286</sup> The catalyst, which has ruthenium particles on the outside of the tubes (from transmission electron microscopy), is more selective than a corresponding material with an  $Al_2O_3$  support in the hydrogenation of cinnamaldehyde to cinnamyl alcohol.

### IX. Other Related Transition Metal–Carbon Compounds

A number of related transition metal–carbon compounds have also attracted interest in recent years. These include complexes of other, all-carbon ligands as well as species in which a carbon–metal framework forms.

As noted earlier, there are extensive studies on fullerenes with a variety of metal ions, general lanthanide and alkaline earth ions, residing on the interior—the endohedral fullerenes.<sup>20</sup> A comprehensive review on these is in preparation. At this stage, there is a considerable body of evidence that indicates that indeed the metal centers reside within the interior of the fullerene. However, definitive structural information regarding details of the metal fullerene interaction remains lacking in this area. Thus as seen in this review, we know in detail how metals bind to the outer surface of fullerenes and how they produce small but significant alterations to the fullerene structure. But comparable information about the structural effects of metals on the inside of fullerenes is lacking.

There has been considerable development of the chemistry of organometallic species with acetylenic and polyacetylene chains. These rodlike  $(-C_2-)_n^{2-}$  units can form bridges between organometallic end caps. The ruthenium and rhenium complexes shown below are examples of the types of complexes that form:<sup>287, 288</sup>



The family of rhenium complexes that have been isolated is really quite remarkable. A set of molecules with 4, 6, 8, 12, 16, and 20 carbon atoms in linear arrays have been produced and isolated as crystalline solids.<sup>288</sup> These molecules have interesting electronic transitions with molar extinction coefficients over  $10^5 M^{-1} cm^{-1}$  in their visible absorption

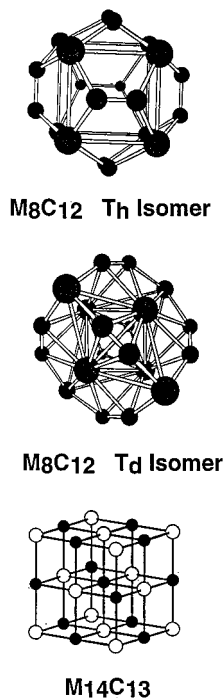


**Figure 64.** Proposed structures for  $M_8C_{12}$  and  $M_{14}C_{13}$  ( $3 \times 3 \times 3$  fcc lattice structure) (from refs 298 and 300).

spectra. The electronic transitions move to the red as the carbon chain length increases. A review on these all-carbon ligands, which also includes discussion of the cyclo- $C_3$  bridging ligand, is available.<sup>289</sup>

Castleman and co-workers and others have identified a family of metal-carbon clusters, "metcars", that are formulated as polyhedral arrays made of carbon and metal atoms.<sup>290-296</sup> The first of these is  $[Ti_8C_{12}]^+$ , for which both the  $T_h$  and  $T_d$  structures shown in Figure 64 have been proposed.<sup>290,297,298</sup> This species has been prepared by reaction of titanium atoms with hydrocarbon ( $CH_4$ ,  $C_2H_2$ ,  $C_6H_6$ , etc.) vapors and identified by mass spectrometry. Evidence that the titanium atoms are on the surface of this cluster comes from its reactivity. In the gas phase  $[Ti_8C_{12}]^+$  reacts with ammonia to form the series of adducts,  $[Ti_8(NH_3)_nC_{12}]^+$  with  $n = 0-8$ , in which the ammonia molecules appear to be coordinated to the titanium atoms.<sup>290</sup> Related adducts are known to be formed with  $\pi$ -bonding molecules such as ethylene and with halogens.<sup>293,295</sup> Clusters of the type  $[M_8C_{12}]^+$  with vanadium, zirconium, and hafnium as well as with chromium, molybdenum, and iron have also been observed via mass spectrometric techniques.<sup>291,296</sup>

Although these metcars are generally studied in the gas phases, there is one report that solid material containing neutral  $M_8C_{12}$  ( $M = Ti, V$ ) has been isolated.<sup>299</sup> This synthesis utilizes the arc discharge method with titanium/graphite or vanadium/graphite composite rods. The procedure yields a soot containing fullerene as well as metal, metal oxides, and the metcars in yields up to 1%. However, no information regarding the solubility or solution-phase properties of  $Ti_8C_{12}$  has yet appeared. Manipulation of these metcars in solution will probably require utilization of a suitable coordinating environment to supply

ligands to bind to the metal atoms and to segregate individual clusters.

In addition to the  $[M_8C_{12}]^+$  clusters, a family of larger clusters can also be observed when laser-evaporated titanium or vanadium reacts with methane or acetylene.<sup>300</sup> Among these, the  $[M_{14}C_{13}]^+$  ( $M = Ti, V$ ) clusters are particularly abundant and stable. These clusters are believed to have the structure of a  $3 \times 3 \times 3$  fcc lattice fragment, as shown in Figure 64. Theoretical calculations relating to the electronic structure and reactivity of this unit are available.<sup>301,302</sup> The  $[M_{14}C_{13}]^+$  is postulated to contain isolated carbon atoms, whereas  $[M_8C_{12}]^+$  contains six  $C_2$  units.

Metal atoms can also be incorporated into the fabric of a fullerene framework.<sup>303,304</sup> Gas-phase  $[NbC_n]^+$  clusters are generated by pulsed laser vaporization of niobium carbide/graphite composite rods and studied by injection-ion drift-tube mass spectrometry.<sup>303</sup> Fullerene, bicyclic ring, and monocyclic ring species are formed in this process. For even-numbered carbon clusters, the drift time behaviors of  $[C_{40}]^+$  and  $[NbC_{40}]^+$  are similar, and an endohedral structure is proposed for  $[NbC_{40}]^+$ . However, for  $[NbC_{39}]^+$  the drift time is longer than for either  $[NbC_{40}]^+$  or  $[C_{40}]^+$ . Additionally,  $[NbC_{n(\text{even})}]^+$  is unreactive toward  $N_2$  and  $O_2$ , whereas  $[NbC_{n(\text{odd})}]^+$  reacts with the added gases. Thus, it is concluded that the  $[NbC_{n(\text{odd})}]^+$  units have a fullerene-type structure with the niobium atoms as an integral part of the shell. However, it is probable that the niobium atom protrudes from the carbon shell because of the greater length of the Nb-C bonds relative to the C-C bonds.<sup>303</sup> Similar data have been obtained for  $[La_2C_n]^+$  ( $n = 28-100$ ) metallofullerenes.<sup>304</sup> Notice that a related structure with a cobalt atom incorporated into the framework of a chemically modified  $C_{60}$  molecule is formed in Scheme 5.<sup>151</sup> Its structure is shown in Figure 43.

## X. Conclusions

Starting with the observations that gas-phase metal ions could be attached to the outer surfaces of the fullerenes,<sup>191,192</sup> there has been extensive development of the condensed phase inorganic and organometallic fullerene chemistry with transition metals. Several types of products of reactions of transition metal complexes with fullerenes have been identified.

Direct coordination of metal centers to fullerenes so far has led almost exclusively to the isolation of the  $\eta^2$ -type of compounds, even in cases of addition of multiple metal centers to the fullerene. Although several metal centers can be appended to a single fullerene; the highest coverage achieved for an isolated complex involves the six platinum atoms bound to  $C_{60}$  in  $C_{60}\{Pt(PEt_3)_2\}_6$  (see Figure 47),<sup>165</sup> as well as the six ruthenium centers attached to  $C_{70}$  in  $C_{70}\{Ru_3(CO)_9\}_2$  (see Figure 13).<sup>70</sup> This coverage does not come close to rivaling the high metal coatings observed in gas-phase studies.<sup>199,200</sup> While bis-fullerene complexes have been observed in the gas phase,<sup>192</sup> an example of an isolated form of such a bis-fullerene complex has yet to be prepared. While the fullerene unit may seem large, from the viewpoint of attach-

ment to a metal center, it is not an exceptionally bulky ligand. The cone angle of C<sub>60</sub> has been estimated to be 120°,<sup>305</sup> and consequently the formation of bis- and even tris-fullerene-ligated metal complexes may be anticipated as sterically feasible.

As seen in reactions 4 and 12 and Scheme 3, metal complexes such as OsO<sub>4</sub> and S<sub>2</sub>Fe<sub>2</sub>(CO)<sub>6</sub> add to fullerenes through ligand sites which become bridges between the fullerene and the metal. The discovery of a wider variety of such ligand additions to fullerene surfaces may be anticipated, as the range of metal complexes used to explore fullerene reactivity increases.

The ability of the fullerene unit to accept electrons means that redox reactions have the potential to occur whenever strongly reducing reagents are involved in reactions with fullerenes. This mode of reaction is particularly predominant in the reactions of many first row transition metal metallocenes with C<sub>60</sub>, where a number of fulleride salts have been prepared.

One of the more remarkable features of fullerenes is their ability to cocrystallize with an array of different molecules. The formation of such crystalline materials is not limited to transition metal complexes, but there are a variety of transition metal complexes that do cocrystallize as can be seen by referring to Figures 17, 18, 19, 45, 53, and 54. In some of these there may be a degree of ground-state electron transfer involved in stabilization of the solid array.

Chemically modified fullerenes promise to present even more varied features to the array of reactions of fullerenes with transition metal complexes. The remarkable reactions shown in Scheme 5, where a fullerene C–C bond is ruptured and a cobalt atom is incorporated into the fullerene core,<sup>151</sup> and those shown in Scheme 7, where a five-membered ring capable of η<sup>5</sup>-coordination is isolated on the fullerene surface,<sup>187</sup> give a good indication of the new directions that can be expected in this area.

## XI. Acknowledgments

The authors express their appreciation for all of the work of their many collaborators who have been involved in the fullerene field. Research at UC Davis on fullerenes has been supported by the National Science Foundation (currently grant CHE 9610507). We especially thank Dr. Saeed Attar, Richard Koerner, Amy Levy, and Eileen Rivera for assistance in the preparation of this manuscript.

## XII. References

- Kroto, H. W.; Heath, J. R.; O'Brien, S. C.; Curl, R. F.; Smalley, R. E. *Nature* **1985**, *318*, 162.
- Krätschmer, W.; Lamb, L. D.; Fostiropoulos, K.; Huffman, D. R. *Nature* **1990**, *347*, 354.
- Hirsch, A. *The Chemistry of Fullerenes*; George Thieme Verlag: Stuttgart, 1994.
- Taylor, R., Ed. *The Chemistry of Fullerenes*; Advanced Series in Fullerenes; World Scientific Publishing Co.: Singapore, 1995; Vol. 4.
- Bürgi, H. B.; Blanc, E.; Schwarzenbach, D.; Liu, S.; Lu, Y.; Kappes, M. M.; Ibers, J. A. *Angew. Chem., Int. Ed. Engl.* **1992**, *31*, 640.
- Hirsch, A.; Lamparth, I.; Karfunkel; H. R. *Angew. Chem., Int. Ed. Engl.* **1994**, *33*, 437.
- Crane, J. D.; Hitchcock, P. B.; Kroto, H. W.; Taylor, R.; Walton, D. R. M. *J. Chem. Soc., Chem. Commun.* **1992**, 1764.
- Dubois D.; Kadish, K. M.; Flanagan, S.; Haufiler, R. E.; Chibante, L. P. F.; Wilson, L. J. *J. Am. Chem. Soc.* **1991**, *113*, 4364. Dubois, D.; Jones M. T.; Kadish, K. M. *J. Am. Chem. Soc.* **1992**, *114*, 6446.
- Xie, Q.; Perez-Cordero, E.; Echegoyen, L. *J. Am. Chem. Soc.* **1992**, *114*, 4. Ohsawa, Y.; Saji, T. *J. Chem. Soc., Chem. Commun.* **1992**, 781.
- Gunnarsson, O. *Rev. Mod. Phys.* **1997**, *69*, 575. Buntar, V.; Weber, H. W. *Supercond. Sci. Tech.* **1996**, *9*, 599.
- Xie, Q.; Arias, F.; Echegoyen, L. *J. Am. Chem. Soc.* **1993**, *115*, 9818.
- Taylor, R.; Hare, J. P.; Abdul-Sada, A. K.; Kroto, H. W. *J. Chem. Soc., Chem. Commun.* **1990**, 1423.
- Hare, J. P.; Dennis, T. J.; Kroto, H. W.; Taylor, R.; Allaf, A. W.; Balm, S.; Walton, D. M. R. *J. Chem. Soc., Chem. Commun.* **1991**, 412.
- Bakowies, D.; Theil, W. *Chem. Phys.* **1991**, *151*, 309.
- Taylor, R. in *The Chemistry of Fullerenes*; Taylor, R., Ed.; Advanced Series in Fullerenes; World Scientific Publishing Co.: Singapore, 1995; Vol. 4, p 43.
- Diederich F.; Whetten, R. L. *Acc. Chem. Res.* **1992**, *25*, 119.
- Fowler, P. W.; Manolopoulos, D. E. *An Atlas of Fullerenes*; Clarendon Press: Oxford, 1995.
- Taylor, R. *J. Chem. Soc., Perkins Trans. 2* **1993**, 813.
- Manolopoulos D. E.; Fowler, P. W. *J. Chem. Phys.* **1992**, *96*, 7603.
- Edelmann, F. T. *Angew. Chem., Int. Ed. Engl.* **1995**, *34*, 981. Nagase, S.; Kobayashi, K.; Akasaka, T. *Bull. Chem. Soc. Jpn.* **1996**, *69*, 2131. Braun, T. *ACH – Models in Chemistry* **1995**, *132*, 245.
- Balch, A. L. In *The Chemistry of Fullerenes*; Taylor, R., Ed.; Advanced Series in Fullerenes; World Scientific Publishing Co.: Singapore, 1995; Vol. 4, p 220.
- Bowser, J. R. *Adv. Organomet. Chem.* **1994**, *36*, 57.
- Stephens, A. H. H.; Green, M. L. H. *Adv. Inorg. Chem.* **1997**, *44*, 1.
- Sliwa, W. *Trans. Met. Chem.* **1996**, *21*, 583.
- Rosseinsky, M. J. *J. Mater. Chem.* **1995**, *5*, 1497.
- Heath, G. A.; McGrady, J. E.; Martin, R. L. *J. Chem. Soc., Chem. Commun.* **1992**, 1272. Boyd, P. D. W.; Bhyrappa, P.; Paul, P.; Stinchcombe, J.; Bolskar, R. D.; Sun, Y.; Reed, C. A. *J. Am. Chem. Soc.* **1995**, *117*, 2907. Sun, Y.; Reed, C. A. *Chem. Commun.* **1997**, 747.
- Ballenweg, S.; Gleiter, R.; Krätschmer, W. *Tetrahedron Lett.* **1993**, *34*, 3737.
- Ballenweg, S.; Gleiter, R.; Krätschmer, W. *J. Chem. Soc., Chem. Commun.* **1994**, 2269.
- Henderson, C. C.; Cahill, P. A. *Science* **1993**, *259*, 1885.
- Douthwaite, R. E.; Green, M. L. H.; Stephens, A. H. H.; Turner, J. F. C. *J. Chem. Soc., Chem. Commun.* **1993**, 1522.
- Cherkasov, V. K.; Rad'kov, Y. F.; Lopatin, M. A.; Bochkarev, M. N. *Russ. Chem. Bull.* **1994**, *43*, 1834.
- Shapley, J. R.; Du, Y.; Hsu, H.-F.; Way, J. J. In *Recent Advances in the Chemistry and Physics of Fullerenes and Related Materials*; Kadish, K. M.; Ruoff, R. S., Eds.; Electrochemical Society Proceedings; Pennington, NJ, 1994; Vol. 94-24, p 1255.
- Balch, A. L.; Cullison, B.; Fawcett, R. W.; Ginwalla, A. S.; Olmstead, M. M.; Winkler, K. *J. Chem. Soc., Chem. Commun.* **1995**, 2287.
- Hsu, H.-F.; Shapley, J. R. In *Recent Advances in the Chemistry and Physics of Fullerenes and Related Materials*; Ruoff R. S.; Kadish, K. M., Eds.; Electrochemical Society Proceedings; Pennington, NJ, 1995; Vol. 95-10, p 1087.
- Song, L.-C.; Zhu, Y.-H.; Hu, Q.-M. *Polyhedron* **1998**, *17*, 469.
- Song, L.-C.; Zhu, Y.-H.; Hu, Q.-M. *Polyhedron* **1997**, *16*, 2141.
- Iglesias, M.; Santos, A. *Inorg. Chim. Acta* **1996**, *248*, 67.
- Tang, K.; Zheng, S.; Jin, X.; Zeng, H.; Gu, Z.; Zhou, X.; Tang, Y. *J. Chem. Soc., Dalton Trans.* **1997**, 3585.
- Pénicaud, A.; Hsu, J.; Reed, C. A.; Koch, A.; Khemani, K. C.; Allemand, P.-M.; Wudl, F. *J. Am. Chem. Soc.* **1991**, *113*, 6698.
- Stinchcombe, J.; Pénicaud, A.; Bhyrappa, P.; Boyd, P. D. W.; Reed, C. A. *J. Am. Chem. Soc.* **1993**, *115*, 5212.
- Zhang, S.; Brown, T. L.; Du, Y.; Shapley, J. R. *J. Am. Chem. Soc.* **1993**, *115*, 6705.
- Beck, W.; Bentele, H.; Hüffer, S. *Chem. Ber.* **1995**, *128*, 1059.
- Selegue, J. P.; Dev, S.; Guarr, T. F.; Brill, J. W.; Fegueroa, E. In *Recent Advances in the Chemistry and Physics of Fullerenes and Related Materials*; Ruoff, R. S., Eds.; Electrochemical Society Proceedings; Pennington, NJ, 1994; Vol. 94-24, p 1245.
- Liu, X. H.; Wan, W. C.; Owens, S. M.; Broderick, W. E. *J. Am. Chem. Soc.* **1994**, *116*, 5489.
- Schröder, M. *Chem. Rev.* **1980**, *80*, 87.
- Wallis, J. M.; Kochi, J. K. *J. Am. Chem. Soc.* **1988**, *110*, 8207.
- Hawkins, J. M.; Lewis, T. A.; Loren, S. D.; Meyer, A.; Heath, J. R.; Shibato, Y.; Saykally, R. J. *J. Org. Chem.* **1990**, *55*, 6250.
- Hawkins, J. M.; Meyer, A.; Lewis, T. A.; Loren, S.; Hollander, F. J. *Science* **1991**, *252*, 312.



- (49) Hawkins, J. M.; Meyer, A.; Lewis, T. A.; Loren, S. In *Fullerenes: Synthesis, Properties and Chemistry of Large Carbon Clusters*; Hammond, G. S., Kuck, V. J., Eds.; ACS Symposium Series 481; American Chemical Society: Washington, DC, 1992; p 91.
- (50) Hawkins, J. M. *Acc. Chem. Res.* **1992**, *25*, 150.
- (51) Hawkins, J. M.; Loren, S.; Meyer, A.; Nunlist, R. *J. Am. Chem. Soc.* **1991**, *113*, 7770.
- (52) Fann, Y. C.; Singh, D.; Jansen, S. A. *J. Phys. Chem.* **1992**, *96*, 6, 5817.
- (53) Hawkins, J. M.; Meyer, A.; Lewis, T. A.; Bunz, U.; Nunlist, R.; Ball, G. E.; Ebbesen, T. W.; Tanigaki, K. *J. Am. Chem. Soc.* **1992**, *114*, 7954.
- (54) Hawkins, J. M.; Meyer, A.; Nambu, M. *J. Am. Chem. Soc.* **1993**, *115*, 9844.
- (55) Sharpless, K. B.; Amberg, W.; Beller, M.; Chen, H.; Hartung, J.; Kawanami, Y.; Lübben, D.; Manoury, E.; Ogino, Y.; Shibata, T.; Ukita, T. *J. Org. Chem.* **1991**, *56*, 4585.
- (56) Sharpless, K. B.; Amberg, W.; Bannani, Y. L.; Crispino, G. A.; Hartung, J.; Jeong, K.-S.; Kwong, H.-L.; Morikawa, K.; Wang, Z.-M.; Xu, D.; Zhang, X.-L. *J. Org. Chem.* **1992**, *57*, 2768.
- (57) Hawkins, J. M.; Meyer, A.; Solow, M. A. *J. Am. Chem. Soc.* **1993**, *115*, 7499.
- (58) Haddon, R. C. *Science* **1993**, *261*, 1545.
- (59) Hawkins, J. M.; Meyer, A. *Science* **1993**, *260*, 1918.
- (60) Li, Q.; Wudl, F.; Thilgen, C.; Whetten, R. L.; Diederich, F. *J. Am. Chem. Soc.* **1992**, *114*, 3994.
- (61) Hawkins, J. M.; Nambu, M.; Meyer, A. *J. Am. Chem. Soc.* **1994**, *116*, 7642.
- (62) Park, J. T.; Cho, J.-J.; Song, H. *J. Chem. Soc., Chem. Commun.* **1995**, 15.
- (63) Park, J. T.; Song, H.; Cho, J.-J.; Chung, M.-K.; Lee, J.-H.; Shu, I. H. *Organometallics* **1998**, *17*, 227.
- (64) Park, J. T.; Cho, J.-J.; Song, H.; Jun, C.-S.; Son, Y.; Kwak, J. *Inorg. Chem.* **1997**, *36*, 2698.
- (65) Hsu, H.-F.; Shapley, J. R. *J. Am. Chem. Soc.* **1996**, *118*, 9192.
- (66) Braun, T.; Wohlers, M.; Belz, T.; Schlögl, R. *Catal. Lett.* **1997**, *43*, 175.
- (67) Braun, T.; Wohlers, M.; Belz, T.; Nowitzke, G.; Wortmann, G.; Uchida, Y.; Pfänder, N.; Schlögl, R. *Catal. Lett.* **1997**, *43*, 167.
- (68) Braga, D.; Grepioni, F.; Johnson, B. F. G.; Lewis, J.; Housecroft, C. E.; Martinelli, M. *Organometallics* **1991**, *10*, 1260.
- (69) Lee, K.; Hsa, H.-F.; Shapley, J. R. *Organometallics* **1997**, *16*, 3876.
- (70) Hsu, H.-F.; Shapley, J. R. *J. Chem. Soc., Chem. Commun.* **1997**, 1125.
- (71) Rasinkangas, M.; Pakkanen, T. T.; Pakkanen, T. A. *J. Organomet. Chem.* **1994**, *476*, C6.
- (72) Gorelsky, S. I.; Magdesieva, T. V.; Butin, K. P. *Russ. Chem. Bull.* **1996**, *45*, 1383.
- (73) Pradeep, T.; Kulkarni, G. U.; Kannan, K. R.; Guru Row, T. N.; Rao, C. N. R. *J. Am. Chem. Soc.* **1992**, *114*, 2272.
- (74) Arce, M.-J.; Viado, A. L.; Khan, S. I.; Rubin, Y. *Organometallics* **1996**, *15*, 4340.
- (75) Fagan, P. J.; Calabrese, J. C.; Malone, B. *Science* **1991**, *252*, 1160.
- (76) Fagan, P. J.; Calabrese, J. C.; Malone, B. *Acc. Chem. Res.* **1992**, *25*, 134.
- (77) Fagan, P. J.; Ward, M. D.; Calabrese, J. C. *J. Am. Chem. Soc.* **1989**, *111*, 1698.
- (78) Rogers, J. R.; Marynick, D. S. *Chem. Phys. Lett.* **1993**, *205*, 197.
- (79) Mavunkal, I. J.; Chi, Y.; Peng, S.-M.; Lee, G.-H. *Organometallics* **1995**, *14*, 4454.
- (80) Westmeyer, M. D.; Galloway, C. P.; Rauchfuss, T. B. *Inorg. Chem.* **1994**, *33*, 4615.
- (81) Westmeyer, M. D.; Rauchfuss, T. B.; Verma, A. K. *Inorg. Chem.* **1996**, *35*, 7140.
- (82) Roth, G.; Adlemann, P.; Knitter, R. *Mater. Lett.* **1993**, *16*, 357.
- (83) Roth, G.; Adlemann, P. *J. Phys. I* **1992**, *2*, 1541.
- (84) Buravov, L. I.; D'yachenko, O. A.; Konovalikhin, S. V.; Kushch, N. D.; Lavrent'ev, I. P.; Spitsyna, N. G.; Shilov, G. V.; Yagubski, E. B. *Russ. Chem. Bull.* **1994**, *43*, 240.
- (85) Bossard, C.; Rigaut, S.; Astruc, D.; Delville, M.-H.; Félix, G.; Février-Bouvier, A.; Amiell, J.; Flandrois S.; Delhaès, P. *J. Chem. Soc., Chem. Commun.* **1993**, 333.
- (86) Foss, C. A., Jr.; Feldheim, D. L.; Lawson, D. R.; Dorhout, P. K.; Eliot, C. M.; Martin, C. R.; Parkinson, B. A. *J. Electrochem. Soc.* **1993**, *140*, L84.
- (87) Crane, J. D.; Hitchcock, P. B.; Kroto, H. W.; Taylor, R.; Walton, D. R. M. *J. Chem. Soc., Chem. Commun.* **1992**, 1764.
- (88) Hao, L.; Olmstead, M. M.; Balch, A. L. *Abstr. Papers. Am. Chem. Soc.* **1996**, *211*, 166-INOR. Olmstead, M. M.; Hao, L.; Balch, A. L. *J. Organometal. Chem.*, in press.
- (89) Crane, J. D.; Hitchcock, P. B. *J. Chem. Soc., Dalton Trans* **1993**, 2537.
- (90) Balch, A. L.; Catalano, V. J.; Lee, J. W. *Inorg. Chem.* **1991**, *30*, 3980.
- (91) McGinnety, J. A.; Ibers, J. A. *J. Chem. Soc., Chem. Commun.* **1968**, 235.
- (92) Vértés, A.; Gál, M.; Wagner, F. E.; Tuzcek, F.; Gütllich, P. *Inorg. Chem.* **1993**, *32*, 4478.
- (93) Vaska, L. *Acc. Chem. Res.* **1968**, *1*, 335.
- (94) Deeming, A. J.; Shaw, B. L. *J. Chem. Soc. A* **1969**, 1802.
- (95) Balch, A. L.; Lee, J. W.; Noll, B. C.; Olmstead, M. M. *J. Am. Chem. Soc.* **1992**, *114*, 10984.
- (96) Balch, A. L.; Lee, J. W.; Noll, B. C.; Olmstead, M. M. *Inorg. Chem.* **1994**, *33*, 5238.
- (97) Cox, E. G.; Cruickshank, D. W. J.; Smith, J. A. S. *Proc. R. Soc. London A* **1958**, *247*, 1.
- (98) Burley, S. K.; Petsko, G. A. *Science* **1985**, *229*, 23.
- (99) Gavezzotti, A.; Desiraju, G. R. *Acta Crystallogr.* **1988**, *B44*, 427.
- (100) Linse, P. *J. Am. Chem. Soc.* **1992**, *114*, 4366.
- (101) Meidine, M. F.; Hitchcock, P. B.; Kroto, H. W.; Taylor, R.; Walton, D. M. R. *J. Chem. Soc., Chem. Commun.* **1992**, 1534.
- (102) Balch, A. L.; Lee, J. W.; Noll, B. C.; Olmstead, M. M. *J. Chem. Soc., Chem. Commun.* **1993**, *56*, Bürgi, H. B.; Restori, R.; Schwarzenbach, D.; Balch, A. L.; Lee, J. W.; Noll, B. C.; Olmstead, M. M. *Chem. Mater.* **1994**, *6*, 1325.
- (103) Balch, A. L.; Catalano, V. J.; Lee, J. W.; Olmstead, M. M. *J. Am. Chem. Soc.* **1992**, *114*, 5455.
- (104) Catalano, V. J.; Parodi, N. *Inorg. Chem.* **1997**, *36*, 537.
- (105) Balch, A. L. *Prog. Inorg. Chem.* **1993**, *41*, 239.
- (106) Balch, A. L.; Davis, B. J.; Lee, J. W.; Noll, B. C.; Olmstead, M. M. Unpublished results.
- (107) Balch, A. L.; Catalano, V. J.; Lee, J. W.; Olmstead, M. M.; Parkin, S. R. *J. Am. Chem. Soc.* **1991**, *113*, 8953.
- (108) Bürgi, H. B.; Venugopalan, P.; Schwarzenbach, D.; Diederich, F.; Thilgen, C. *Helv. Chim. Acta*, **1993**, *76*, 2155.
- (109) Balch, A. L.; Lee, J. W.; Olmstead, M. M. *Angew. Chem., Int. Ed. Engl.* **1992**, *31*, 1356.
- (110) Scuseria, G. E. *Chem. Phys. Lett.* **1991**, *180*, 451.
- (111) Hedberg, K.; Hedberg, L.; Bethune, D. S.; Brown, C. A.; Dorn, H. C.; Johnson, R. D.; deVries, M. *Science*, **1991**, *254*, 410.
- (112) Hedberg, K.; Hedberg, L.; Bühl, M.; Bethune, D. S.; Brown, C. A.; Johnson, R. D.; *J. Am. Chem. Soc.*, **1997**, *119*, 5314.
- (113) Haddon, R. C. *J. Am. Chem. Soc.* **1990**, *112*, 3385. Haddon, R. C. *J. Am. Chem. Soc.* **1997**, *119*, 1797.
- (114) Fowler, P. W.; Manolopoulos, D. E.; Ryan, R. P. *J. Chem. Soc., Chem. Commun.* **1992**, 408.
- (115) Stone A. J.; Wales, D. J. *Chem. Phys. Lett.* **1986**, *128*, 501.
- (116) Zhang, B. L.; Wang, C. Z.; Ho, K. M. *J. Chem. Phys.* **1992**, *96*, 7183. Wang, X.-Q.; Wang, C. Z.; Zhang, B. L.; Ho, K. M. *Phys. Rev. Lett.* **1992**, *69*, 69. Wang, X.-Q.; Wang, C. Z.; Zhang, B. L.; Ho, K. M. *Chem. Phys. Lett.* **1993**, *207*, 349.
- (117) Kikuchi K.; Nakahara, N.; Wakabayashi, T.; Suzuki, S.; Shiro-maru, H.; Miyake, Y.; Saito, K.; Ikemoto, I.; Kainosho, M.; Achiba, Y. *Nature (London)* **1992**, *357*, 142.
- (118) Manolopoulos, D. E.; Fowler, P. W.; Taylor, R.; Kroto, H. W.; Walton, D. R. M. *J. Chem. Soc., Faraday Trans.* **1992**, *88*, 3117.
- (119) Dennis, T. J. S.; Kai, T.; Tomiyama, T.; Shinohara, H. *Chem. Commun.* **1998**, 619.
- (120) Sanders, M.; Jiménez-Vázquez, H. A.; Cross, R. J.; Billups, W. E.; Gesenberg, C.; Gonzalez, A.; Luo, W.; Haddon, R. C.; Diederich, F.; Herrmann, A. *J. Am. Chem. Soc.* **1995**, *117*, 9305.
- (121) Okada, S.; Saito, S. *Chem. Phys. Lett.* **1996**, *252*, 94.
- (122) Balch, A. L.; Ginwalla, A. S.; Noll, B. C.; Olmstead, M. M. *J. Am. Chem. Soc.* **1994**, *116*, 2227.
- (123) Creegan, K. M.; Robbins, J. L.; Robbins, W. K.; Millar, J. M.; Sherwood, R. D.; Tindall, P. J.; Cox, D. M.; Smith, A. B., III; McCauley, J. P., Jr.; Jones, D. R.; Gallagher, R. T. *J. Am. Chem. Soc.* **1992**, *114*, 1103.
- (124) Elemes, Y.; Silverman, S. K.; Sheu, C.; Kao, M.; Foote, C. S.; Alvarez, M. M.; Whetten, R. L. *Angew. Chem., Int. Ed. Engl.* **1992**, *31*, 351.
- (125) Vaughan, G. B. M.; Heiney, P. A.; Cox, D. E.; McGhie, A. R.; Jones, D. R.; Strongin, R. M.; Cichy, M. A.; Smith, A. B., III. *Chem. Phys.* **1992**, *168*, 185.
- (126) Balch, A. L.; Costa, D. A.; Lee, J. W.; Noll, B. C.; Olmstead, M. M. *Inorg. Chem.* **1994**, *33*, 2071.
- (127) Lenarda, M.; Ros, R.; Traverso, O.; Pitts, W. D.; Baddley, W. H.; Graziani, M. *Inorg. Chem.* **1977**, *16*, 3178. Schlodder, R.; Ibers, J. A.; Lenarda, M.; Graziani, M. *J. Am. Chem. Soc.* **1974**, *96*, 6893.
- (128) Balch, A. L.; Costa, D. A.; Noll, B. C.; Olmstead, M. M. *Inorg. Chem.* **1996**, *35*, 458–462.
- (129) Balch, A. L.; Costa, D. A.; Noll, B. C.; Olmstead, M. M. *J. Am. Chem. Soc.* **1995**, *117*, 8926–8932.
- (130) Penn, S. G.; Costa, D. A.; Balch, A. L.; Lebrilla, C. B. *Int. J. Mass Spectrosc. Ion Processes* **1997**, *169*, 371.
- (131) Smith, A. B., III; Strongin, R. M.; Brard, L.; Furst, G. T.; Atkins, J. H.; Romanow, W. J.; Saunders, M.; Jiménez-Vázquez, H. A.; Owens, K. G.; Goldschmidt, R. J. *J. Org. Chem.* **1996**, *61*, 1904.
- (132) Balch, A. L.; Costa, D. A.; Olmstead, M. M. *Chem. Commun.* **1996**, 2449–2450.
- (133) Rasinkangas, M.; Pakkanen, T. T.; Pakkanen, T. A.; Ahlgrén, M.; Rouvinen, J. *J. Am. Chem. Soc.* **1993**, *115*, 4901.
- (134) Tuzcek, F.; Gál, M.; Wagner, F. E.; Vértés, A. *Fullerene Science Tech.* **1997**, *5*, 443.

- (134) Tuzcek, F.; Gál, M.; Wagner, F. E.; Vértes, A. In *Recent Advances in the Chemistry and Physics of Fullerenes and Related Materials*; Ruoff R. S., Kadish, K. M., Eds.; Electrochemical Society Proceedings; Pennington, NJ, 1995; Vol. 95-10, p 1092.
- (135) Koefod, R. S.; Hudgens, M. F.; Shapley, J. R. *J. Am. Chem. Soc.* **1991**, *113*, 8957.
- (136) Koefod, R. S.; Xu, C.; Lu, W. Y.; Shapley, J. R.; Hill, M. G.; Mann, K. R. *J. Phys. Chem.* **1992**, *96*, 2928.
- (137) Zhang, Y.; Du, Y.; Shapley, J. R.; Weaver, M. J. *Chem. Phys. Lett.* **1993**, *205*, 508.
- (138) Zhu, Y.; Koefod, R. S.; Devadoss, C.; Shapley, J. R.; Schuster, G. B. *Inorg. Chem.* **1992**, *31*, 3505.
- (139) Jardine, F. H. *Polyhedron* **1982**, *1*, 569.
- (140) Balch, A. L.; Lee, J. W.; Noll, B. C.; Olmstead, M. M. *Inorg. Chem.* **1993**, *32*, 55.
- (141) Becker, L.; Evans, T. P.; Bada, J. L. *J. Org. Chem.* **1993**, *58*, 7630.
- (142) Denisovich, L. I.; Peregudova, B. M.; Usatov, A. V.; Sigán, A. L.; Novikov, Y. N. *Russ. Chem. Bull.* **1997**, *46*, 1251.
- (143) Usatov, A. V.; Blumenfeld, A. L.; Voronstov, E. V.; Vinogradova, L. E.; Novikov, Y. N. *Mendeleev Commun.* **1993**, 229.
- (144) Usatov, A. V.; Voronstov, E. V.; Vinogradova, L. E.; Novikov, Y. N. *Russ. Chem. Bull.* **1994**, 1572. Usatov, A. V.; Kudin, K. N.; Voronstov, E. V.; Vinogradova, L. E.; Novikov, Y. N. *J. Organomet. Chem.* **1996**, *522*, 147.
- (145) Usatov, A. V.; Kudin, K. N.; Voronstov, E. V.; Vinogradova, L. E.; Novikov, Y. N. *J. Organomet. Chem.* **1996**, *522*, 147.
- (146) Schreiner, S.; Gallaher, T. N.; Parsons, H. K. *Inorg. Chem.* **1994**, *33*, 3021.
- (147) Ishii, Y.; Hoshi, H.; Hamada, Y.; Hidai, M. *Chem. Lett.* **1994**, 801.
- (148) Green, M. L. H.; Stephens, A. H. H. *Chem. Commun.* **1997**, 793.
- (149) Iyoda, M.; Sultana, F.; Sasaki, S.; Butenschön, H. *Tetrahedron Lett.* **1995**, *36*, 579.
- (150) Angermund, K. P.; Betz, P.; Butenschön, H. *Chem. Ber.* **1993**, *126*, 713.
- (151) Arce, M.-J.; Viado, A. L.; An, Y.-Z.; Kahn, S. I.; Rubin, Y. *J. Am. Chem. Soc.* **1996**, *118*, 3775.
- (152) Rubin, Y. *Chem. Eur. J.* **1997**, *3*, 1009.
- (153) Balch, A. L.; Lee, J. W.; Noll, B. C.; Olmstead, M. M. In *Recent Advances in the Chemistry and Physics of Fullerenes and Related Materials*; Ruoff, R. S., Kadish, K. M., Eds.; Electrochemical Society Proceedings; Pennington, NJ, 1994; Vol. 94-24, p 1231.
- (154) Patel, D. K.; Thompson, D. M.; Baird, M. C.; Thomson, L. K.; Preston, K. F. *J. Organomet. Chem.* **1997**, *546*, 607.
- (155) Costa, D. A.; Olmstead, M. M.; Balch, A. L. Unpublished results.
- (156) Xiao, J.; Savina, M. R.; Martin, G. B.; Francis, A. H.; Meyerhoff, M. E. *J. Am. Chem. Soc.* **1994**, *116*, 9341.
- (157) Lerke, S. A.; Parkinson, B. A.; Evans, D. H.; Fagan, P. J. *J. Am. Chem. Soc.* **1992**, *114*, 7807.
- (158) Fagan, P. J.; Calabrese, J. C.; Malone, B. In *Fullerenes, Synthesis, Properties and Chemistry of Large Carbon Clusters*; Hammond, G. S., Kuck V. J., Eds.; ACS Symposium Series 481; American Chemical Society: Washington, DC, 1992; p 177.
- (159) Cheng, P. T.; Nyburg, S. C. *Can. J. Chem.* **1972**, *50*, 912.
- (160) Bashilov, V. V.; Petrovskii, P. V.; Sokolov, V. I.; Lindeman, S. V.; Guzey, I. A.; Struchkov, Y. T. *Organometallics* **1993**, *12*, 991.
- (161) Brady, F. J.; Cardin, D. J.; Domin, M.; *J. Organomet. Chem.* **1995**, *491*, 169-172.
- (162) Bashilov, V. V.; Tumanskii, B. L.; Petrovskii, P. V.; Sokolov, V. I. *Russ. Chem. Bull.* **1994**, *43*, 1069.
- (163) Bashilov, V. V.; Petrovskii, P. V.; Sokolov, V. I.; Dolgushin, F. M.; Yanovsky, A. I.; Struchkov, Y. T.; *Russ. Chem. Bull.* **1996**, *45*, 1207.
- (164) Sul'man, E. M.; Matveeva, V. G.; Bashilov, V. V.; Sokolov, V. I. *Kinetics Catal.* **1997**, *38*, 251-252.
- (165) Fagan, P. J.; Calabrese, J. C.; Malone, B. *J. Am. Chem. Soc.* **1991**, *113*, 9408.
- (166) Djojo, F.; Herzog, A.; Lampath, I.; Hampel, F.; Hirsch, A. *Chem. Eur. J.* **1996**, *2*, 1537.
- (167) Magdesieva, T. V.; Bashilov, V. V.; Gorel'sky, S. I.; Sokolov, V. I.; Butin, K. P. *Russ. Chem. Bull.* **1994**, *43*, 2034.
- (168) Lerke, S. A.; Evans, D. H.; Fagan, P. J. *J. Electroanal. Chem.* **1995**, *383*, 127.
- (169) Chase, B.; Fagan, P. J. *J. Am. Chem. Soc.* **1992**, *114*, 2252.
- (170) Denisov, N. N.; Lobach, A. S.; Nadochenko, V. A. *Russ. Chem. Bull.* **1996**, *45*, 1103-1106.
- (171) Kunkely, H.; Vogler, A. *Inorg. Chim. Acta* **1996**, *250*, 375.
- (172) Tumanskii, B. L.; Bashilov, V. V.; Bubnov, N. N.; Solodovnikov, S. P.; Sokolov, V. I. *Russ. Chem. Bull.* **1994**, *43*, 884.
- (173) Balch, A. L.; Hao, L.; Olmstead, M. M. *Angew. Chem., Int. Ed. Engl.* **1996**, *35*, 188.
- (174) Nagashima, H.; Nakaota, A.; Saito, Y.; Kato, M.; Kawanishi, T.; Itoh, K. *J. Chem. Soc., Chem. Commun.* **1992**, 377.
- (175) Nagashima, H.; Nakaoka, A.; Tajima, S.; Saito, Y.; Itoh, K. *Chem. Lett.* **1992**, 1361.
- (176) Shul'ga, Y. M.; Lobach, A. S.; Ivleva, I. N.; Spektor, V. N.; Ovchinnikov, A. A. *Dokl. Chem.* **1996**, *348*, 162.
- (177) Cowley, J. M.; Liu, M.-Q.; Ramakrishna, B. L.; Peace, T. S.; Wertsching, A. K.; Pena, M. R. *Carbon* **1994**, *32*, 393.
- (178) Nagashima, H.; Yamaguchi, H.; Kato, Y.; Saito, Y.; Haga, M.; Itoh, K. *Chem. Lett.* **1993**, 2153.
- (179) Nagashima, H.; Kato, Y.; Yamaguchi, H.; Kimura, E.; Kawanishi, T.; Kato, M.; Saito, Y.; Haga, M.; Itoh, K. *Chem. Lett.* **1994**, 1207.
- (180) van Wijnkoop, M.; Meidine, M. F.; Avent, A. G.; Darwish, A. D.; Kroto, H. W.; Taylor, R.; Walton, D. R. M. *J. Chem. Soc., Dalton Trans.* **1997**, 675.
- (181) Nagashima, H.; Nakazawa, M.; Furukawa, T.; Itoh, K. *Chem. Lett.* **1996**, 405.
- (182) Balch, A. L.; Costa, D. A.; Winkler, K. To be published.
- (183) Ginwalla, A. S.; Balch, A. L.; Kauzlarich, S. M.; Irons, S. H.; Klavins, P.; Shelton, R. N. *Chem. Mater.* **1997**, *9*, 278.
- (184) Wan, W. C.; Liu, X.; Sweeney, G. M.; Broderick, W. E. *J. Am. Chem. Soc.* **1995**, *117*, 9580.
- (185) Olmstead, M. M.; Ginwalla, A. S.; Noll, B. C.; Tinti, D. S.; Balch, A. L. *J. Am. Chem. Soc.* **1996**, *118*, 7737.
- (186) Fabiaski, R.; Kuchta, Adv. Mater. Opt. Electron. **1996**, *6*, 297. Król, S.; Łpiński, A.; Graja, A. *Adv. Mater. Opt. Electron.* **1996**, *6*, 255.
- (187) Ikeda, A.; Fukuhara, C.; Shinkai, S. *Tetrahedron Lett.* **1996**, *37*, 7091. Ikeda, A.; Fukuhara, C.; Shinkai, S. *Chem. Lett.* **1997**, 407.
- (188) Sawamura, M.; Iikura, H.; Nakamura, E. *J. Am. Chem. Soc.* **1996**, *118*, 12850.
- (189) (a) Avent, A. G.; Birkett, P. R.; Crane, J. D.; Darwish, A. D.; Langley, J.; Kroto, H.; Taylor, R.; Walton, D. R. M. *J. Chem. Soc., Chem. Commun.* **1994**, 1463. (b) Iikura, H.; Mori, S.; Sawamura, M.; Nakamura, E. *J. Org. Chem.* **1997**, *62*, 7912.
- (190) Schumann, H.; Janiak, C.; Khan, M. A.; Zuckerman, J. J. *J. Organomet. Chem.* **1988**, *354*, 7.
- (191) Roth, L. M.; Huang, Y.; Schwedler, J. T.; Cassidy, C. J.; Ben-Amotz, D.; Kahr, B.; Freiser, B. S. *J. Am. Chem. Soc.* **1991**, *113*, 6298.
- (192) Huang, Y.; Freiser, B. S. *J. Am. Chem. Soc.* **1991**, *113*, 8186.
- (193) Huang, Y.; Freiser, B. S. *J. Am. Chem. Soc.* **1991**, *113*, 9418.
- (194) Jiao, Q.; Huang, Y.; Lee, S. A.; Gord, J. R.; Freiser, B. S. *J. Am. Chem. Soc.* **1992**, *114*, 2726.
- (195) Kan, S. Z.; Byun, Y. G.; Freiser, B. S. *J. Am. Chem. Soc.* **1994**, *116*, 8815.
- (196) Kan, S. Z.; Byun, Y. G.; Freiser, B. S. *J. Am. Chem. Soc.* **1995**, *117*, 1177.
- (197) Kan, S. Z.; Xu, Y. C.; Byun, Y. G.; Freiser, B. S. *J. Mass Spectrom.* **1995**, *30*, 834.
- (198) Basir, Y.; Anderson, S. L. *Chem. Phys. Lett.* **1995**, *243*, 45.
- (199) Tast, F.; Malinowski, N.; Frank, S.; Heinebrodt, M.; Billas, I. M. L.; Martin, T. P. *Z. Phys. D.* **1997**, *40*, 351.
- (200) Tast, F.; Malinowski, N.; Frank, S.; Heinebrodt, M.; Billas, I. M. L.; Martin, T. P. *Phys. Rev. Lett.* **1996**, *77*, 3529.
- (201) Guo, B. C.; Wei, S.; Purnell, J.; Buzza, S.; Castleman, Jr., A. W. *Science* **1992**, *256*, 515.
- (202) Zimmermann, U.; Malinowski, N.; Burkhardt, A.; Martin, T. P. *Carbon* **1995**, *33*, 995.
- (203) Zimmermann, U.; Malinowski, N.; Näher, U.; Frank, S.; Martin, T. P. *Phys. Rev. Lett.* **1994**, *72*, 3542.
- (204) Martin, T. P.; Malinowski, N.; Zimmermann, U.; Näher, U.; Schaber, H. *J. Chem. Phys.* **1993**, *99*, 4210.
- (205) Lichtenberger, D. L.; Wright, L. L.; Gruhn, N. E.; Rempe, M. E. *Synth. Met.* **1993**, *59*, 353.
- (206) Fujimoto, H.; Nakao, Y.; Fukui, K. *J. Mol. Struct.* **1993**, *300*, 425.
- (207) Koga, N.; Morokuma, K. *Chem. Phys. Lett.* **1993**, *202*, 330.
- (208) López, J. A.; Mealli, C. *J. Organomet. Chem.* **1994**, *478*, 161.
- (209) Lichtenberger, D. L.; Wright, L. L.; Gruhn, N. E.; Rempe, M. E. *J. Organomet. Chem.* **1994**, *478*, 213.
- (210) Bo, C.; Costas, M.; Poblet, J. M. *J. Phys. Chem.* **1995**, *99*, 5914.
- (211) Gal'pern, E. G.; Gambaryan, N. P.; Stankevich, I. V.; Chistyakov, A. L. *Russ. Chem. Bull.* **1994**, *43*, 547.
- (212) Haddon, R. C. *J. Comput. Chem.* **1998**, *19*, 139.
- (213) Goldberg, N.; Hoffmann, R. *J. Am. Chem. Soc.* **1996**, *118*, 3315.
- (214) Goldberg, N.; Hoffmann, R. *Inorg. Chem.* **1996**, *35*, 4369.
- (215) Yamago, S.; Yanagawa, M.; Mukai, H.; Nakamura, E. *Tetrahedron* **1996**, *52*, 5091.
- (216) Yamago, S.; Yanagawa, M.; Nakamura, E. *J. Chem. Soc., Chem. Commun.* **1994**, 2093.
- (217) Armspach, D.; Constable, E. C.; Diederich, F.; Housecroft, C. E.; Nierengarten, J. *Chem. Commun.* **1996**, 2009.
- (218) Maggini, M.; Donò, A.; Scorrano, G.; Prato, M. *J. Chem. Soc., Chem. Commun.* **1995**, 845.
- (219) Diederich, F.; Dietrich-Buchecker, C.; Nierengarten, J.-F.; Sauvage, J.-P. *J. Chem. Soc., Chem. Commun.* **1995**, 781.
- (220) Sariciftci, S.; Wudl, F.; Heeger, A. J.; Maggini, M.; Scorrano, G.; Prato, M.; Bourassa, J.; Ford, P. C. *Chem. Phys. Lett.* **1995**, *247*, 510.
- (221) Guldi, D. M.; Maggini, M.; Scorrano, G.; Prato, M. *J. Am. Chem. Soc.* **1997**, *119*, 974.
- (222) Maggini, M.; Karlsson, A.; Scorrano, G.; Sandonà, G.; Farnia, G.; Prato, M. *J. Chem. Soc., Chem. Commun.* **1994**, 589.

- (223) Diederich, F.; Jonas, U.; Gramlich, V.; Herrmann, A.; Ringsdorf, H.; Thilgen, C. *Helv. Chim. Acta* **1993**, *76*, 2445.
- (224) Osterodt, J.; Nieger, M.; Winscheif, P.; Vögtle, F. *Chem. Ber.* **1993**, *126*, 2331.
- (225) Davey, S. N.; Leigh, D. A.; Moody, A. E.; Tetler, L. W.; Wade, F. A. *J. Chem. Soc., Chem. Commun.* **1994**, 397.
- (226) Ikeda, A.; Fukuhara, C.; Shinkai, S. *Chem. Lett.* **1997**, 407.
- (227) Drovetskaya, T.; Reed, C. A.; Boyd, P. *Tetrahedron Lett.* **1995**, *36*, 7971.
- (228) Imahori, H.; Hagiwara, K.; Akiyama, T.; Taniguchi, S.; Okada, T.; Sakata, Y. *Chem. Lett.* **1995**, 265. Imahori, H.; Sakata, Y. *Chem. Lett.* **1996**, 199.
- (229) Akiyama, T.; Imahori, H.; Ajawakom, A.; Sakata, Y. *Chem. Lett.* **1996**, 907.
- (230) Kuciauskas, D.; Lin, S.; Seely, G. R.; Moore, A. L.; Gust, D.; Drovetskaya, T.; Reed, C. A.; Boyd, P. D. W. *J. Phys. Chem.* **1996**, *100*, 15926.
- (231) Liddell, P. A.; Kuciauskas, D.; Sumida, J. P.; Nash, B.; Nguyen, D.; Moore, A. L.; Gust, D. *J. Am. Chem. Soc.* **1997**, *119*, 1400.
- (232) Sun, Y.; Drovetskaya, T.; Bolskar, R. D.; Bau, R.; Boyd, P. D. W.; Reed, C. A. *J. Org. Chem.* **1997**, *62*, 3642.
- (233) Imahori, H.; Yamada, K.; Hasegawa, M.; Taniguchi, S.; Okada, T.; Sakata, Y. *Angew. Chem., Int. Ed. Engl.* **1997**, *36*, 2626.
- (234) Imahori, H.; Sakata, Y. *Adv. Mater.* **1997**, *9*, 537.
- (235) Banim, F.; Cardin, C. J.; Cardin, D. J.; Pistocchi, M.; Todd, A. *J. Phys. Chem. Solids* **1997**, *58*, 1919.
- (236) Chiang, L. Y.; Swirczewski, J. W.; Hsu, C. S.; Chowdhury, S. K.; Cameron, S.; Creagan, K. *J. Chem. Soc., Chem. Commun.* **1992**, 1791.
- (237) Chiang, L. Y.; Wang, L. Y.; Swirczewski, J. W.; Saled, S.; Cameron, S. *J. Org. Chem.* **1994**, *59*, 3960.
- (238) Iglesias, M.; Santos, A. *J. Organomet. Chem.* **1997**, *549*, 213.
- (239) Scott, L. T. *Pure Appl. Chem.* **1996**, *68*, 291.
- (240) Rabideau, P. W.; Sygula, A. *Acc. Chem. Res.* **1996**, *29*, 235.
- (241) Faust, R. *Angew. Chem., Int. Ed. Engl.* **1995**, *34*, 1429.
- (242) Barth, W. E.; Lawton, R. G. *J. Am. Chem. Soc.* **1966**, *88*, 380–381. Barth, W. E.; Lawton, R. G. *J. Am. Chem. Soc.* **1971**, *93*, 1730.
- (243) Scott, L. T.; Bratcher, M. S.; Hagen, S. *J. Am. Chem. Soc.* **1996**, *118*, 8743.
- (244) Hanson, J. C.; Nordman, C. E. *Acta Crystallogr.* **1976**, *B32*, 1147.
- (245) Forkey, D. M.; Attar, S.; Noll, B. C.; Koerner, R.; Olmstead, M. M.; Balch, A. L. *J. Am. Chem. Soc.* **1997**, *119*, 5766.
- (246) Fedurco, M.; Olmstead, M. M.; Fawcett, W. R. *Inorg. Chem.* **1995**, *34*, 390.
- (247) Seiders, T. J.; Baldrige, K. K.; O'Connor, J. M.; Siegel, J. S. *J. Am. Chem. Soc.* **1997**, *119*, 4781.
- (248) Shaltout, R. M.; Sygula, R.; Sygula, A.; Fronczek, F. R.; Stanley, G. G.; Rabideau, P. W. *J. Am. Chem. Soc.* **1998**, *120*, 835.
- (249) Attar, S.; Forkey, D. M.; Olmstead, M. M.; Balch, A. L. *Chem. Commun.* **1998**, 1255.
- (250) Iijima, S. *Nature* **1991**, *354*, 56.
- (251) Ajayan, P. M. *Prog. Crystal Growth Charact.* **1997**, *34*, 37.
- (252) (a) Chu, A.; Cook, J.; Heesom, R. J. R.; J. L. Hutchison, J. L.; Green, M. L. H.; Sloan, J. *Chem. Mater.* **1996**, *8*, 2751. (b) Chen, Y. K.; Chu, A.; Cook, J.; Green, M. L. H.; Harris, P. J. F.; Heesom, R.; Humphries, M.; Sloan, J.; Tsang, S. C.; Turner, J. F. C. *J. Mater. Chem.* **1997**, *7*, 545.
- (253) Ebbesen, T. W.; Ajayan, P. M. *Nature* **1992**, *358*, 220.
- (254) Iijima, S.; Ichihashi, T. *Nature* **1993**, *363*, 603.
- (255) Bethune, D. S.; Kiang, C. H.; de Vries, M. S.; Gorman, G.; Savoy, R.; Vazquez, J.; Beyers, R. *Nature* **1993**, *363*, 605.
- (256) Ajayan, P. M.; Lambert, J. M.; Bernier, P.; Barbedette, L.; Colliex, C.; Planeix, J. M. *Chem. Phys. Lett.* **1993**, *215*, 509.
- (257) Zhou, D.; Seraphin, S.; Wang, S. *Appl. Phys. Lett.* **1994**, *65*, 1593.
- (258) Cassell, A. M.; Scrivens, W. A.; Tour, J. M. *Chem. Mater.* **1996**, *8*, 1545.
- (259) Kiang, C.-H.; Goddard, W. A., III; Beyers, R.; Salem, J. R.; Bethune, D. S. *J. Phys. Chem. Solids* **1996**, *57*, 35.
- (260) José-Yacamán, M.; Miki-Yoshida, M.; Rendon, L.; Santiesteban, J. G. *Appl. Phys. Lett.* **1993**, *62*, 657.
- (261) Ivanov, V.; Nagy, J. B.; Lambin, Ph.; Lucas, A.; Zhang, X. B.; Zhang, X. F.; Bernaerts, D.; Van Tendello, G.; Amelinckx, S.; Van Landuyt, J. *Chem. Phys. Lett.* **1994**, *223*, 329.
- (262) Hernadi, K.; Fonseca, A.; Nagy, J. B.; Bernaerts, D.; Lucas, A. A. *Carbon* **1996**, *34*, 1249.
- (263) Hernadi, K.; Fonseca, A.; Piedigrosso, P.; Delvaux, M.; Nagy, J. B.; Bernaerts, D.; Riga, J. *Catal. Lett.* **1997**, *48*, 229.
- (264) Guo, T.; Nikolaev, P.; Thess, A.; Colbert, D. T.; Smalley, R. E. *Chem. Phys. Lett.* **1995**, *243*, 49.
- (265) Thess, A.; Lee, R.; Nikolaev, P.; Dai, H.; Petit, P.; Robert, J.; Xu, C.; Lee, Y. H.; Kim, S. G.; Rinzler, A. G.; Colbert, D. T.; Scuseria, G. E.; Tománek, D.; Fischer, J. E.; Smalley, R. E. *Science* **1996**, *273*, 483.
- (266) Yudasaka, M.; Komatsu, T.; Ichihashi, T.; Iijima, S. *Chem. Phys. Lett.* **1997**, *278*, 102.
- (267) Dai, H.; Rinzler, A. G.; Nikolaev, P.; Thess, A.; Colbert, D. T.; Smalley, R. E. *Chem. Phys. Lett.* **1996**, *260*, 471.
- (268) Maiti, A.; Brabec, C. J.; Bernholc, J. *Phys. Rev. B* **1997**, *55*, R6097.
- (269) Birkett, P. R.; Cheetham, A. J.; Eggen, B. R.; Hare, J. P.; Kroto, H. W.; Walton, D. M. R. *Chem. Phys. Lett.* **1997**, *281*, 111.
- (270) Ugarte, D. *Chem. Phys. Lett.* **1993**, *209*, 99.
- (271) Ruoff, R. S.; Lorents, D. C.; Chan, B.; Malhotra, R.; Subramoney, S. *Science* **1993**, *259*, 346.
- (272) Saito, Y.; Nishikubo, K.; Kawabata, K.; Matsumoto, T. *J. Appl. Phys.* **1996**, *80*, 3062.
- (273) Ata, M.; Yamaura, K.; Hudson, A. J. *Adv. Mater.* **1995**, *7*, 286.
- (274) Guerret-Plécourt, C.; Le Bouar, Y.; Loiseau, A.; Pascard, H. *Nature* **1994**, *372*, 761.
- (275) Tsang, S. C.; Chen, Y. K.; Harris, P. J. F.; Green, M. L. H. *Nature* **1994**, *372*, 159.
- (276) Lago, R. M.; Tsang, S. C.; Lu, K. L.; Chen, Y. K.; Green, M. L. H. *J. Chem. Soc., Chem. Commun.* **1995**, 1355.
- (277) Sloan, J.; Hammer, J.; Zwiefka-Sibley, M.; Green, M. L. H. *Chem. Commun.* **1998**, 347.
- (278) Ajayan, P. M.; Stephan, O.; Redlich, Ph.; Colliex, C. *Nature* **1995**, *375*, 564.
- (279) Chen, Y. K.; Green, M. L. H.; Tsang, S. C. *Chem. Commun.* **1996**, 2489.
- (280) Dai, H.; Wong, E. W.; Lu, Y. Z.; Fan, S.; Lieber, C. M. *Nature* **1995**, *375*, 769.
- (281) Wong, E. W.; Maynor, B. W.; Burns, L. D.; Lieber, C. M. *Chem. Mater.* **1996**, *8*, 2041.
- (282) Sen, R.; Govindaraj, A.; Rao, C. N. R. *Chem. Mater.* **1997**, *9*, 2078.
- (283) Yu, R.; Chen, L.; Liu, Q.; Lin, J.; Tan, K.-L.; Ng, S. C.; Chan, H. S. O.; Xu, G.-Q.; Hor, T. S. A. *Chem. Mater.* **1998**, *10*, 718.
- (284) Kyotani, T.; Tsai, L. F.; Tomita, A. *Chem. Commun.* **1997**, 701.
- (285) Chu, A.; Cook, J.; Heesom, R. J. R.; Hutchinson, J. L. *Chem. Mater.* **1996**, *8*, 2751.
- (286) Planeix, J. M.; Coustel, N.; Coq, B.; Brotons, V. *J. Am. Chem. Soc.* **1994**, *116*, 7935.
- (287) Bruice, M. I.; Hinterding, P.; Tiekink, E. T. R.; Skelton, B. W.; White, A. H. *J. Organomet. Chem.* **1993**, *450*, 209.
- (288) Bartik, T.; Bartik, B.; Brady, M.; Dembinski, R.; Gladysz, J. A. *Angew. Chem., Int. Ed. Engl.* **1996**, *35*, 415.
- (289) Bruce, M. I. *Coord. Chem. Rev.* **1997**, *116*, 91.
- (290) Guo, B. C.; Kerns, K. P.; Castleman, A. W., Jr. *Science* **1992**, *255*, 1411.
- (291) Guo, B. C.; Wei, S.; Purnell, J.; Buzza, S.; Castleman, A. W., Jr. *Science* **1992**, *256*, 515.
- (292) Wei, S.; Guo, B. C.; Purnell, J.; Buzza, S.; Castleman, A. W., Jr. *Science* **1992**, *256*, 818.
- (293) Guo, B. C.; Kerns, K. P.; Castleman, A. W., Jr. *J. Am. Chem. Soc.* **1993**, *115*, 7415.
- (294) Kerns, K. P.; Guo, B. C.; Deng, H. T.; Castleman, A. W., Jr. *J. Am. Chem. Soc.* **1995**, *117*, 4026.
- (295) Deng, H. T.; Kerns, K. P.; Castleman, A. W., Jr. *J. Am. Chem. Soc.* **1996**, *118*, 446.
- (296) Pilgrim, J. S.; Duncan, M. A. *J. Am. Chem. Soc.* **1993**, *115*, 6958.
- (297) Dance, I. *J. Chem. Soc., Chem. Commun.* **1992**, 1779.
- (298) Dance, I. *J. Am. Chem. Soc.* **1996**, *118*, 6309.
- (299) Cartier, S. F.; Chen, Z. Y.; Walder, G. J.; Sleppy, C. R.; Castleman, A. W., Jr. *Science* **1993**, *260*, 195.
- (300) Pilgrim, J. S.; Duncan, M. A. *J. Am. Chem. Soc.* **1993**, *115*, 9724.
- (301) Reddy, B. V.; Khanna, S. N.; Jena, P. *Science* **1992**, *258*, 1640.
- (302) Dance, I. *J. Am. Chem. Soc.* **1996**, *118*, 2699.
- (303) Clemmer, D. E.; Hunter, J. M.; Shellmow, K. B.; Jarrold, M. F. *Nature* **1994**, *372*, 248.
- (304) Shelimov, K. B.; Jarrold, M. F. *J. Am. Chem. Soc.* **1995**, *117*, 6404.
- (305) Balch, A. L. In *Applications of Organometallic Chemistry in the Preparation and Processing of Advanced Materials*; Harrod, J. F., Laine, R. M., Eds.; Kluwer Academic Publishers: Boston, MA, 1995; p 283.

